A strategy to assess the effect of microgravity on the neuronal cytoskeleton and intracellular trafficking

by

Matthew Danesh

B.Sc., University of Toronto, 2018

Thesis Submitted in Partial Fulfillment of the
Requirements for the Degree of
Master of Science

in the
Department of Biological Sciences
Faculty of Science

SIMON FRASER UNIVERSITY
Summer 2022

Declaration of Committee

Name:	**Matthew Danesh**
Degree:	**Master of Science**
Title:	**A strategy to assess the effect of microgravity on the neuronal cytoskeleton and intracellular trafficking**
Committee:	**Chair:** **Eirikur Palsson** Associate Professor, Biological Sciences
	Michael Silverman Supervisor Professor, Biological Sciences
	Timothy Audas Committee Member Associate Professor, Molecular Biology and Biochemistry
	Devin Ridgley Committee Member Vice President of Biotechnology HNu Photonics LLC
	Rene Harrison Examiner Professor, Biological Sciences University of Toronto

Abstract

Microgravity exposure plays a role in the onset of physiological dysfunction among crew onboard the International Space Station. Cognitive effects including impaired motor control and mood disturbance are difficult for astronauts, as they decrease quality of life and are risk factors for neurological conditions. However, it remains difficult to investigate the underlying cause of such conditions via cellular experimentation in actual microgravity. Here, in collaboration with HNu Photonics (Maui, HI), I report a framework for use of the imaging and microfluidics platform Mobile SpaceLab™ for cell biology research in microgravity. We plan to send SH-SY5Y neuroblastoma cells cultured in the MoSL to the ISS (SpaceX27, Jan.2023) and will investigate the effect of microgravity on neurite outgrowth, microtubule dynamics and axonal transport of mitochondria. In this thesis, I establish the culture and imaging conditions for the ground control, a data set which will serve as a negative control for the effect of microgravity on SH-SY5Y cells sent to outer space. Furthermore, I establish and validate protocols for post-flight analysis; a regimen of immunostaining and quantitative analyses to identify cell stress and mitochondrial dysfunction post-microgravity exposure. The data collected in this thesis will allow for analysis of the first representations of neurite outgrowth dynamics and axonal transport in actual microgravity conditions. These results may aid in uncovering mechanistic pathways involving microtubule disruption and help explain maladaptive responses to microgravity in neurons. Furthermore, success in this mission may open the hatch for follow-up experiments using this framework and MoSL across cell biology.

Keywords: microgravity; cytoskeleton; axonal transport; mitochondria; neuron development; cell stress

Acknowledgements

I extend my thanks to my senior supervisor, Dr Michael Silverman for giving me the opportunity to work in his lab and grow as a student and as an individual. I will fondly remember the amount of patience and guidance he showed me throughout my struggles to navigate one of the more uncertain times of my life. And to Andrew, who not only played an instrumental role in this project, but also for teaching me so much about enjoying life and introducing me to sous vide cooking, my steaks have never been so perfect. Thank you to my collaborators at HNu Photonics for allowing me the opportunity to contribute to just a small part of an incredibly large and fascinating project. I'd also like to extend my gratitude to my supervisory committee, Dr. Timothy Audas and Dr. Devin Ridgley for their role in shaping my progression through this thesis and providing me with invaluable advice along the way. And of course, the undergrads Kelly and Akshit, for their numerous contributions to this project.

Finally, to those closest to me. My mother and father, and grandmother. And to my brother Mark: best of luck in your own pursuit of a Master's. I pray there is no covid-2022 to affect your progression. Thank you to my rabbit, Simon, who selectively makes a commotion when I have a meeting or presentation. And most importantly, to Anita, my love, who I would not have made it this far without. Thank you for always having my back and believing in me with all your heart. These last 7 years have been amazing, and many more adventures await us next.

Table of Contents

List of Tables

List of Figures

List of Acronyms

+TIP	Microtubule Plus-End Tracking Protein
AD	Alzheimer's Disease
ALS	Amyotrophic Lateral Sclerosis
BDNF	Brain Derived Neurotrophic Factor
DAPI	4′,6-diamidino-2-phenylindole
EB3	End-Binding Protein 3
ECM	Extracellular Matrix
EXPRESS	Expedite the Processing of Experiments to Space Station
FAT	Fast Axonal Transport
FCCP	Carbonyl cyanide-p-trifluoromethoxyphenylhydrazone
GC	Ground Control
GFP	Green Fluorescent Protein
ISS	International Space Station
KIF	Kinesin Superfamily Proteins
MAP	Microtubule Associated Protein
MiNA	Mitochondrial Network Analysis
MoSL	Mobile Space Lab
MPS	Membrane-Associated Periodic Skeleton
MSC	Mechanosensitive Ion Channel
MT	Microtubule
MTOC	Microtubule Organizing Center
MTS	Mitochondrial Targeting Sequence
PD	Parkinson's Disease
RA	Retinoic Acid
RFP	Red Fluorescent Protein
TIA1	T cell-Restricted Intracellular Antigen

Chapter 1. Introduction

The unique environmental conditions of outer space apply pressure on animal physiology in ways that many species will never encounter on Earth. While spacecraft engineering may mitigate the effects of space radiation, extreme temperatures, and space debris, any organism sent into space must independently adapt to the effects of microgravity, vacuum, and acceleration (Iwase et al., 2020). As time spent in microgravity increases, crew members onboard the International Space Station (ISS) become more likely to experience physiological dysfunction. Some of the most common effects of extended microgravity exposure include immune system dysregulation, skeletal muscle atrophy, cardiovascular dysregulation, bone loss, cognitive impairments, and decreased motor control (Bloomfield et al., 2016; Crucian et al., 2008; Fitts et al., 2000; Manzey et al., 1998; Shen & Frishman, 2019; Wang et al., 2013). These adaptations impair quality of life in both the short-term and long-term, especially upon re-entry to Earth's gravitational field after extended microgravity exposure (Goswami et al., 2021). As such, it is critical to understand how microgravity affects human physiology and identify mitigating factors to help attenuate these deleterious effects on human physiology. Due to the widespread dysfunction across several tissue and organ systems, it is likely that there may be fundamental alterations to cellular function at the subcellular level, rather than specific organ and tissue-level interactions with microgravity.

It is hypothesized that intracellular gravity perception is mediated by the cell cytoskeleton, which is primarily composed of actin filaments and microtubules (Hayakawa et al., 2008; Hughes-Fulford, 2003; Takahashi et al., 2021)**.** Microtubules are important regulators of cell structure and shape, and they provide a platform for the transport of various intracellular cargos. Neurons are especially reliant on proper microtubule function due to their high degree of compartmentalization and polarization. Without microtubule support, neurons become unable to maintain their morphology and have difficulty establishing and maintaining synapses, thus impairing neuronal transmission. Furthermore, disruption of microtubule-dependent axonal transport leads to compromised energetics, failure to clear toxins, synaptic loss, and ultimately cell death (Guedes-Dias & Holzbaur, 2019; Kelliher et al., 2019; Rolls et al., 2020).

Previous experiments in simulated and actual microgravity conditions have shown that indeed, cytoskeletal organization is disrupted in a variety of cell lines. Model systems such as cardiocytes, osteoblasts, and neuroblastoma cells have been used to highlight various degrees of microtubule and actin cytoskeleton disruption which is likely dependent on time spent exposed to microgravity (Hughes-Fulford, 2003; Lin et al., 2016; Lin et al., 2020; Nabavi et al., 2011; Rösner et al., 2006; Nassef et al., 2019; Tan et al., 2018; Wang et al., 2016; Yang et al., 2008). Knowing that proper neuronal organization and function is heavily dependent on the regulation of cytoskeletal organization makes the effects of microgravity evermore so concerning. The onset and progression of many human neurological diseases such as Charcot-Marie-Tooth disease, amyotrophic lateral sclerosis (ALS), Alzheimer's Disease (AD) and Parkinson's Disease (PD) are related to dysfunctional microtubules and microtubule-related processes (Cappelletti et al., 2015; Jean & Baas, 2013; Kametani & Hasegawa, 2021; Lazarov, 2005; Liu et al., 2012; Millecamps & Julien, 2013). Thus, if cellular models of neurological disease and microgravity-exposed cells exhibit similar behaviours and phenotypes, we may be able to uncover connections between microtubular organization and the irregular cognitive side-effects experienced by humans enduring long-term stays in space.

The objective of this thesis is to describe a strategy for the capture and analysis of cytoskeletal and neurophysiological dysfunction resulting from long-term microgravity exposure using the microfluidics platform Mobile SpaceLab. In this chapter, I begin with a brief introduction to classical microgravity research models and how the use of the Mobile SpaceLab (MoSL), an automated microfluidics and imaging platform can collect various first-of-its-kind types of dynamic data in living cells onboard the International Space Station (ISS). I will then provide a comprehensive overview of neuronal cytoskeletal structure and cytoskeletal-dependent functions including neurite outgrowth and axonal transport, and how microgravity may affect these systems. I will also discuss the idea of stress markers and mitochondrial morphology as markers for overall cellular health, and the role microgravity may play in causing cellular stress. Lastly, I will outline my research objectives which revolve around building a framework for utilization of the MoSL to capture the first recordings and analyses of microtubule dynamics and axonal transport in microgravity.

1.1. Cellular Research in Microgravity

Conducting research on cellular systems in microgravity environments presents a technological and logistical challenge. The first consideration before planning and conducting microgravity research is consideration of the prohibitive costs, and scarcity of spaceflight missions. For this reason, planned spaceflights are rich in collaborative research opportunity, where over 3000 experiments have been conducted within the ISS to date (Witze, 2020).

A second consideration is technology. There are immense amounts of prerequisite training and accreditations required for each person assigned to a spaceflight mission. It is not practical for primary scientific researchers to be present in space to conduct experiments. Thus, innovations in space-research methodologies have been ongoing for decades. One such innovation has been the creation of simulated microgravity models. The clinostat, for example, is a motorized device which rotates on a singular axis and uses this rotation to negate the net effect of gravity in one vector (Lyon, 1970). One problem with the clinostat is that weightlessness is only felt along the axis of rotation, while actual microgravity affects all axes equally (Brown et al., 1976). This problem has been combated with the invention of the random-positioning machine, a two-axis clinostat which averages gravitational pull over all directions (Wuest, et al., 2015). Another alternative is the free fall machine, where a suspension of cells is allowed to fall under the influence of gravity for a short time before being pulled back up by a strong force (Schwarzenberg et al., 1999). These simulated microgravity models significantly reduce the costs and coordination required to conduct experiments in space and have provided a tremendous amount of insight into candidate sub-cellular systems that may be worthwhile for the investment of future resources. However, it should be noted that gravitational effects still occur in simulated microgravity, but without a net direction. Another criticism of rotation-based simulated microgravity is the potential confounding effect of centrifugal force experienced by the biological specimen, which is inversely proportional to reductions in gravitational force (Brown et al.,1976).

To conduct cell research in actual microgravity, a variety of technological advancements in automated laboratory engineering have occurred since the induction of the first biomedical space program, SkyLab, in 1973. The first cell culture experiment was completed on the ISS in 2001, where colon, kidney, neuroendocrine, and ovarian cell

cultures were housed in an incubator and fixed by hand before returning to Earth for analysis ("ISS Expedition Three Science Operations Weekly Science Status Report 29 Aug 2001"). Today, a variety of cell and molecular biology platforms exist on the ISS, such as BioCell Habitat, Bioculture system, WetLab-2, MinION, and Space Automated Bioproduct Laboratory. These various platforms are largely automated and allow for a plethora of cell culture experiments, especially in the -omics research space (genomics, proteomics, lipidomics, etc.) to be conducted on the ISS. These experiments have greatly enhanced our current understanding of changes in cellular physiology during microgravity exposure and have enabled researchers to hypothesize the mechanisms in which microgravity affects mammalian cells. However, due to the hardships in performing such experiments and the sheer amount of research that must be conducted to gain a full understanding of any biological system, there remain many holes in our knowledge of mechanisms by which microgravity affects cell and tissue cultures.

1.1.1. Mobile SpaceLab

The Mobile SpaceLab (MoSL), developed by HNu Photonics (Maui, HI, USA) is a novel microfluidics and imaging platform capable of maintaining mammalian cell cultures in constant temperature and humidity. Microfluidic ports allow for the maintenance and replacement of the cell-media environment, ensuring cells can stay healthy for extended durations without human interaction. The MoSL is also equipped with digital cameras capable of recording up to two fluorescent wavelengths with adjustable y and z-axis positioning. Further explanation of MoSL hardware design and capabilities will be covered in Section 2.9. The MoSL enables researchers to observe living cell cultures over time in microgravity and provides near real-time data about cell and tissue behaviour. Historically, this has not been possible, and most studies performed in actual microgravity have presented data from fixed cell or tissue sections, absent of any dynamic data or imaging. As such, various dynamic cell processes such as neurite outgrowth or axonal transport have never been studied in actual microgravity. In this thesis, I describe a strategy for the analysis of neurite outgrowth and microtubule dynamics from data captured in outer space using MoSL. I also describe and validate a plan for post-flight experimentation on fixed cells returned to our lab on Earth post-microgravity exposure.

1.1.2. The SH-SY5Y Cell Line as a "Neuron-Like" Model

Neuroscience research requires neuronal models to elucidate the molecular and cellular processes involved in nervous system disorder. However, *in vitro* models of neuronal systems are historically difficult to culture and require human maintenance to ensure survival. This introduces challenges in actual microgravity, where cell culture methodologies are often inflexible and regulated by automated systems. Thus, alternative neuronal models which express key features of mature human neurons are often sought after and used to approximate neurons. One popular model is the SH-SY5Y neuroblastoma cell line. This cell line, while acknowledged as not being true neurons, proliferates continuously and is resilient to environmental pressures, making them an apt model to survive with little human interference in an automated microgravity environment (Agholme et al., 2010).

The SH-SY5Y cell line undergoes neuronal differentiation when treated with an inducing agent such as retinoic acid (RA). The most common differentiation paradigm is RA followed by brain-derived neurotrophic factor (BDNF), which is the only differentiation protocol that causes SH-SY5Y cells to exhibit electrophysiological properties that are similar to neurons (Şahin et al., 2021; Xicoy et al., 2017). Furthermore, this cell line is purported to express many biochemical neuronal markers, such as tyrosine hydroxylase (TH), neuron-specific enolase (NSE), neuronal nuclei protein (NeuN), and the dopamine transporter (DAT) (Agholme et al., 2010; de Medeiros et al., 2019). However, it has been observed by others and myself that these cells do not form mature axonal and synaptic connections, and thus may not truly approximate the physiology of mature neurons (Figure A.1. (Goldie et al., 2014).

While recognized as not being true neurons, the physical, electrical, and biochemical properties of these cells are widely regarded as being neuron-like, and literature often equates findings in neuronal-research to being applicable in SH-SY5Y cells. Thus, for the purposes of this thesis, all upcoming discussion of neuronal processes and physiology may be considered as also applying to SH-SY5Y cells, and references to works done in actual SH-SY5Y cells are made whenever possible.

1.2. Overview of Neuronal Cytoskeletal Structure and Function

Neurons are the fundamental unit of the brain and nervous system, responsible for the transmission of information. Using electrical impulses and chemical messengers, neurons transmit information between different regions of the brain, or between the brain and the rest of the physiological systems. This communicative ability is dependent on neuronal polarization, the process wherein neurons develop into highly compartmentalized cells with distinct borders between their processes (Schelski & Bradke, 2017). These processes consist of the axon and dendrites, which are responsible for the transmission and reception of complex chemical and electrical signaling pathways. The formation and maintenance of these structures is dependent on the cytoskeleton, a complex and dynamic molecular megastructure known for its stabilizing role in shaping cells and providing mechanical resistance to deformation. The eukaryotic cytoskeleton is primarily composed of three main components: microfilaments (actin filaments), intermediate filaments (neurofilaments), and microtubules (Leterrier, 2021).

1.2.1. Microtubule Dynamics

Microtubules constitute one of the three main classes of cytoskeletal filaments in eukaryotic cells and are found in all eukaryotic organisms (Sweeney & Holzbaur, 2018). They are longer and more rigid compared to actin and intermediate filaments due to their larger diameter and tubular construction (Figure 1.1.) (Gittes et al., 1993). They play major roles in various important cellular activities. Most notably, microtubules and their accessory proteins form the mitotic spindle, which separates chromosomes during mitosis and is the basis for cellular division (McIntosh, 2016). In addition, microtubules constitute the building blocks of the microtubule cytoskeleton, the architecture of which serves as the basis for various forms of cell motility, cell shape, and transport of organelles, vesicles, and other cellular components or structures (Barlan & Gelfand, 2017; Guedes-Dias & Holzbaur, 2019; Viswanadha et al., 2017). Microtubule structure is most straightforwardly described as comprising of 13 linear protofilaments constructed from head-to-tail polymerization of α- and β-tubulin heterodimers (commonly referred to as just “tubulin”), which then associate laterally and are closed into a hollow tube (Figure 1.1.). α- and β-tubulins are just two of the six families of tubulins, and even within families, there may be upwards of 20 isoforms of α- and β-tubulin, which allows for specificity in expression

patterns among eukaryotic cells (Dutcher, 2001; Oakley, 2000). For example, Class III β-tubulin is exclusively expressed in neurons (Karki et al., 2013). Because αβ-tubulin heterodimers are assembled with the α-tubulin facing one end (minus-end) and β-tubulin the other (plus-end) of the microtubule, the overall polymer structure is polar. The microtubule minus-end region is relatively stable and embedded within the “microtubule organizing center” (MTOC), whereas the plus-end is more dynamic, actively growing and shrinking by addition and subtraction of tubulin heterodimers (Arnal et al., 1996; Chaaban & Brouhard, 2017; Guedes-Dias & Holzbaur, 2019; Sui & Downing, 2010; Tian & Cowan, 2013). This dynamicity allows for a constant turnover of tubulin subunits driven by nucleotide hydrolysis. Interestingly, the assembly of microtubules is spontaneous while the energy released from GTP hydrolysis is used to power disassembly. Furthermore, microtubule dynamicity can be regulated via a variety of post-translational modifications or associations with microtubule associated proteins (MAPs). (Hyman et al., 1992; Vulevic & Correia, 1997).

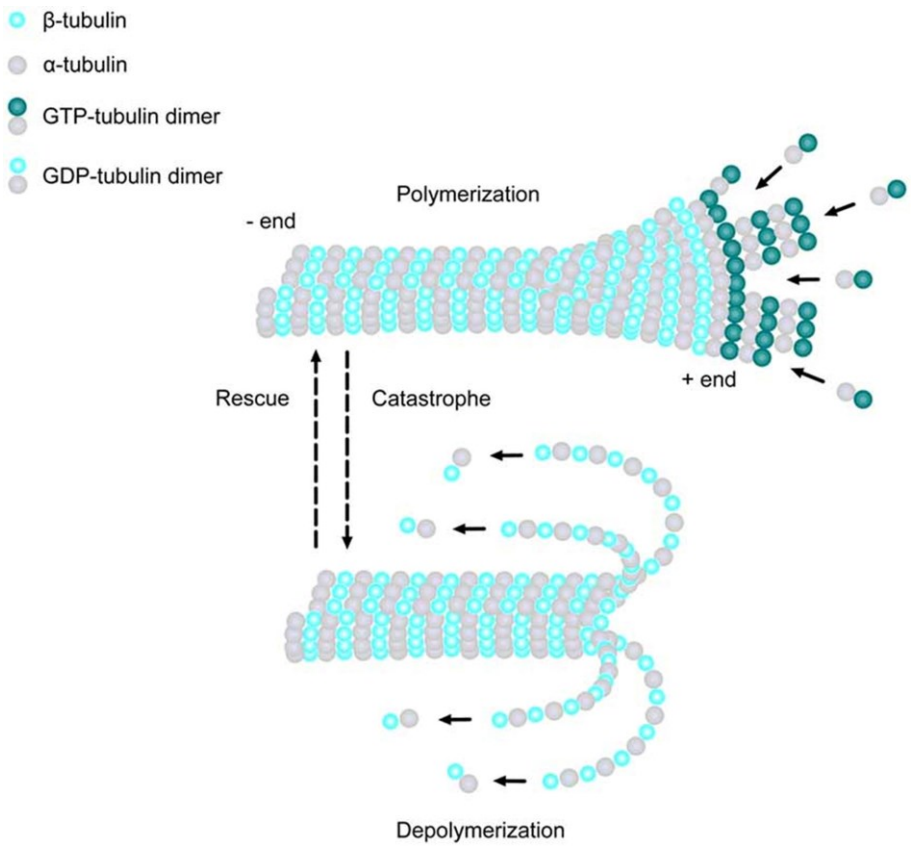

Figure 1.1. Basics of microtubule structure
MTs are linear structures comprised of α-tubulin and β-tubulin heterodimers. MTs are highly dynamic, existing in either a growing state (polymerization) or shrinking state (depolymerization), and can rapidly switch from growth to shrinkage (catastrophe) or from shrinkage to growth (rescue). Addition of new GTP-bound heterodimers occurs at the MT plus end during polymerization. Shortly thereafter, the tubulin subunits hydrolyze their bound GTP to GDP. When the addition of GTP-bound heterodimers slows and the MT lattice is composed of predominantly GDP-tubulin, the protofilaments splay apart and the MT depolymerizes.

In neurons, microtubules are essential for many fundamental cellular and developmental processes, such as migration, polarity, and differentiation. Microtubules have been regarded as critical structures for stable neuronal morphology because they serve as tracks for long-distance transport, provide dynamic and mechanical functions, and control local signaling events (Kapitein & Hoogenraad, 2015). Dysfunctional microtubule organization and dynamics are thought to be causative in many well-known neurological diseases, and controlled disruption to microtubules or their associated proteins is sufficient to generate cell lines with disease phenotypes that mimic neurological

disease *in vivo* (Franker & Hoogenraad, 2013; Matamoros & Baas, 2016; Millecamps & Julien, 2013; Sorbara et al., 2014). The neuronal microtubule cytoskeleton is heterogeneous, and microtubule orientation, stability, modifications, and associated proteins can differ depending on location in the cell (Figure 1.2.). Fluorescence microscopy has allowed for selective labeling of various microtubule-related targets, but visualization of individual microtubules is difficult and 3D reconstruction of the microtubule cytoskeleton from thin sections is time-consuming and error prone (Kapitein & Hoogenraad, 2015). Thus, the precise organization of the overall neuronal microtubule cytoskeleton is largely unresolved.

1.2.1.1. +TIPs and EB3

Plus-end tracking proteins (+TIPs) are a diverse group of MAPs that accumulate at the ends of growing microtubules. In general, they are thought to be involved in regulation of microtubule dynamics and act as mediators between microtubules and other cellular components (Akhmanova & Hoogenraad, 2005). Because of their propensity to track the plus-end, a common strategy to assess changes in microtubule dynamics is to monitor the direction and velocity of +TIPs (Zwetsloot, et al., 2018). This strategy is robust, as even within the same cell the quantitative aspects of microtubule dynamics may differ depending on sub-cellular location. For example, neuronal dendrites, axons, and the soma all may exhibit differing velocities and direction of +TIPs (Stepanova et al., 2003). This is a reasonable conclusion, as we know that each neuronal compartment has unique microtubule organization and associated function (Discussed in section 1.2.1.).

Previous works have shown that local microtubule polymerization events occur throughout neuronal differentiation, and that changes in microtubule polymerization dynamics are reflective of changes in the microtubule network (Stepanova et al., 2003). End-Binding Protein 3 (EB3) is one such +TIP that has been used to track microtubule polymerization and generate such data. EB3 has a specific role in regulating the morphology of differentiating muscle and neuronal cells and is upregulated during differentiation (Straube & Merdes, 2007). By conjugating EB3 to a fluorophore, e.g., RFP-EB3, and expressing this fusion protein in mammalian cells, we can monitor the velocity and directionality of EB3 throughout growing neurites and quantitatively assess changes in microtubule dynamics. Previous studies using transgenic models to visualize EB3 dynamics have demonstrated that overexpressed EB3 does not have any significant effect

on microtubule organization or EB3 protein distribution patterns, however increased mushroom-type dendritic spines and spine head area have been observed (Jaworski et al., 2009; Komarova et al., 2005; Pchitskaya et al., 2022). Furthermore, the manipulation of microtubule dynamics by pharmacological intervention can be quantified via EB3 dynamics and has been previously done so in the cases of taxol and nocodazole, microtubule stabilizing and destabilizing drugs, respectively (Stepanova et al., 2003). The quantification of EB3 dynamics in this manner only requires fluorescently captured timelapses, and as such, we utilized a similar experiment design in the MoSL to monitor EB3 velocity during differentiation in microgravity conditions. While microtubule structure and dysfunction are well-documented in various cell lines exposed to microgravity conditions (Discussed in section 1.2.4.), the capture of real time changes in axonal transport and microtubule dynamics is novel and possible because of the MoSL.

1.2.2. Actin and Intermediate Filaments

Actin is ubiquitously expressed and is the most abundant protein in eukaryotic cells. Despite being one of the three major cytoskeletal proteins, actin is not limited to cytoskeletal functions, and its ability to transition between monomeric (G-actin) and filamentous (F-actin) states allows it to play a role in various other cellular functions including cell motility, muscle contraction, cell division and cytokinesis, and cell signaling (Doherty & McMahon, 2008; Dominguez & Holmes, 2011). F-actin is assembled linearly at the barbed-end (plus-end) of the structure, via polymerization of repeating ATP-bound G-actin monomers, while monomer release occurs more commonly at the opposite minus-end. (Campellone et al., 2013). The most notable use of actin is in the formation of the actin cytoskeleton, which gives cells their shapes and resistance to deformation from mechanical stress. The actin cytoskeleton is reliant on several protein classes to maintain its shape and function: nucleation-promoting factors, which initiate filament formation; capping proteins, which terminate filament growth; polymerases, which promote faster or more sustained filament growth; depolymerizing factors and severing factors, which disassemble filaments; and crosslinkers and stabilizing proteins, which organize and reinforce higher-order network structures. The expression of any one of these regulatory proteins can be influenced by change in mechanical forces inside or outside the cell, and in turn can affect local organization of cytoskeletal architecture, cell adhesion dynamics, and cytoskeletal stability (Coles & Bradke, 2015; Fletcher & Mullins, 2010).

In neurons, actin serves different functions within each domain of the cell and may interact with different accessory proteins depending on the required function and location within the neuron (dendrite, soma, or axon). Within the soma, the actin cytoskeleton is expressed in a similar fashion to other somatic cells, providing neurons with the means to withstand compressive forces and maintain structural integrity. Unique to neurons, however, is F-actin assembly into the “membrane-associated periodic skeleton” (MPS), which is composed of actin and various accompanying proteins (Baines, 2010; Bennett and Baines, 2001). The MPS is a supramolecular protein structure consisting of periodic, transverse F-actin rings. It is highly expressed in axons, where it is thought to support the extreme physical and structural conditions that axons must resist during their lifespans (Figure 1.2.) (Xu et al., 2013). Actin is also heavily involved in formation of the growth cone, a large actin-supported extension of developing neurites (Figure 1.2.). Growth cones and F-actin polymerization will be discussed in further detail in section 1.2.3. Numerous actin-based structures also exist both in the shafts of and surface of dendrites. Small patches of branched F-actin (actin patches) serve as outgrowth points for filopodia (Korobova and Svitkina, 2010). Dendritic spines are small membranous protrusions that form synapses with neighboring neurons and are found on the surfaces of dendrites. These spines contain dense F-actin arrangements and respond dynamically to local synaptic activity, thus forming the basis for one of the ways in which neurons exhibit plasticity (Figure 1.2.) (Bär et al., 2016; Okamoto et al., 2004). Synapses serve as essential structures for the transmission of chemical and electrical impulses and serve as the basis for neuronal communication and physiology. While F-actin arrangements are important in early neurite outgrowth and later growth cone dynamics, our preliminary work in SH-SY5Y cells has demonstrated to us that these cells do not form mature synapses that are identifiable by standard neuronal protein markers, such as synapsin (Figure A.1.) With this in mind, the data presented here in SH-SY5Y cells serves only as a proxy for neuronal physiology, and results in traditional neuronal models may not fully reflect the data presented in this thesis.

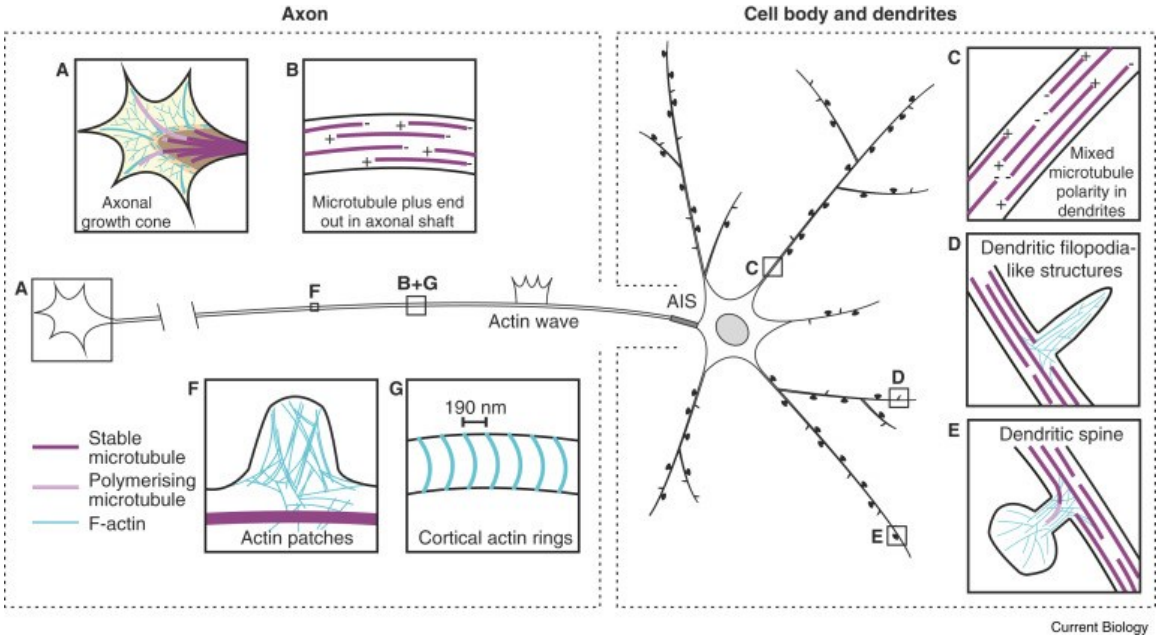

Figure 1.2. Microtubule and actin organization in neurons
In axons, MTs form stable, polarized bundles, which provide structural integrity and serve as tracks to guide MT-dependent motor proteins. Actin filaments form equidistance ring-shaped structures to resist mechanical forces and maintain axon shape. The growth cone contains an array of both stable and dynamic MTs, which prompt growth cone advancement and turning. Various +TIPs accumulate at the growing MT plus ends in the growth cone, where they regulate MT dynamics during axon outgrowth and guidance. MTs of mixed polarity and dense F-actin bundles are located within dendrites.

Image: Coles, C., & Bradke, F. (2015). Coordinating Neuronal Actin–Microtubule Dynamics. Current Biology, 25(15), R677-R691. doi: 10.1016/j.cub.2015.06.020. Reproduced with permission from Elsevier and Copyright Clearance Center for reuse in a thesis.

Intermediate filaments are termed as such due to their “intermediate” diameter (10 nm) as compared to actin filaments (6 nm) and microtubules (25 nm). Their role in the eukaryotic cell is primarily to provide structural support both intra and extracellularly (Cooper, 2000). Intermediate filaments are classified among 6-groups based on amino acid sequencing, one of which is the Type IV intermediate filaments, which includes neurofilament proteins (NF) (Yuan et al., 2017). NFs are unique in that they are expressed selectively in neurons, providing structural support for asymmetric neuronal geometry. NFs are primarily found in axons, where they are essential for the radial growth and structural stability of myelinated axons. (Eyer and Peterson 1994; Friede and Samorajski 1970; Ohara et al. 1993; Yum et al. 2009; Zhu et al. 1997). In mature axons, the NF network is largely stable, and turnover of NF protein subunits is slow compared to other cytoskeletal proteins (Nixon and Shea 1992). Due to the difficulties of investigating living neurons in microgravity and the stable nature of the NF cytoskeleton, NFs have thus far

not been a topic of interest among microgravity researchers, and literature on the topic remains sparse.

1.2.3. Microtubule Dynamics in Neurite Outgrowth

The basis of neuronal physiology is founded upon the concept of electrical and chemical synaptic communication over distance in large, interconnected networks of individual neurons. (Südhof, 2021). Neuronal polarization is a process that serves to establish the axons and dendrites that will eventually come together and form a mature synapse. The establishment of polarity is highly dependent on the organization of and feedback between the actin and microtubule cytoskeletons. The role of each cytoskeletal component varies dependent on the stage of neurite outgrowth and differentiation. In general, mammalian neuronal polarization can be divided into five stages: (1) Formation of lamellipodia and filopodia, (2) outgrowth of minor processes, (3) formation and growth of the axon, (4) growth of dendrites, and (5) and maturation of axonal and dendritic arbors (Dotti & Banker, 1988; Leondaritis & Eickholt, 2015; Schelski & Bradke, 2017). In the context of this thesis, SH-SY5Y cells are treated as neuron-like and the following chapters may be interpreted as if SH-SY5Y cells exhibit similar physiology, having noted that this process is not completed in full due to the lack of mature neuronal synapses expressing traditional synaptic protein markers in SH-SY5Y cells (Figure A.1.) (Discussed in section 1.2.2).

Microtubules play their most prominent role during stages 2 and 3 of neuronal differentiation. During stage 2, the emergence and extension of minor processes (neurites) begins. Neurites are immature projections from the cell body of a neuron packed with microtubule bundles serving as a backbone and an actin-rich growth cone, from which neurite elongation is regulated (Dent & Gertler, 2003; Schelski & Bradke, 2017). The transition from stage 2 to 3 is marked by the simultaneous presence and outgrowth of multiple undifferentiated neurites, until one neurite becomes dominant and will proceed to form the axon. The outgrowth of neurites begins with microtubule extension into filopodia. Elongated microtubules extend into the filopodia either by distributing stabilized microtubules into the actin rich protrusions or through polymerization, both of which contribute to the maturation of filopodia into neurites in neuronal cultures (Sainath & Gallo, 2014). Regulation of microtubule dynamics directly influences neurite outgrowth. For example, microtubule stabilizing proteins promote microtubule nucleation and

polymerization both *in vitro* and *in vivo.* (Dehmelt et al., 2003; Li et al., 2009; Teng et al., 2001; Vandecandelaere et al., 1996). Conversely, microtubule destabilizers can inhibit MT assembly, increasing the number of neurites but decreasing the likelihood of differentiation into the axon. (Riederer et al., 1997). Collectively, these results indicating that a balance of microtubule polymerization and depolymerization is required in neurite outgrowth, a phenomenon often referred to as dynamic instability. Following several hours of growth within the minor processes, neurite differentiation begins with the abrupt appearance of one minor process growing at an approximately 5-10 times greater rate than the other processes of the cell. The remaining neurites will then become the shorter dendrites (Dotti et al., 1988; Schelski & Bradke, 2017).

While neuronal polarization and neurite outgrowth are hallmarks of neuroscience research, the effect of microgravity on the dynamics of these processes has never been investigated. In section 1.2.4., I detail our current understanding of changes in microtubule dynamics resulting from microgravity exposure. Because microtubule dynamics are affected by microgravity, it is likely that neurite outgrowth, a microtubule-dependent process will also be affected. Thus, neurite outgrowth is an interesting and novel target for microgravity research which will be expanded upon in later sections of this thesis.

1.2.4. Cytoskeletal Dynamics in Microgravity

Despite the challenges in conducting microgravity research (Discussed in section 1.1.), the net effect of research in various cell lines paints a clear picture of cytoskeletal dysfunction resulting from exposure to both simulated and actual microgravity. Model systems such as cardiocytes, osteoblasts, and neuroblastoma cells have been used to consistently highlight various degrees of microtubule and actin cytoskeletal disruption across a variety of tests and assays (Vorselen et al., 2013).

In vitro proteomic and genomic analyses of neurons and SH-SY5Y cells, have found significant changes and deleterious reductions in the expression of various cytoskeleton and ECM-associated proteins when exposed to simulated and actual microgravity (Grosse et al., 2001; Ulbrich et al., 2011). These deleterious changes in cytoskeletal protein expression are subsequently used as justification to pursue investigations into *in vitro* cytoskeletal visualization experiments in simulated and actual microgravity. Simulated microgravity models have confirmed these suspicions, with a

variety of cell lines expressing disruptions to actin and microtubule cytoskeletal organizations. For example, irregular actin organization, increased G-actin expression, shortened microtubules, poorly defined microtubule-organizing centers and loss of cell shape have been observed in short-term simulated microgravity (Buravkova & Romanov, 2001**;** Chen et al., 2016; Lewis, 1996; Meyers et al., 2005; Rijken et al., 1992; Uva et al., 2002).

Experiments in short-term actual microgravity demonstrate similar effects to the actin and microtubule cytoskeletons, but there remain gaps in the literature due to limitations in performing experiments in actual microgravity versus simulated. Disruptions to the actin cytoskeleton include reduced amount of, and thinning of actin stress fibers, clustering and perinuclear relocalization of G-actin, and disrupted radial organization of the actin cytoskeleton (Carlsson et al., 2003; Grenon et al., 2013; Hughes-Fulford & Lewis, 1996; Rijken et al., 1992; Ulbrich et al., 2011). In an extreme case, the complete collapse of the actin cytoskeleton was reported within the first 4-days of microgravity exposure (Hughes-Fulford, 2003). Disruptions to the microtubule cytoskeleton in short-term actual microgravity include disrupted radial organization, shortened microtubule filaments, reduced tubulin subunit expression, loss of tubulin bundles, and perinuclear organization of tubulin (Gaboyard et al., 2002; Grosse et al., 2012; Lewis et al., 1998; Meloni et al., 2011; Vassy et al., 2001). In section 4.3., I outline how disruption to the actin and microtubule cytoskeletons are linked to neuronal phenotypes that mildly mimic early-stage characteristics of various neurodegenerative diseases, and how a link between neurological side effects experienced in actual microgravity may lie in system-wide cytoskeletal disorganization caused by prolonged microgravity exposure. To this end, further investigation of the long-term effects of microgravity on cytoskeletal organization in neurons are warranted.

1.3. Overview of Axonal Transport

Microtubule-based intracellular transport is required by all eukaryotic cells for proper spatiotemporal delivery of organelles, mRNA and soluble proteins. Intracellular transport is particularly critical for neurons due to their extreme morphological dimensions, polarity, and need for efficient communication between the cell body and distal processes (Bentley & Banker, 2016). Because axonal transport is a microtubule-dependent process, it is likely that microgravity-mediated disruptions to microtubule structure will affect axonal

trafficking dynamics. Axonal transport of any cargo has never been analyzed in microgravity conditions, and as such, they are an interesting target for such experiments. The results of these experiments will greatly expand upon our collective knowledge regarding microtubule dynamics and axonal physiology in microgravity conditions.

Cytosolic and cytoskeletal proteins, such as neurofilaments, tubulin, and tau are moved from the cell body by slow transport, ranging from 0.2 to 2.5 mm per day (Roy, 2014). By contrast, membranous organelles are moved to the axon terminals by fast axonal transport (FAT), which can exceed 400 mm per day (Hirokawa & Tanaka, 2015). Because the axon is largely devoid of biosynthetic machinery, it relies on FAT to supply axon terminals with neurotrophic factors, lipids, and mitochondria, and to prevent accumulation of toxic aggregates by clearing recycled or misfolded proteins (Maday et al., 2014; Millecamps and Julien, 2013). Retrograde transport from distal portions of the neuron is of equal importance to prevent accumulation of toxic aggregates by clearing recycled or misfolded proteins (Hinckelmann et al., 2013; Millecamps and Julien, 2013). The movement and distribution of each axonal component is determined by where and how frequently it engages with and disengages from the microtubule-based transport machinery. Because axonal microtubules are organized uniformly with their plus ends toward the terminal (Hirokawa et al., 2010), anterograde transport involves translocation toward microtubule plus ends, using kinesin motors, whereas retrograde transport requires translocation toward minus ends, using dynein motors (Figure 1.3.). The balance between anterograde and retrograde transport can be strongly biased in favor of one direction over the other; for example, movement of vesicles filled with neuropeptides is strongly biased toward sites of secretion at axon terminals (Barkus et al., 2008) whereas organelles that carry endocytic and signaling cargoes move mainly back toward the cell body (Hollenbeck, 1993; Lalli and Schiavo, 2002).

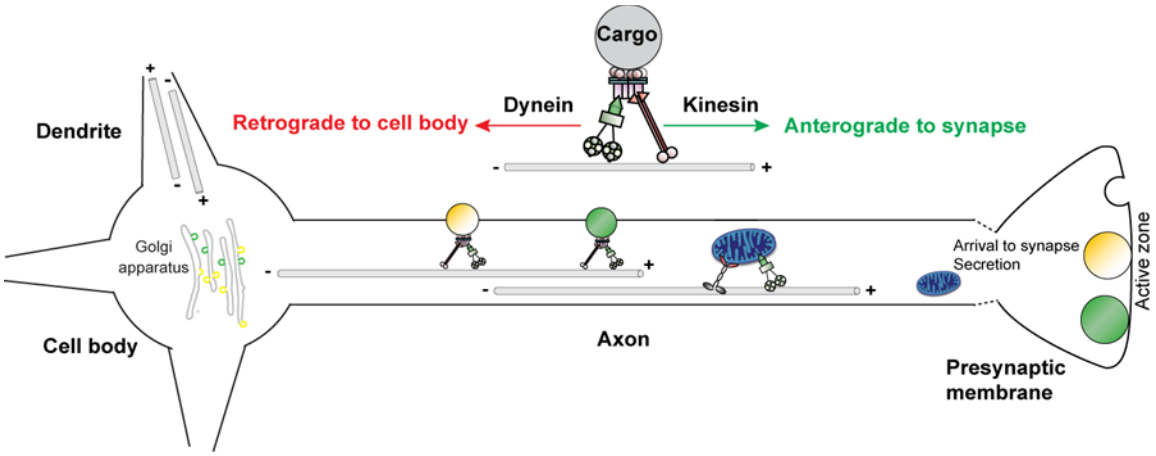

Figure 1.3. Schematic of bidirectional, intraneuronal transport
The bidirectional transport of cellular cargos via motor proteins is important for the development, maintenance, and viability of neurons. The kinesins drive anterograde transport of cargos such as SVPs and DCVs from the soma to the axon, while dynein drives retrograde transport of cargos such as mitochondria from the axon and the dendrites towards the soma.

The kinesin superfamily of motor proteins comprises 45 different members organized in 15 major families. Approximately half of the kinesin family is responsible for intracellular cargo transport while the remaining act in cell division (Hirokawa et al., 2009). In contrast, the dynein protein family is less diverse, but plays an equally important role in cargo transport. Although kinesin and dynein are different in size, they are both ATP dependent and have specialized domains to interact with the microtubules and cargo they are transporting (Goldstein & Yang, 2000). All kinesins have a motor domain, which can be located either at the N-terminal, the middle region, or the C-terminal. Kinesins with a motor domain in the middle region are involved in regulation of microtubule polymerization and cell division. Kinesins with an N-terminal motor are responsible for plus-end transport, while those with a C-terminal motor domain function primarily in negative-end transport (Hirokawa et al., 2009). In addition to a motor domain, they all have a distinct stalk and a tail region. Cargo selectivity in kinesin family members relies on different binding domains in the tail region (Hirokawa et al., 2010). In addition to cargo binding, the stalk and tail domains also play a role in dimerization of kinesins and thus regulate motor activation. (Goldstein & Yang, 2000).

In contrast to kinesin, the dynein family of proteins is less diverse but has a more complex structure. The dynein family is comprised of two types of motor complexes: cytoplasmic dynein and axonemal dynein. Of the two types of dynein, cytoplasmic dynein acts as a negative-end motor protein for vesicle transport and it moves by hydrolyzing

ATP (Hirokawa, 1998). Dyneins are multi-domain proteins made up of a heavy chain, intermediate chains, light intermediate chains, and light chains; interaction between the various domains and associated proteins allows for cargo binding and regulation (Goldstein & Yang, 2000). Specifically, cytoplasmic dynein interacts with the dynactin complex to regulate cargo binding and movement. (Hirokawa & Takemura, 2005). Furthermore, interaction between dynactin, dynein, and kinesins appear to regulate coordinated bidirectional transport (Chen et al., 2019).

1.3.1. Mitochondrial Transport

Neurons are among the most metabolically active cells in the human body, consuming 20% of resting energy. Mitochondria, being the sole source of energy production in the body are thus extremely important in fulfilling the continuous energy requirements to maintain neuronal physiology (Kann & Kovács, 2006). Synaptic communication and axonal signal transduction are among the most metabolically demanding functions in neurons, and due to the long-distance synapses may be situated away from the cell soma, proper transport of mitochondria towards these energetically active regions is required to maintain proper neuronal physiology (Figure 1.4.). Anterograde and retrograde transport dynamics of mitochondria are tightly regulated and may be biased to either direction based on signaling stimuli or disruptions to neuronal physiological function. (Chada and Hollenbeck, 2004; Morris and Hollenbeck, 1993). Furthermore, some mitochondria move persistently over long distances while others appear to be largely stationary. Among the moving subset of mitochondria, continuous runs are interspersed with periods of brief pause or reversal of direction before resuming their initial path (Miller and Sheetz, 2004; Morris and Hollenbeck, 1993; Morris and Hollenbeck, 1995; Ohno et al., 2011). The transport of mitochondria is mainly regulated by either kinesin-1 or kinesin-3 in the anterograde direction, and dynein in the retrograde direction (Figure 1.4.) (Kanai et al., 2000; Nangaku et al., 1994; Pilling et al., 2006; Tanaka et al., 1998; Wozniak et al., 2005).

The kinesin 3 family motor KIF1Bα and the kinesin-1 associated KIF5 motors are thought to be involved in mitochondrial transport. KIF1Bα colocalizes with mitochondria and can transport them *in vitro* (Nangaku et al., 1994). Furthermore, KIF1Bα binding protein (KBP) is localized to mitochondria (Wozniak et al., 2005). In the case of KIF5, there is evidence that disruption to the Kif5b gene in mice causes mitochondria to accumulate

in the center of cells (Tanaka et al., 1998). This accumulation in the cell body can be undone via exogenous expression of any of the KIF5 motors (Kanai et al., 2000), suggesting that the KIF5 motors are essential for mitochondrial transport (Hirokawa, Noda, Tanaka & Niwa, 2009). The mechanism by which KIF5 delivers mitochondria to presynaptic sites is controlled by local Ca2+ influx, which causes the accessory protein Miro on the mitochondrial outer membrane to change conformation and inhibit kinesin mediated transport (MacAskill et al., 2009; Wang & Schwarz, 2009). The acetylation state of Miro inversely affects the sensitivity of Miro to Ca2+ (Kalinski et al., 2019). Because both kinesin and dynein interact with Miro via TRAK proteins (van Spronsen et al., 2013), it is likely that this mechanism affects dynein-mediated transport as well (Guedes-Dias & Holzbaur, 2019).

Disruptions to normal mitochondrial trafficking such as disrupted axonal microtubule organization or knockout of Miro are sufficient in mimicking the early pathological dysfunctions observed in many neurodegenerative diseases, including AD, PD, ALS, and Huntington's Disease (HD) (Panchal & Tiwari, 2021). While dynamic trafficking of mitochondria has never been observed under microgravity conditions, there does exist evidence of mitochondrial dysfunction and mitochondrial-associated increases in oxidative stress resulting from microgravity conditions (Discussed in section 1.4.). Thus, the experiments outlined in this thesis may expound upon our current understanding of mitochondrial dysfunction in microgravity and help uncover the potential underlying mechanisms regulating these dysfunctions. Furthermore, they will represent the first analyses of the dynamic trafficking of organelles in microgravity conditions, and any result obtained following these experiments will significantly enhance our understanding of axonal transport in microgravity conditions.

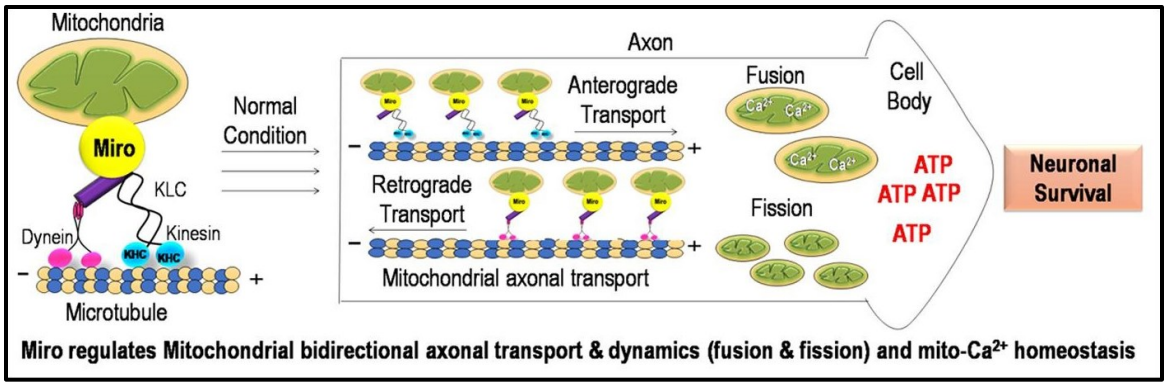

Figure 1.4. Overview of mitochondrial transport and axonal energetics
The bidirectional axonal transport of mitochondria plays a key role in maintaining axonal and synaptic energetics. Mitochondrial transport is mediated by kinesin and dynein association with microtubule tracks along the axon. The conformation of Miro, a mitochondrial outer membrane accessory protein mediates mitochondrial attachment to molecular motors.

Image: Panchal, K., & Tiwari, A. (2021). Miro (Mitochondrial Rho GTPase), a key player of mitochondrial axonal transport and mitochondrial dynamics in neurodegenerative diseases. Mitochondrion, 56, 118-135. doi: 10.1016/j.mito.2020.10.005. Reproduced with permission from publisher for reuse in a thesis.

1.4. Effects of microgravity on cellular stress

Mammalian cells must regularly adapt to environmental stressors including extreme temperature, nutrient deprivation, ionizing radiation, toxins, viral infection, and hypoxia (Alao & Sunnerhagen, 2008; Fulda et al., 2010; McCormick & Khapersky, 2017). DNA damage, global translational inhibition, and protein misfolding are some of the sub-cellular effects that must be overcome to reattain cellular homeostasis following stress (Aulas et al., 2018; Ciccia & Elledge, 2010; Richter et al.,2010). While there are specific molecular mechanisms responsible for undoing the effects of stress, there is also a general stress response in the form of stress-inducible membrane-less domains. These domains include cytoplasmic stress granules (SGs), processing bodies (P-bodies), nuclear stress bodies, and paraspeckles (Anderson & Kedersha, 2006; Marijan et al., 2019). These membrane-less domains are generally composed of proteins and RNA, and the specific molecular composition of the proteins and RNA in each membrane-less domain dictates its likely function (Anderson & Kedersha, 2006). For example, SGs uniquely contain translation initiation factors while P-bodies are associated with miRNA/siRNA silencing (Luo et al., 2018). Following a stressful stimulus, the generalized upregulation of multiple stress-pathways occurs in most cell types. This result is useful in cell biology experimentation, where the quantification and analysis of stress marker

expression patterns can be used to help identify mechanisms of stress and the relative effectiveness of therapeutic agents. For example, neurodegenerative diseases such as ALS, AD, and MS have been shown to generate permanent SGs resultant from chronic cellular stress, and mechanisms to disaggregate these pathological stress granules is of interest to neurobiologists (Asadi et al., 2021; Wolozin, 2012).

Interestingly, there is evidence that microgravity exposure acts as a stressful stimulus on cells. Space flight has been associated with increased production of free radicals (Maillet et al., 2001). Increases in free radicals are responsible for increased oxidative stress, thus contributing to cellular and molecular damage (Stein, 2002). Proteomic and genomic analyses in microgravity have found differential expression of proteins involved in oxidative stress-related pathways and they are among the most affected by microgravity exposure (Feger et al., 2016; Kumar et al., 2021; Kwon et al., 2006; Ulbrich et al., 2011). To show that physiological function is affected by differentially expressed stress-response genes, various cell lines have been used to demonstrate increased oxidative stress following simulated and actual microgravity (Beck et al., 2014; Tan et al., 2017; Zhang et al., 2020). The nervous system has been shown to be especially vulnerable to oxidative stress during microgravity exposure. *In vivo* simulated microgravity experiments have detected increased lipid peroxidation products and decreased expression of antioxidant proteins in the brain stem and frontal cortex of mice (Chowdhury & Soulsby, 2002; Soulsby et al., 2004. *In vitro* studies demonstrate increased nitric oxide (NO) production in PC-12 and SH-SY5Y cells, and oxidoreductase gene expression is significantly altered following simulated microgravity (Qu et al., 2006; Wang & Good, 2001; Wang et al., 2009). To counteract the effects of microgravity on cellular stress and damage caused by ROS, astronauts are often prescribed antioxidant cocktails. However, mammalian physiological systems do not utilize exogenous antioxidants to equal effect, and research in mechanisms of the effects of stress on independent cell systems is required to help develop antioxidant formulations that better protect astronaut health (Gómez et al., 2021). For example, flavonoid antioxidants have been shown to be effective in reducing simulated microgravity induced oxidative stress in SH-SY5Y cells, but because little is known about microgravity stress on neuronal systems in actual microgravity, we cannot assume these effects will persist (Qu et al., 2010). Thus, in this thesis I outline experiments that are designed to characterize and quantify the neuronal stress response

via stress marker expression and staining following exposure to actual microgravity conditions.

1.4.1. Influence of microgravity on mitochondrial morphology

Mitochondria play a critical role in the mechanisms of cell stress through their involvement in pathways that modulate energetics, cell signaling, and apoptosis (Lenaz, 1998). As a by-product of electron transfer during ATP production, mitochondria produce ROS using extra electrons from the electron transport chain (Oyewole & Birch-Machin, 2015). Under normal circumstances, mitochondria are capable of detoxifying ROS. However, if mitochondria are damaged or dysfunctional, their ability to detoxify ROS may become impeded leading to increased ROS levels (Oyewole & Birch-Machin, 2015). Because oxidative stress is observed in microgravity conditions (described in section 1.4.), disruptions to mitochondrial physiology are suspected of playing a role in the onset of oxidative stress during microgravity exposure. Disruptions to mitochondrial function have indeed been observed in simulated and actual microgravity, but the mechanism linking microgravity to these dysfunctions remains unknown (Nguyen et al., 2021; Rubinstein et al., 2021; Singh et al., 2021; Zhang et al., 2020). To this end, most authors have pursued quantitative analyses of mitochondrial dysfunction in microgravity, while visualization of mitochondrial morphology remains rare. One interesting method to quantify mitochondrial morphology which will be applicable in the context of methods applied in this thesis is mitochondrial network analysis (MiNA) (Valente et al., 2017). In living cells, mitochondria undergo dynamic fusion and fission, continuously remodeling a network of interconnected mitochondria (Chen et al., 2010). Dysregulation of mitochondrial dynamics can be visualized by observing changes in this network such as increased fragmentation or decreases in network branching and complexity (Valente et al., 2017). In this thesis, I utilize MiNa to visualize the mitochondrial network and quantify changes in network dynamics during microgravity exposure. These experiments are significant, as visualization and analysis of mitochondrial morphology has never been performed in cells exposed to microgravity conditions. The results of these analyses may then be used to assess and validate proposed mechanisms of mitochondrial dysfunction resulting from microgravity exposure.

1.5. Project Overview

The primary goal of my thesis is construct and validate a strategy that will determine the effects of long-term microgravity exposure on cytoskeletal dynamics, axonal trafficking, and cellular health in SH-SY5Y cells cultured in the MoSL. To accomplish this, I have collected and analyzed the ground control (GC) experiment data set in normal cell culture conditions. Furthermore, I have established protocols for post-flight analysis of SH-SY5Y cells that have been fixed following differentiation. The results of this thesis will validate the use of these proposed experiment protocols for use in our transformed SH-SY5Y cell line post microgravity exposure. This goal can be subdivided into 2 main aims:

1. Quantify the effects of microgravity on neuronal cytoskeletal dynamics and axonal transport

a) Determine the effects of microgravity on cytoskeletal dynamics via analysis of neurite outgrowth during differentiation. I hypothesize that microgravity-induced cytoskeletal disruption will impair neurite outgrowth, resulting in slower neurite outgrowth velocity and less time spent in stages of active growth.

b) Quantify the effects of microgravity on microtubule dynamics via analysis of EB3 velocity in neurites. I hypothesize that microgravity-induced microtubule disorganization will result in slower EB3 velocity in differentiating neurites.

c) Determine the effects of microgravity on cytoskeletal structure in fixed, fully differentiated SH-SY5Y cells. I hypothesize that microgravity will induce cytoskeletal disruption and induce F-actin and microtubule network depolymerization and disorganization.

d) Determine the effects of microgravity on axonal transport by quantifying the transport of fluorescently tagged mitochondria. I hypothesize that microgravity-induced disruptions to microtubule organization will impair mitochondrial transport, resulting in reduced number of trafficking events, velocity, and run length of trafficking events.

2. Evaluate neuronal and mitochondrial health in differentiated SH-SY5Y cells after long-term microgravity exposure.

a) Investigate the impact of microgravity on mitochondrial network dynamics. I hypothesize that microgravity-induced increases in cellular stress will impair mitochondrial physiology, resulting in fragmentation and disorganization of mitochondrial networks and mitochondrial morphology.

b) Investigate the impact of microgravity on stress marker expression and stress granule formation. I hypothesize that microgravity-induced increases in cell stress will cause increased nuclear relocalization and expression of the stress marker TIA1, and an increase in cytoplasmic SGs.

This work is significant as cytoskeletal and axonal trafficking dynamics have never been investigated in actual microgravity. Furthermore, visualization of mitochondrial networks and stress markers has never been conducted on fixed cells returning from actual microgravity. Data collected in this thesis will be used as a guideline for the analysis of data collected in the MoSL at a future date, resulting in the first report of changes to dynamics in sub-cellular neuronal systems resulting from long-term microgravity exposure.

Chapter 2. Materials and Methods

2.1. Plasmid and Stable Cell Line Generation

Work described in section 2.1. was conducted by Andrew Wieczorek of the Silverman Lab at Simon Fraser University, BC, Canada.

SH-SY5Y cells (ATCC.org, Manassas, VA, USA) were dually transformed for the stable expression of GFP-MTS and RFP-EB3. The first step in this process was to amplify lentiviral plasmid DNA from *E. coli* stocks and confirm plasmid DNA structure. The following lentiviral plasmids were received in *E. coli* glycerol stocks from Profacgen (New York, NY, USA): pLVX-EGFP-MTS-PGK-Puro and pLVX-TagRFP-EB3-EF1a-SV40-Hygro (Figure 2.1.). *E. coli* (XL1-Blue) were streaked on 50 µg/mL ampicillin-agar plates and grown overnight at 37°C. Following *E. coli* growth, plasmids were obtained using Qiagen miniprep spin kit (Qiagen, Hilden, Germany), as per manufacturer's instructions. Confirmation of plasmid structure was performed via multiple restriction enzyme (RE) digestions (Table 2.1.). To conduct RE reactions, 1 µL of RE and 1 µg of DNA were added to a solution containing water, bovine serum albumin (BSA), and NEB buffer 3.1. (New England BioLabs, Ipswich, MA, USA). Each plasmid was cut with 3 different RE's and 1 no enzyme control. Each reaction was run simultaneously at 37°C for 1-hour, as per manufacturers instructions. Following RE digestion, cut DNA was loaded into a 0.7% agarose gel in Tris-acetate-EDTA (TAE) running buffer. The agarose gel was then imaged, and DNA bands were compared to the expected band lengths per RE digest (Table 2.1.; Figure 2.2.). Upon confirmation of plasmid structure*, E. coli* containing the plasmids of interest were seeded in 250 mL Erlenmyer flasks with 50 mL of Miller LB (Sigma Aldrich, St. Louis, MO, USA) and 200 µg/mL ampicillin (BioShop Canada Inc., Burlington, ON). Following growth overnight at 37°C plasmids were purified using the Qiagen plasmid PLUS midi kit (Qiagen, Hilden, Germany) as per manufacturers instructions.

Following plasmid purification, Lenti-X™ human embryonic kidney 293T cells (HEK293T) (via Takara Bio Inc, San Jose, CA, USA) were transfected with the purified lentiviral DNA to produce lentivirus. The Lenti-X 293T cell line is known for high transfectability and high-titer of lentivirus. This step is necessary to produce lentivirus containing our plasmids of interest, which will subsequently be used to infect SH-SY5Y cells and will result in the stable expression of GFP-MTS and RFP-EB3. This approach

was chosen because retroviral vectors such as lentivirus are known to cause a stable integration of transgene into the host genome (Merten et al., 2016). Transfection of HEK293 cells was performed according to "Lenti-X^{TM} Packaging Single Shots Protocol-At-A-Glance" (TaKaRa Bio Inc, San Jose, CA, USA). HEK293T cells were seeded at 50% confluency in 10 cm^2 cell culture dishes with media composed of: 90% DMEM with high glucose (4.5 g/L), 4 mM L-glutamine and sodium bicarbonate, 10% FBS, 100 units/mL penicillin G sodium and 100 µg/mL streptomycin sulfate with 1 mM sodium pyruvate. Once cell culture dishes reached 80% confluency of HEK293 cells, cells were transfected with lentiviral plasmid DNA. First, 7 µg lentiviral DNA was added to 600 µL sterile 18 MegOHM H_2O. This mixture was then added to the manufacturer supplied Xfect™ Transfection Reagent (TaKaRa Bio Inc, San Jose, CA, USA). The final transfection mixture was vortexed, incubated for 10-minutes at room temperature for complexes to form, and lastly centrifuged for 2 seconds before the full 600 uL plasmid/packaging compound was added dropwise to the plated HEK293T cells. These cells were then incubated overnight at 37°C, 5% CO_2 conditions. 48 and 72-hours post transfection, culture media (containing lentivirus) was collected in 50 mL conical tubes and subsequently centrifuged at 1200 rpm for 5-minutes to pellet cell debris. The lentivirus-containing supernatant was transferred to sterile 50 mL conical tubes and stored at 4°C for immediate use.

Following lentivirus collection, SH-SY5Y cells were infected with lentivirus derived from either MTS-GFP or RFP-EB3 containing plasmids. SH-SY5Y cells were grown in a 1:1 mixture of DMEM:F12 with 10% FBS on collagen-treated glass coverslips in 12-well tissue culture plates. Once cells reached 50% confluence, either 1 µg/mL puromycin (for MTS-GFP infection) or 100 µg/mL hygromycin (for RFP-EB3 infection) were added to cell culture media along with 500 µL of a 250-fold dilution of lentivirus-containing supernatant harvested either 48 or 72-hours post transfection of HEK293T cells (Figure 2.3.). Viral solution was prepared from a 5-step serial dilution process in 1:1 DMEM:F12 + 10% FBS with the addition of 4 µg/mL polybrene. Cells were then returned to a standard cell culture incubator at 37°C, 5% CO_2 conditions for 24-hours overnight. On the subsequent day, the infected SH-SY5Y cells (Either with RFP-EB3 or GFP-MTS-derived lentivirus) were split and grown in T25 cell culture flasks with selective antibiotic (hygromycin or puromycin for RFP-EB3 or GFP-MTS, respectively). Cells were allowed to grow until multiple flasks containing SH-SY5Y colonies expressing 1 of the 2 transgene constructs were collected. Once cells in T25 flasks were approximately 90% confluent, one flask from each

population of transformed cells was harvested and 100 µL of cell-containing media was added to individual wells in a 96-well tissue culture plate. Over the following days, 96-well plates containing a pooled population of singly transformed SH-SY5Y cells were screened for (1) survival using a phase microscope, and (2) for GFP or RFP fluorescence using a wide-field fluorescent microscope (Leica, DMI, 6000B; Leica, Wetzlar, Germany) equipped with a CCD camera (Hamamatsu ORCA-ER-1394; Shizuoka, Japan) at 200X magnification. Select wells were then expanded into T25 flasks and 6-well plates, and the aforementioned procedure for lentiviral infection was repeated using lentivirus constructed from plasmid that each cells had not previously been infected with. Cells were once again grown in T25 tissue culture flasks, transferred to 96 well plates, and screened for viability and fluorescence of pooled colonies. Candidate colonies dually expressing GFP-MTS and RFP-EB3 were selected for and expanded in T25 cell culture flasks. Two populations of reclones (F11 and G12) were viable and demonstrated stable expression of both GFP-MTS and RFP-EB3 following expansion. These reclones were further expanded and subsequently sorted via Fluorescence-activated cell sorting (FACS), selectively sorting for cells that dually fluoresced using a fluorescein isothiocyanate (FITC) filter for GFP-MTS, and Texas Red filter for RFP-EB3 (Figure 2.4.). This final population of sorted SH-SY5Y cells dually expressing GFP-MTS and RFP-EB3 were expanded in T75 flasks, and multiple aliquots of cells in 1 mL cryotubes were stored in a liquid nitrogen freezer for future use.

Confirmation of fluorescent marker expression, stability, and parental cell line phenotype is evaluated in section 3.1.

Figure 2.1. Lentiviral plasmids for transfection of HEK293T cells
The two plasmids, pLVX-EGFP-MTS-PGK-Puro and pLVX-TagRFP-EB3-EF1a-SV40-Hygro were obtained from Profacgen (New York, NY, USA) and were used in the transfection of HEK293T cells to induce production of lentivirus.

Table 2.1. Confirmation of plasmid structure via multiple restriction enzyme digestions

Restriction enzyme	Expected # of fragments	Expected fragment size (bp)
AseI	4	6584 1232 1075 59
BamHI	1	8950
EcoRV	6	5365 2985 219 219 79 79
No enzyme	N/A	N/A

pLVX-EGFP-MTS-PGK-Puro

Restriction enzyme	Expected # of fragments	Expected fragment size (bp)
BamHI	2	9848 741
NotI	1	10589
PstI	2	6285 4304
No enzyme	N/A	N/A

pLVX-TagRFP-EB3-EF1a-SV40-Hygro

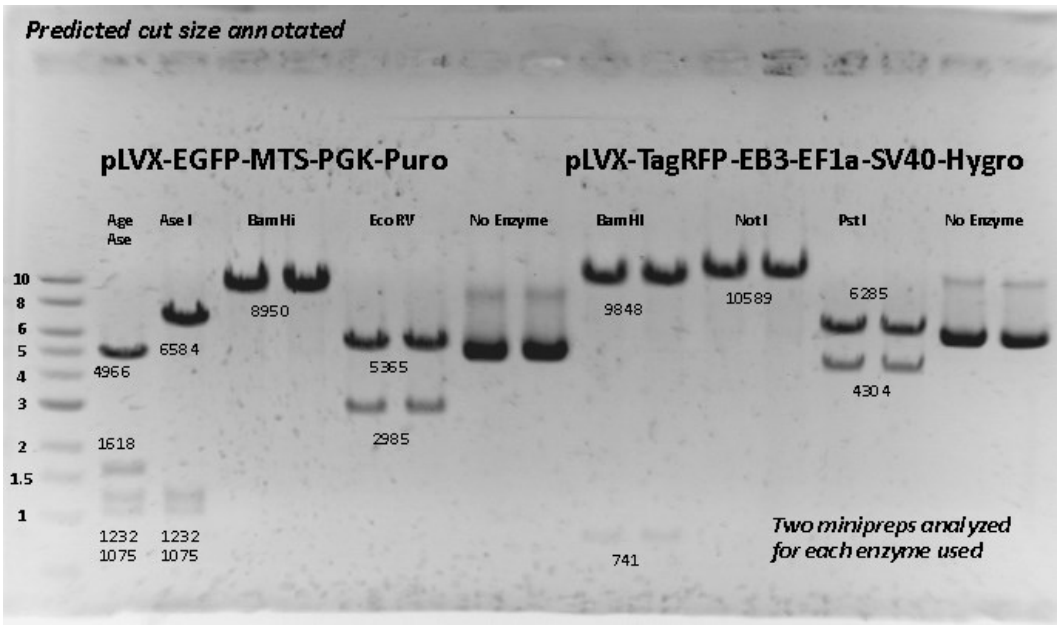

Figure 2.2. Confirmation of plasmid structures via gel electrophoresis of RE products

Results of electrophoresis in a 0.7% agarose gel of restriction enzyme products from table 2.1. are represented here. Each RE digestion was repeated once. All band lengths correspond to expected fragment size (in bp) listed in table 2.1., thus positively affirming the structure of the two plasmids.

Figure 2.3. Strategy for lentiviral infection of SH-SY5Y cells

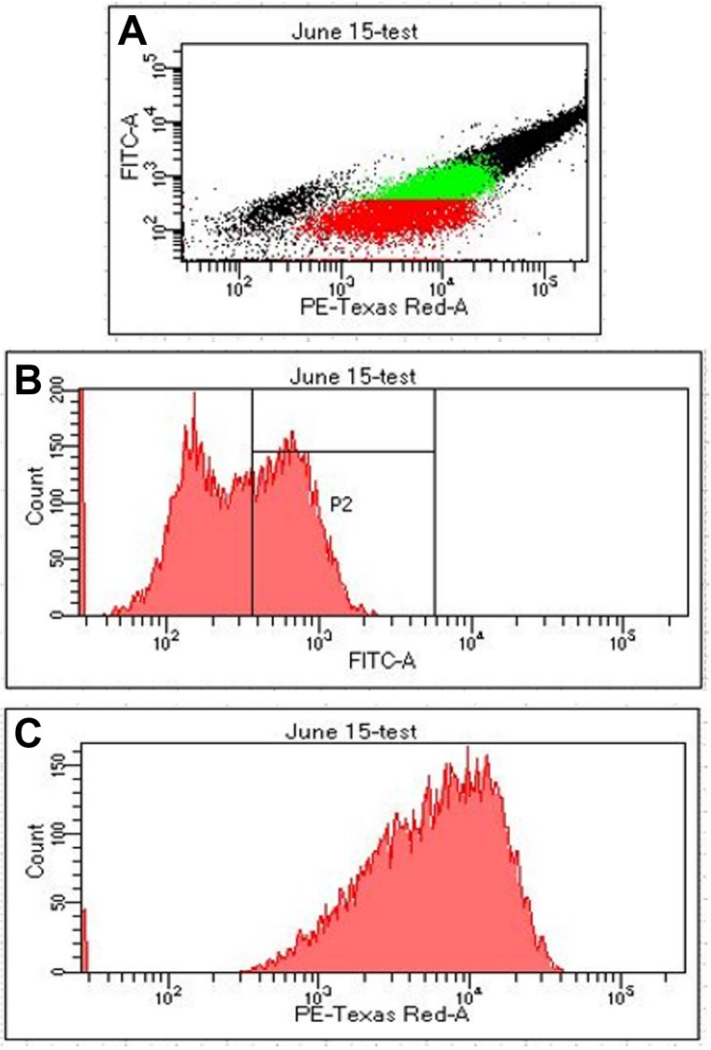

Figure 2.4. FACS parameters for selection of dually transformed SH-SY5Y cells
SH-SY5Y cells dually transformed to express RFP-EB3 and GFP-MTS were sorted using the fluorescence activated cell sorting capabilities of a flow cytometer. A) Scatterplot of relative GFP-MTS and RFP-EB3 intensities in cells expressing fluorescence in both culture channels. Black and red dots indicate discarded cells. Green dots indicate collected cells, comprising the parental line of cells utilized in experiments outlined in this thesis. Axes represent relative fluorescent intensities on a logarithmic scale. B) Histogram representing the distribution of SH-SY5Y cells by GFP fluorescence intensity. C) Histogram representing the distribution of SH-SY5Y cells by RFP fluorescence intensity.

2.2. Cell Culture and Differentiation

SH-SY5Y cells were grown and maintained in a 1:1 mixture of Minimum Essential Media (MEM) and Ham's F-12 Nutrient Mixture (F12), supplemented with 10% fetal bovine serum (FBS), 100 µg/mL hygromycin and 1 µg/mL puromycin at 37°C/5% CO_2 conditions. Prior to neuronal differentiation, cells were transferred onto glass coverslips in standard 12-well tissue culture plates at a density of 50 cells/mm^2. Following 5-days of unperturbed

growth on glass coverslips, media was exchanged to a mixture containing 1:1 MEM+F12 supplemented with 1% FBS, 100 µg/mL hygromycin, 1 µg/mL puromycin, and 10 µM retinoic acid (RA). The inclusion of RA induces morphological differentiation of SH-SY5Y cells (Encinas et al., 2002). Following 5-days of RA-mediated growth, media was exchanged for a mixture containing 1:1 MEM+F12 supplemented with 1% FBS, 100 µg/mL hygromycin, 1 µg/mL puromycin, and 50 ng/mL brain derived neurotrophic factor (BDNF). The inclusion of BDNF incudes biochemical differentiation in SH-SY5Y cells (Encinas et al., 2002). Cells remained in BDNF for 10-additional days, at which point they were deemed mature (Figure 2.5.).

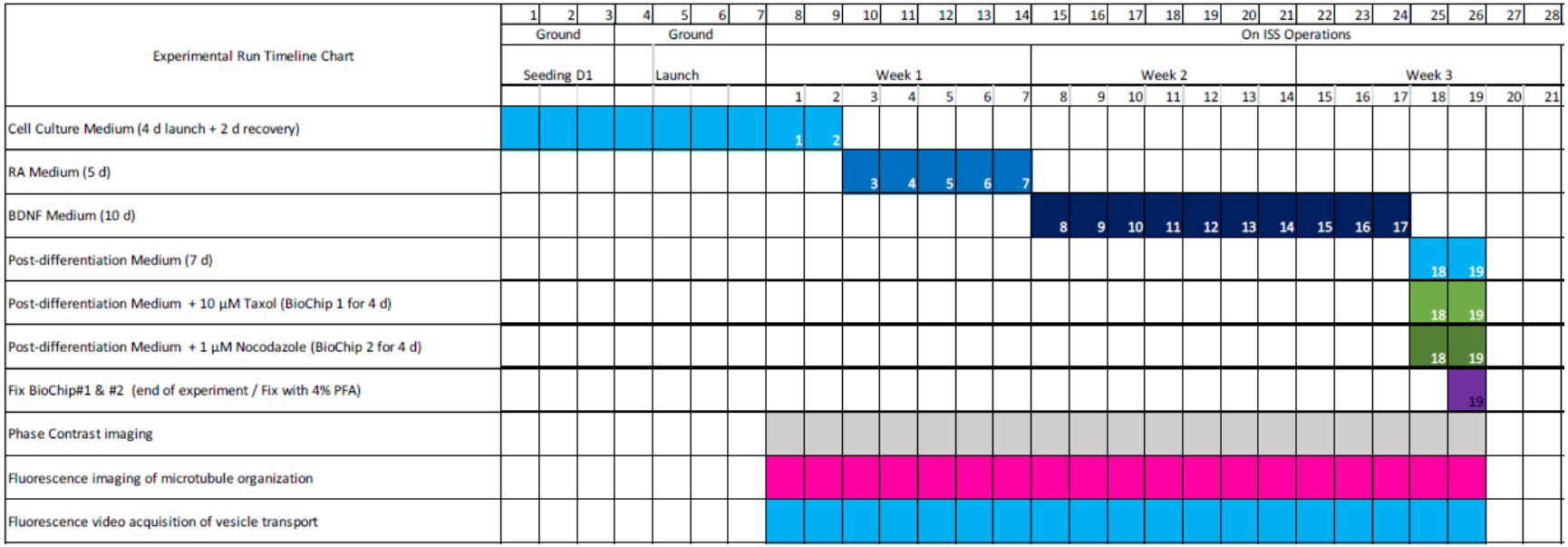

Figure 2.5. MoSL experiment run timeline chart

Proposed experiment timeline chart for cells cultured in the MoSL. GC experiment timelines described in section 2.2. are adapted to closely mirror this timeline and differentiation protocol.

2.3. Pre-Fixation Treatment

2.3.1. Pharmacological Treatment

Cells exposed to pharmacological treatment prior to fixation and antibody staining were done so under the following conditions:

Nocodazole: A 16 μM stock solution of Nocodazole (Sigma Aldrich, St. Louis, Missouri, USA) was diluted in fresh cell growth media (1:1 MEM/F12) to a final concentration of 1 μM. Glass coverslips with differentiated SH-SY5Y cells had their media replaced with 1 mL of 1 μM nocodazole media. Cells were then returned to 37°C/5% CO_2 conditions and incubated for 1-hour. Following incubation, cells were immediately subjected to fixation and immunostaining as per instructions in section 2.4.

FCCP: A 1mM stock solution of FCCP (a gift from Dr. Gordon Rintoul, Simon Fraser University) was diluted in fresh cell growth media (1:1 MEM/F12) to a final concentration of 1 μM. Glass coverslips with differentiated SH-SY5Y cells had their media replaced with 1 mL of 1 μM FCCP media. Cells were then returned to 37°C/5% CO_2 conditions and incubated for 30-minutes. Following incubation, cells were immediately subjected to fixation and immunostaining as per instructions in section 2.4.

2.3.2. Heat Shock

Glass coverslips with differentiated SH-SY5Y cells were transferred to a fresh 12-well cell culture plate with 2 mL cell growth media (1:1 MEM/F12) before being placed in a cell culture incubator heated to 43°C for 2-hours. Following heat-shock incubation, cells were immediately subjected to fixation and immunostaining as per instructions in section 2.4.

2.4. Fixation and Immunocytochemistry

Post-pharmacological treatment or heat-shock incubation, coverslips were prepared for immunocytochemical antibody staining. Glass coverslips with adhered SH-

SY5Y cells were removed and washed with 1x Dulbecco's phosphate-buffered saline (DPBS). DPBS was removed and cells were fixed with 4% paraformaldehyde (PFA) solution for 20-minutes at 37°C. PFA was removed, and cells were washed twice in one-minute intervals with DPBS, and once with tris-buffered saline (TBS). Processing of coverslips for utilization in experiments outlined in section 2.7.2. was complete by this stage. Remaining coverslips were then permeabilized using a 0.1% solution of Triton-X-100 diluted in DPBS, and subsequently blocked with 0.5% fish skin-gelatin. Following permeabilization and blocking, cells were subjected to either antibody staining, or phalloidin staining.

Antibody staining: All antibodies were diluted using 0.5% fish-skin gelatin solution (Kwinter et al., 2009). To observe microtubules, cells were stained with mouse anti-DM1A α-Tubulin antibody (1:500, Sigma Aldrich, St. Louis, Missouri, USA). To observe the stress marker TIA1, cells were stained with mouse anti-TIA1 monoclonal antibody (1:50, Santa Cruz Biotechnology, Dallas, Texas, USA). All cells were incubated with the primary antibodies at 4°C overnight. After the incubation period, excess of primary antibody was rinsed using PBS, and cells were incubated with secondary antibody, goat anti-mouse-Cy5 (1:1000, Thermo Fisher Scientific, Waltham, MA, USA).

Phalloidin staining: Phalloidin is a highly selective bicyclic peptide that binds to all variants of actin filaments and is conjugated to a fluorescent dye. Following permeabilization, coverslips were treated with a solution of phalloidin conjugated to Alexa Fluor-647 dye (Invitrogen, Waltham, MA, USA) and incubated in the dark at room temperature for 90-minutes.

Following antibody or phalloidin staining, cell nuclei were stained using a 1 μM DAPI solution (Sigma Aldrich, St. Louis, Missouri, USA) diluted in ultrapure water for 5-minutes in the dark. Coverslips were then washed 3 times in 5-minute intervals and mounted on glass microscope slides using elvanol.

2.5. Fluorescence Microscopy and Live Imaging

Imaging of microscope slides prepared with fixed and stained SH-SY5Y cell were imaged using a wide-field fluorescent microscope (Leica, DMI, 6000B; Leica, Wetzlar,

Germany) equipped with a CCD camera (Hamamatsu ORCA-ER-1394; Shizuoka, Japan). Images were captured at 630X magnification with a 63X/1.2NA lens.

To analyze bidirectional mitochondrial transport and EB3 comet velocity, living SH-SY5Y cells were recorded using the same wide-field fluorescent microscope equipped with CCD camera. Images were captured at 400X magnification with a 40X/0.9NA lens. At 24-hour intervals, new coverslips were mounted in a heated chamber containing a clear imaging media (1:1 ratio of translucent, phenol-free MEM/F12). After identification of three microscope stage positions containing unobstructed views of individual cells and their processes, an automated program in MetaMorph (Molecular Devices, Sunnyvale, CA) captured 1) a phase-contrast image every 15-minutes at each stage position, 2) a 1-minute, 1 frame per second video of RFP-EB3 transport every 45-minutes, and 3) a 2-minute, 1 frame per second video of mitochondrial transport every 45-minutes. The total experiment run time was 12-hours (A total of 16, 45-minute intervals between fluorescent video capture).

2.6. Kymograph Analysis

Videos obtained depicting axonal transport of fluorescent RFP-EB3 and GFP-MTS were used to generate kymographs, time versus position graphs, using MetaMorph (Kwinter et al., 2009). Movement parameters, such as velocity and run length were then quantified by tracking particle movement in the kymographs. Anterograde and retrograde movements were quantified by tracing positive and negative slopes, respectively; stationary particles were represented by straight flat lines. Only runs over 0.2 μm long were traced to avoid tracing movement that could be due to diffusion rather than motor protein movement. After the kymographs were traced, they were analyzed using a custom software described in Kwinter et al.,2009. All data obtained were calculated with the calibration that at a 400X magnification, 1 pixel = 0.2538 μm; the generated values were collected and further analyzed in GraphPad Prism 9 Software (San Diego, CA, USA).

2.7. Image Analysis

2.7.1. Neurite Outgrowth

To conduct analysis of neurite outgrowth dynamics, all phase-contrast images acquired during the automated 12-hour recording sessions (Described in section 2.5.) were compiled into stacked .tiff filetypes and analyzed using the TrackPoints function in MetaMorph software. TrackPoints allows for the manual tracking of the tip (growth cone) of dynamic neurite outgrowth. Data was exported to an excel spreadsheet, where the quantification of net outgrowth velocity was calculated (Withers & Wallace, 2020).

A secondary, non-dynamic analysis for reporting the mean length of neurites from still images was conducted using the "NeuronJ" plugin for the ImageJ software package. In this analysis, phase-contrast images with unobstructed neurites were manually traced, measured, and logged within software (Torres-Espín et al., 2014). Aggregate data of neurite lengths and number of neurites at each day in differentiation media was exported into an Excel spreadsheet and GraphPad Prism 9 for statistical analysis.

2.7.2. Mitochondrial Analysis (MiNA)

Analysis of mitochondrial network morphology was performed using a procedure described in Valente et al., 2017. The Mitochondrial Network Analysis (MiNA) toolset is a pair of macros making use of existing ImageJ plug-ins, allowing for semi-automated analysis of mitochondrial networks in cultured mammalian cells. The basic protocol utilized in this analysis is as follows: fluorescent images of GFP-MTS are opened in ImageJ and individual cells are manually cropped. A custom macro is activated which automatically performs a sequence of built-in commands to pre-process the image and increase mitochondrial network visibility (Unsharp Mask → Enhance Local Contrast → Median Filter). Following pre-processing, a second custom macro is activated to produce a simplified morphological model of the mitochondrial network (Convert image to binary → Skeletonize → Analyze Skeleton). A detailed explanation of each processing step is found in the original protocol published by Valente et al., 2017. Several descriptive parameters are compiled by the program, such as number of mitochondrial networks, number of branches, branch lengths, and number of punctate mitochondria. This data was then exported to GraphPad Prism 9 software for statistical analysis.

2.7.3. Corrected Total Cell Fluorescence

Corrected total cell fluorescence (CTCF) is a simple quantification protocol for ImageJ Software. CTCF generates a relative fluorescent intensity score for isolated cells in an image and corrects for background fluorescence. This analysis was performed to quantify actin cytoskeletal disassembly (Results section 3.2.3.) and nuclear stress granule intensity (Results section 3.4.1.).

To conduct this analysis, the outline of a single cell was traced by hand and the measure function in ImageJ was selected. Relevant outputs were manually selected from the measure function. These outputs were: area, integrated density (IntDen), and min & max gray value. These outputs were exported to Excel software. An additional region of approximately equal size to 1 cell without cells was also traced and measured to serve as control for background fluorescence. The following formula was then applied to each individual cell for calculation of a CTCF score:

$$CTCF = IntDen - (Area\ of\ selected\ cell \times\ Mean\ background\ fluorescence)$$

These values were then exported to GraphPad Prism 9 for statistical analysis.

2.7.4. Stress Marker Analysis

Quantification of TIA1 stress granules was conducted using ImageJ software in a protocol initially described in Apicco et al., 2017. TIA1 stained cells were thresholded (TIA1 fluorescence intensity above 69.6) with nuclear masking using DAPI. The number of cytoplasmic (defined by exclusion from $DAPI^+$ nuclei) puncta with diameter greater than or equal to 2 μm positive for TIA1 were counted and divided by the total number of $DAPI^+$ nuclei per image. For quantification of nuclear TIA1 nuclear fluorescence, images were processed via CTCF analysis, as described in section 2.7.3.

2.8. Statistical Analysis

Data obtained from all experiments was exported to a Microsoft Excel spreadsheet and imported to GraphPad Prism 9 (GraphPad Software, San Diego, CA, USA) for further analysis. For neurite length and EB3 comet velocity experiments, data is presented as mean ± SD. All data from these experiments were collected from at least 100 independent

EB3-comets (EB3 comet velocity) or 50 individual neurites (neurite length and outgrowth). Following data collection in actual microgravity, statistical analyses will be performed on these experiments using two-way ANOVAs with Tukey's post hoc test, comparing the mean EB3 velocity or neurite length at 24-hour intervals between 3 categorical variables (ground control, ground-BioChip-control and Microgravity). For fluorescent intensity distribution experiments, data is presented as mean ± SEM. All fluorescent intensity distribution experiments were performed on at least 10-cells, imaged from different fields of view on at least 3-independent coverslips. Statistical analyses of these experiments were performed using an unpaired Student's *t*-test.

2.9. Spaceflight and Mobile SpaceLab Hardware

BioChip and Mobile SpaceLab hardware are property of HNu Photonics LLC, (Maui, Hawaii, USA), who have permitted disclosure of the following information within this thesis.

MoSL is a microfluidics and imaging platform designed to withstand the environmental pressures of microgravity exposure on cell culture. MoSL has an environmental control system housed in the docking station with connectors for power, data downlink and command. (Figure 2.6.). MoSL is a closed system consisting of three main components (ordered from most exterior to most interior): the Outer Chassis, Inner Chamber, and Science Platform.

The Outer Chassis has four main functions: 1) Acts as a protective shell to isolate the Inner Hermetic Chassis. 2) Provides box section structural rigidity. 3) Provides thermal isolation of components. The Outer Chassis contains a mountain platform for warm power bricks, printed circuit boards (PCB), and a fan. A cold box for storing liquid media and reagents is also located in the Outer Chassis, regulated by four thermoelectric coolers (TECs) which transport heat away from the cold box to maintain ideal temperature. 4) Acts as a thermal barrier, providing safe front touch temperature.

The Inner Chassis is completely hermetic except at the gas permeable polytetrafluoroethylene (PTFE) port, which is part of the microfluidic system. The flow path of the microfluidic system consists of a closed fluidic path of tubing, biospecimen chambers (BioChips), pumps, valves, and bags (media, fixative) in a cool zone,

maintaining fixative solution at 4°C before injection to culture wells. Furthermore, the fluidic system is impermeable to gas except at the PTFE port, and resistant to high pressure leaks (Figure 2.7.).

The Science Platform, located entirely within the inner chamber of MoSL is the main containment site for biological specimens and data collection (Figure 2.8.). Two removable bioreactors (BioChips) are stored within the Science Platform. Each BioChip contains four cell culture wells (Figure 2.9.). The living SH-SY5Y cell culture will be housed in each of the eight BioChip wells, which are constructed using transparent polycarbonate glass. SH-SY5Y cells are known to adhere to polycarbonate glass without surface treatments such as collagen.

Once BioChips are loaded into the Science Platform, the BioChips will maintain the cell culture at 37°C and 5% CO_2 for the duration of the mission until the samples have been fixed for post-flight immunofluorescence analysis. MoSL performs automated microfluidic replacements of the medium and/or reagents within the wells via a series of pumps, valves and flow sensors within the microfluidic manifold. Another component of the Science Platform includes a dual digital camera system equipped for phase-contrast (Dual Back LED illuminators) and fluorescent (Dual illuminators: 1x 60 mW Laser at 488 nm and 1x 100 mW Laser at 532 nm) imaging techniques, which will collect images at periodic intervals as described in section 2.2. Imaging capabilities are accompanied with adjustable Y and Z-axis stage positioning, controllable from a command center on Earth to ensure adequate plane of focus during experimentation.

Based on current projections, the MoSL will depart Kennedy Space Center (Merritt Island, Florida, USA) aboard SpaceX flight CRS-27 in January 2023. After berth of the ascent vehicle, MoSL is moved to ISS Expedite the Processing of Experiments to Space Station (EXPRESS) Rack and the experiment initiated by remote command. All data will be captured automatically and stored on the MoSL hard drive as well as sent down to the SCORPIO-V command center via the ISS's Ku-IP link in near real-time for immediate analysis of the fluorescent videos as well as monitoring of system status (microfluidic delivery rates, delivery times, temperatures, focus, etc.). MoSL is a fully enclosed facility that requires little to no crew operations once on-orbit. The MoSL facility can perform the required operations autonomously to maintain a living cell culture, deliver reagent treatments and image the culture for the duration of a 4-week mission on-orbit.

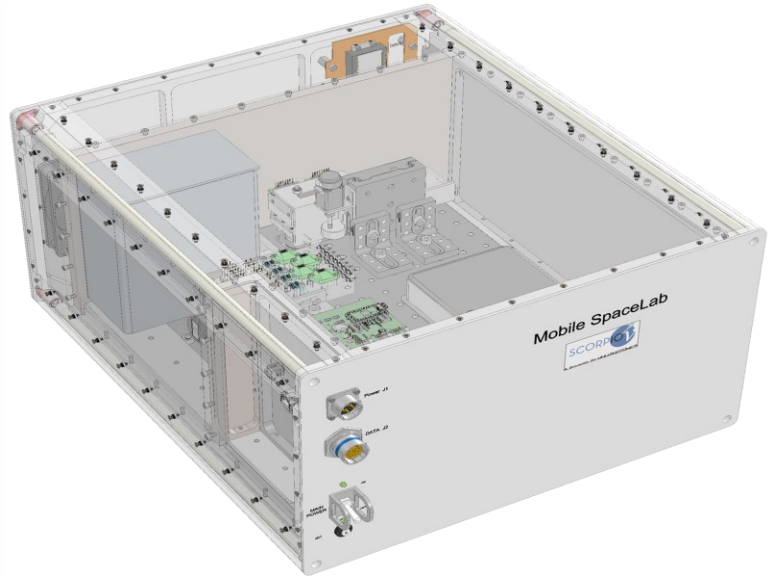

Figure 2.6. HNu Photonics Mobile SpaceLab (MoSL)
AutoCAD rendering of MoSL with view of Inner Chamber, Outer Chassis, and connectors for power, data downlink and command.

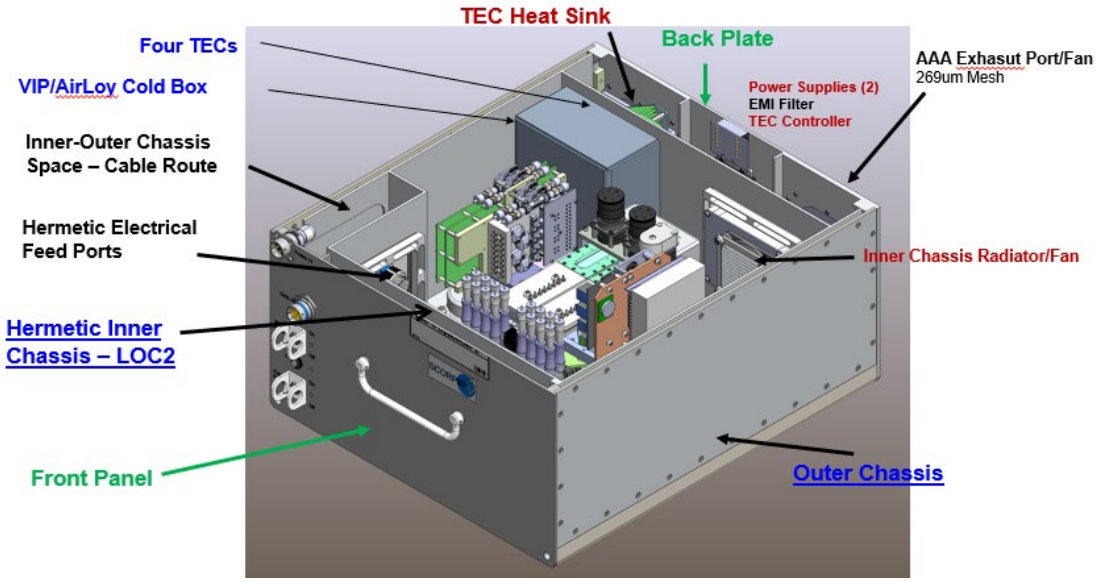

Figure 2.7. MoSL Inner Chamber and Outer Chassis Components
MoSL has an environmental control system housed in the docking station with connectors for power, data downlink and command. The flow path consists of a closed fluidic path of tubing, biospecimen chamber (BioChips), pumps, valves, and bags (media, fixative) in a cool zone, maintaining fixative solution at 4°C before injection to culture wells.

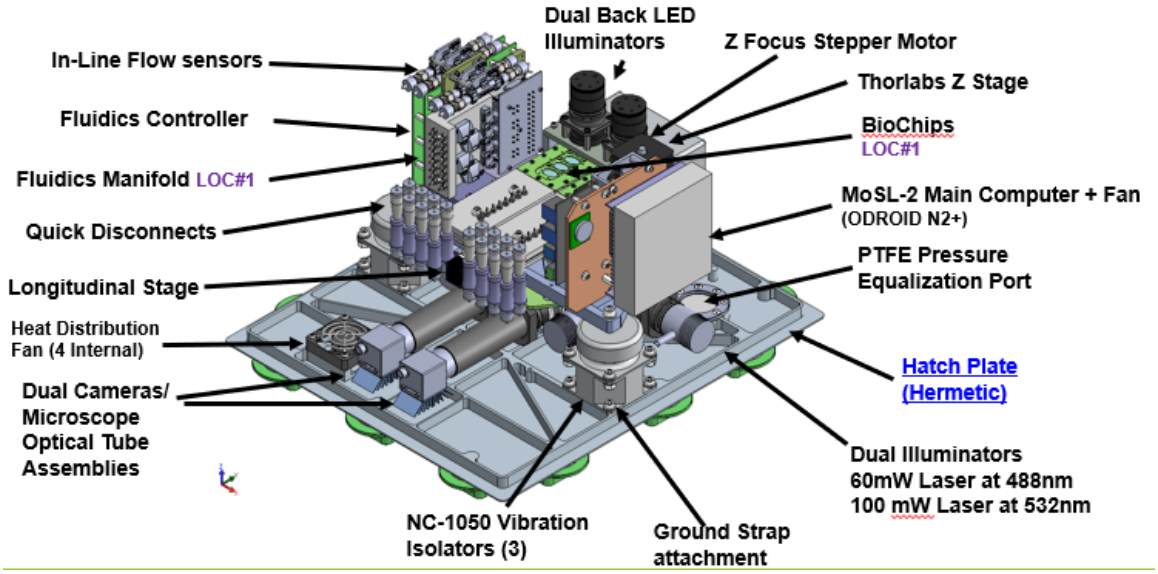

Figure 2.8. MoSL Science Platform

The Science Platform houses two BioChips, each containing four cell culture wells. Living cells in BioChips are maintained at 37°C and 5% CO2 conditions for the duration of the mission, controlled via a series of sensors, controllers, and fans. The automated microfluidic system replaces cell culture media daily and can administer drugs into media as required. The Science Platform also houses a dual digital camera system for automatic phase contrast and fluorescence imaging, with two adjustable axes.

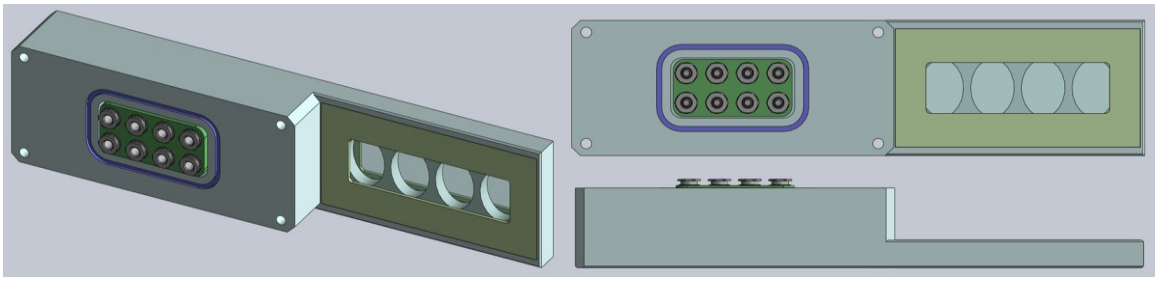

Figure 2.9. HNu Photonics BioChips for Mobile SpaceLab

The Biochips each contain 4 polycarbonate glass wells for cell culture. Samples are loaded into BioChips prior to spaceflight before being inserted into MoSL. After insertion, MoSL is responsible for maintaining cell culture conditions prior to and during launch.

Chapter 3. Results

The goals of my thesis were to assess the effect of microgravity on cytoskeletal dynamics, axonal transport, and cellular stress. My hypotheses followed the notion that microgravity will disrupt cytoskeletal organization and have deleterious effects on neurite outgrowth, axonal transport of mitochondria, mitochondrial physiology, and cytoskeletal ultrastructure. To pursue these hypotheses, experiments were designed in collaboration with HNu Photonics to utilize their MoSL hardware in actual microgravity and obtain data demonstrating cytoskeletal dynamics in a neuron-like model. The data obtained in microgravity can then be compared to two control groups: a ground control (Earth, normogravity) (GC) for normal cell culture conditions, and a ground control for cell culture conditions in a MoSL situated on Earth. Unfortunately, due to the unforeseen circumstances of the CoViD-19 pandemic, various delays have affected our ability to send the MoSL to the ISS (Discussed in Section 4.4), and this portion of experiments will be performed at a later date. The experiments presented in this thesis represent the validation and quantification of GC experiments within a normal cell culture environment. Upon completion of microgravity-based experimentation the data presented here will be combined with data obtained in the MoSL, and a full comparison of the effects of microgravity on cytoskeletal dynamics, axonal transport, and cell health will be performed.

3.1. SH-SY5Y Pre-Flight Characterization

3.1.1. Neuronal Morphology and Phenotype

My first goal was to characterize if transformed SH-SY5Y cells exhibit normal parental cell line characteristics. Virus-mediated transfections are prone to immunogenic and cytotoxic responses in host cells due to the random insertion of viral vectors into the host genome. If viral vector insertion disrupts expression of tumor suppressor genes or essential protein expression, unwanted cancerous or unviable cell phenotypes may emerge (Kim & Eberwine, 2010). To accomplish this, I monitored cell morphology throughout the time course of differentiation. Normal characteristics of mature neuron-like cells includes the expression of thin, long neurites, and an overall decrease in the surface area of the soma in favour of rounded, phase-bright cell bodies.

Figure 3.1. demonstrates representative SH-SY5Y cells at various stages of differentiation. Over the time-course of differentiation, SH-SY5Y cells grew long, thin neurites that continuously grew proportionally to the time spent in differentiation media (RA and subsequent BDNF). Furthermore, many cell bodies had a reduced surface area and exhibited a characteristic rounded phase-bright morphology. Thus, I concluded that the transformed cell line exhibited normal characteristics of differentiated neuron-like cells. SH-SY5Y cells differentiated in RA and BDNF were also positive for the neuron-specific tubulin subunit, βIII-Tubulin (Figure A.2.). This result indicates that the transformed cell line exhibits typical biochemical differentiation comparable to literature (Jing et al., 2016; Kazemi et al., 2020).

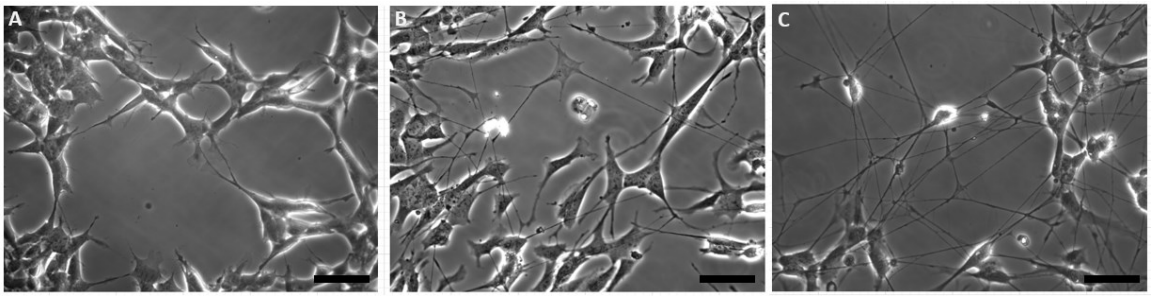

Figure 3.1. Characterization of transformed SH-SY5Y cell line
A) Representative phase-contrast image of undifferentiated SH-SY5Y cells aged 5-days on glass coverslips. B) Representative phase-contrast image of partially differentiated SH-SY5Y cells, aged 5-days in RA (10-days since plating on coverslips). C) Representative phase-contrast image of differentiated SH-SY5Y cells aged 10-days in BDNF (20-days since plating on coverslips). Scale bars: 25μm.

My second goal was to determine the survivability of differentiated SH-SY5Y cells. Decreased long-term viability of differentiated cells has been reported due to prolonged nutrient deprivation (Encinas et al., 2002; Strother et al., 2021). Because our differentiation protocol and follow-up experimentation in actual microgravity will take place over a 21-day period (Figure 2.1.), it was important to ensure the transformed cell line would remain viable for a minimum of 21-days following induction. SH-SY5Y survival over the course of differentiation was assessed and quantified in MoSL hardware by Brittany Willebrand, a collaborator employed by HNu Photonics. This data was shared with me and included within this section with permission (Figure 3.2.). Over a 21-day period, the estimated percent of remaining viable cells was visually assessed and quantified (Figure 3.3.). Approximately 75% of cells remained viable by the end of the 21-days. Cells were then continually monitored to determine the maximum duration of SH-SY5Y viability post-induction. These results indicated significant reductions in cell survival by 24-days post-

induction, and almost no viable cells remained by day-28 (Figure 3.2.E-F; Figure 3.3.). The observed viability of SH-SY5Y cells for at least 21-days supports the conclusion that the parental SH-SY5Y phenotype was not altered post-transformation. Furthermore, these results confirm that SH-SY5Y viability is not altered by incubation in BioChips and MoSL hardware on Earth.

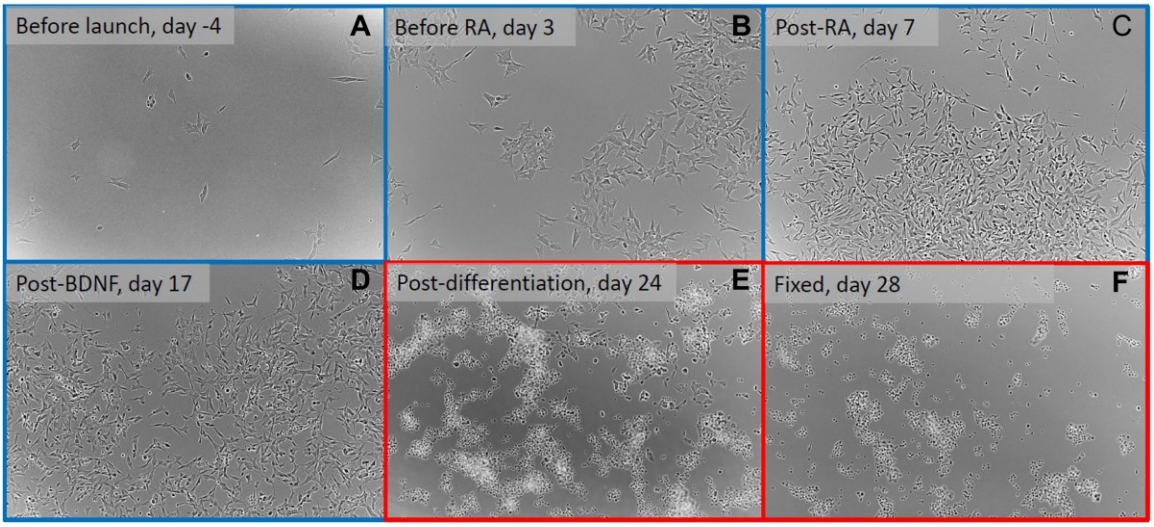

Figure 3.2. SH-SY5Y long-term survivability and death on MoSL hardware
Representative images of SH-SY5Y cells cultured in MoSL hardware, imaged at 10X magnification. A) Undifferentiated cells, freshly plated on polycarbonate glass BioChips. B) Undifferentiated cells aged 2-days in BioChip. C) Partially differentiated cells, aged 5-days in RA (10-days total). D) Differentiated cells, aged 10-days in BDNF (20-days total). E) Differentiated cells, aged 24-days total. F) Differentiated cells, aged 28-days total.

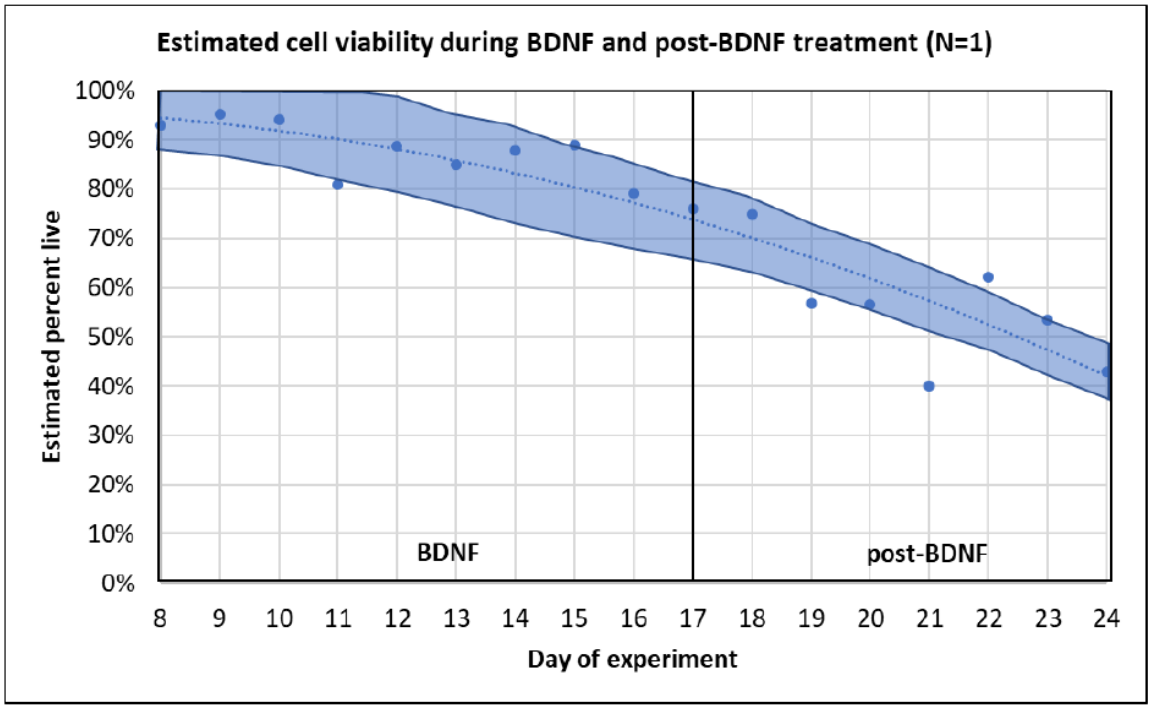

Figure 3.3. Quantification of SH-SY5Y survivability on MoSL hardware
Quantification of estimated cell viability in transfected SH-SY5Y cells. Reduced viability was noted after BDNF treatment but without significant effect on 3-week experiment timeline.

3.1.2. Fluorescent Marker Stability

Next, I investigated the long-term expression and resistance to photobleaching of the two transfected fluorescent proteins in our cell line. A stably transfected cell line should ideally express the transgene in all cells with consistency in expression patterns over time. However, it has been noted that modifications such as transcriptional silencing triggered by epigenetic modifications of exogenous DNA may be responsible for nonuniform, mosaic expression patterns observed in some transgenes over time. Certain promoters are known to be susceptible to methylation proportionally to the number of DNA replication cycles (Brooks et al., 2004; Hsu et al., 2-10; Moritz et al., 2015). To ensure that 1) fluorophores properly localize to target proteins and 2) fluorophore expression patterns remained consistent throughout the time-course of differentiation, I monitored and quantified the relative fluorescent intensities of the two markers at the beginning and end of differentiation.

To confirm fluorophore localization to target proteins, high resolution images of fixed SH-SY5Y cells stained for ATP5A or α-tubulin were captured and analyzed. Mitochondrial membrane ATP-synthase F1 subunit alpha (ATP5A) localizes to

mitochondrial ATP synthase on the inner mitochondrial membrane, and antibody staining can be utilized for localization and visualization of mitochondria (Goldberg et al., 2018). The stably transfected protein, GFP fused to a mitochondrial targeting sequence (MTS) was imaged at high resolution and its localization compared to that of ATP5A via visual colocalization analysis. It was found that GFP-MTS fluorescent expression patterns were highly correlated to sites of ATP5A fluorescence, thus leading to the conclusion that GFP-MTS was properly localizing to endogenous mitochondria (Figure 3.4.). Similarly, fluorescent RFP-EB3 was confirmed to localize to the plus-end of microtubule tracks via visualization of the microtubule heterodimer subunit, α-tubulin (Figure 3.5.). To further confirm proper EB3-localization, distance-time graphs (kymographs) indicated that RFP moved in anterograde comet patterns, which is a distinct characteristic of +TIP proteins including EB3 (Reviewed in section 1.2.1.1.) (Figure 3.9.).

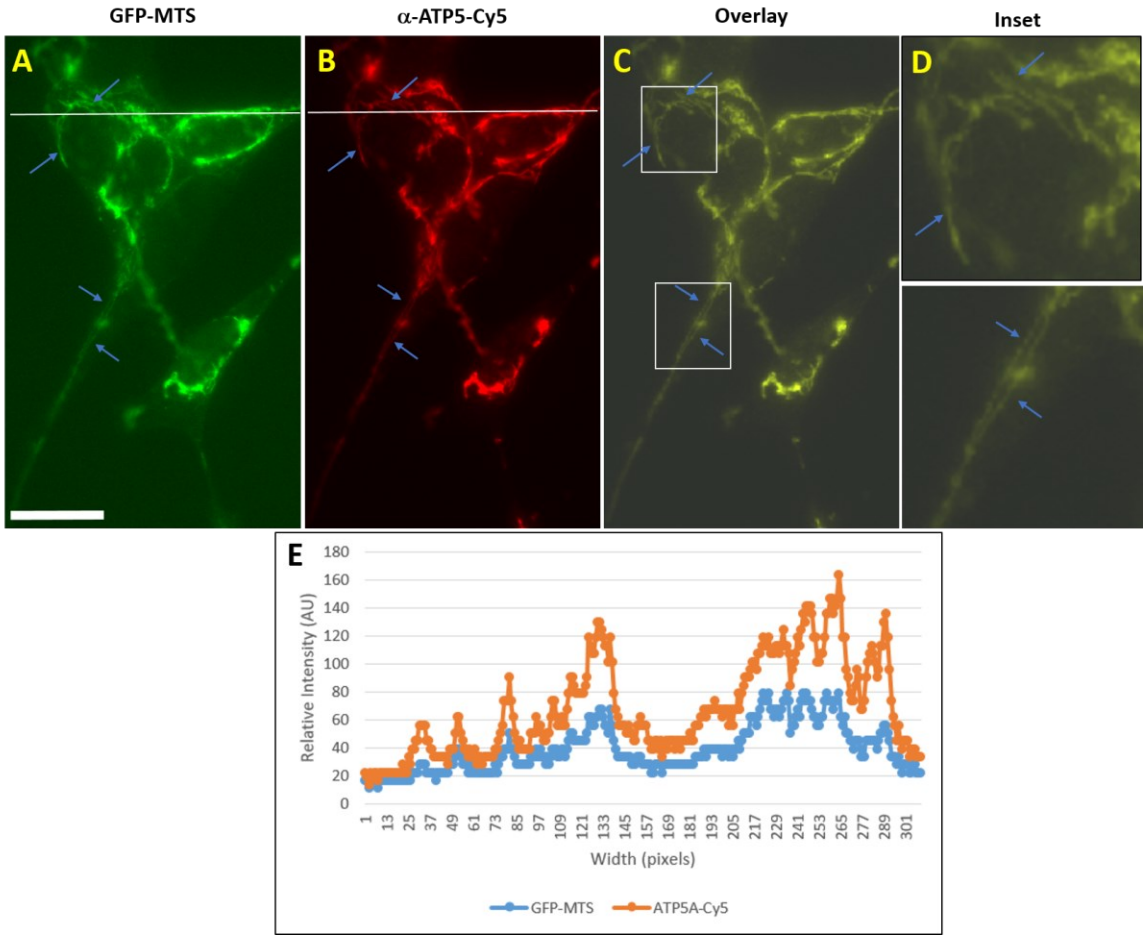

Figure 3.4. Expressed GFP-MTS colocalizes with ATP5A
A) Expression of transfected GFP-MTS in SH-SY5Y cells. B) Expression of immunologically stained ATP5A. C) Overlay and colocalization between GFP-MTS and ATP5A. D) Insets of C) highlighting mitochondrial network structures and complete colocalization of GFP-MTS and

ATP5A. Scale bar: 25μm. E) Linescan analysis of relative pixel intensies comparing GFP-MTS and ATP5A-Cy5 across the horizontal line present in A) and B).

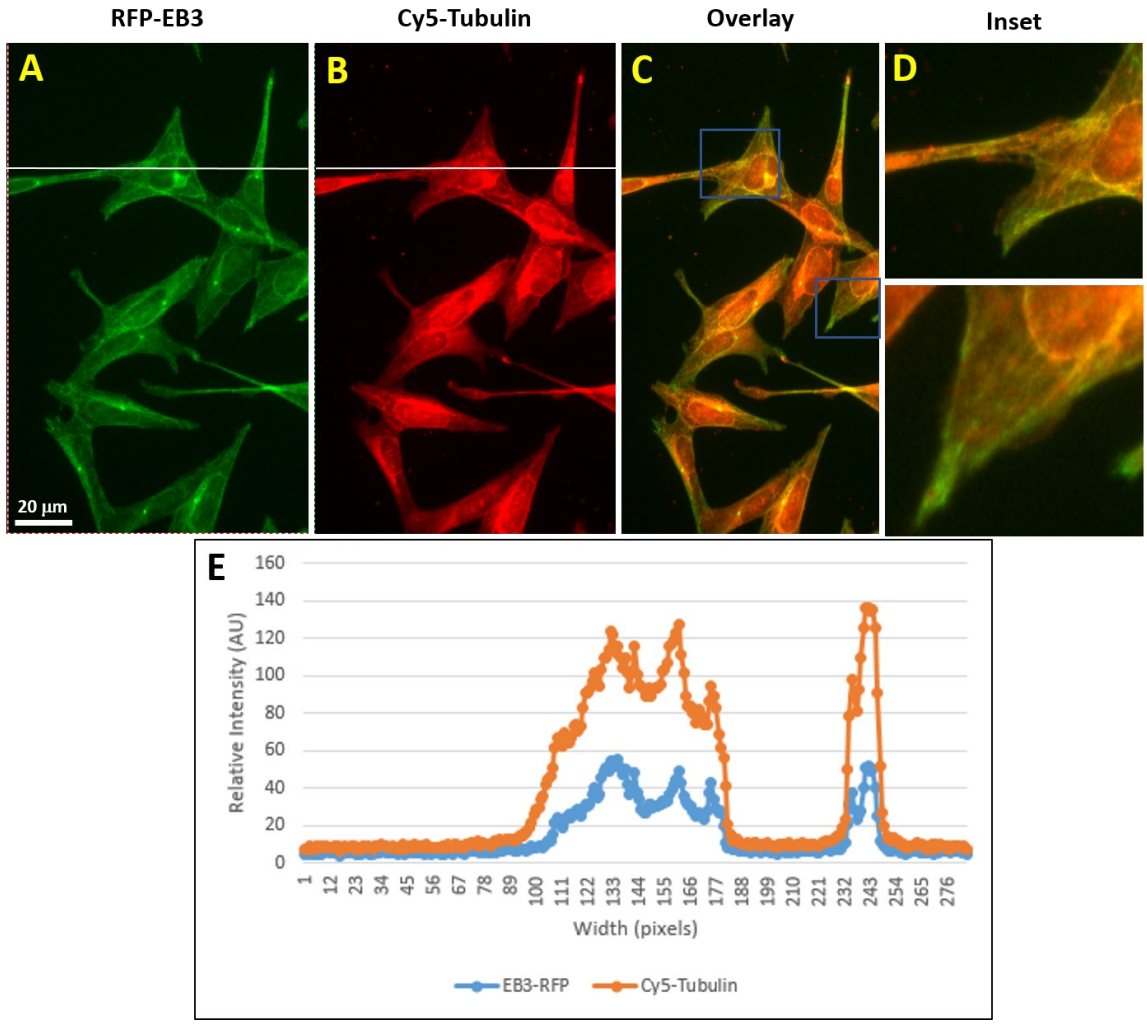

Figure 3.5. Expressed RFP-EB3 colocalizes with tubulin
A) Expression of transfected RFP-EB3 in SH-SY5Y cells. B) Expression of immunologically stained α-Tubulin. C) Overlay and colocalization between RFP-EB3 and Tubulin. D) Insets of C) highlighting RFP presence and colocalization to tips of linear microtubules. Scale bar: 25μm. E) Linescan analysis of relative pixel intensies comparing GFP-MTS and ATP5A-Cy5 across the horizontal line present in A) and B).

I then aimed to quantify the stability of fluorophore expression patterns throughout the time-course of differentiation. To accomplish this, fluorescence intensities of RFP-EB3 and GFP-MTS were quantified in either undifferentiated or fully differentiated SH-SY5Y cells using 400X magnification images obtained from videos captured overnight with an automated recording protocol as described in section 2.5. It was found that both GFP-MTS and RFP-EB3 displayed stable and consistent expression patterns throughout the time course of differentiation (Figures 3.6., 3.7.) Mean fluorescence intensity was then

compared between undifferentiated and differentiated cells, and no statistically significant differences were found (Figure 3.8.). These results imply that the expression of the two transfected markers is stable for at least the duration of the experimental timeframes in this thesis, and their expression is not reduced in the long-term due to repeated cycles of fluorescent video capture.

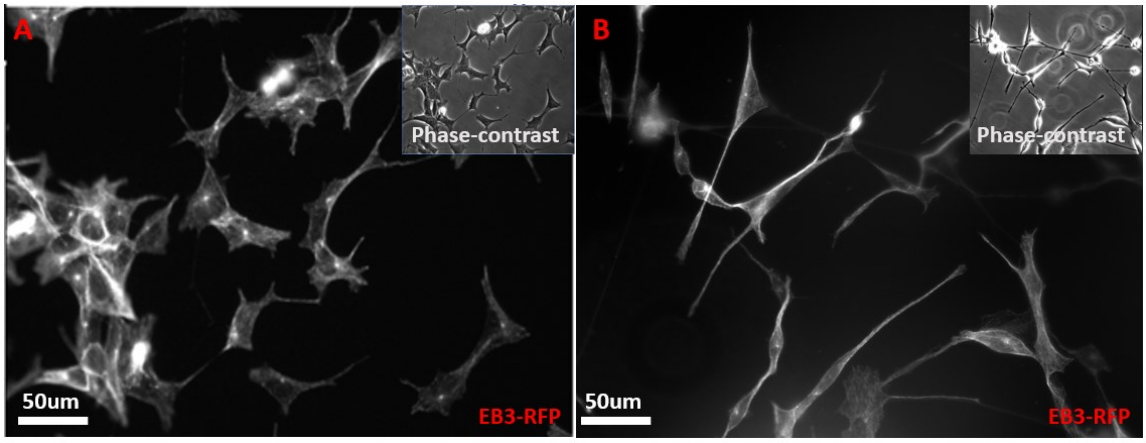

Figure 3.6. EB3-RFP expression is stable throughout differentiation
A) Representative image of undifferentiated SH-SY5Y cells aged 5-days on glass coverslips. B) Differentiated SH-SY5Y cells, aged 10-days in BDNF on glass coverslips (20-days since plating on coverslips). Overall fluorescent intensity level is consistent between conditions and expression patterns of RFP-EB3 remain consistent throughout differentiation. Scale bars: 50µm.

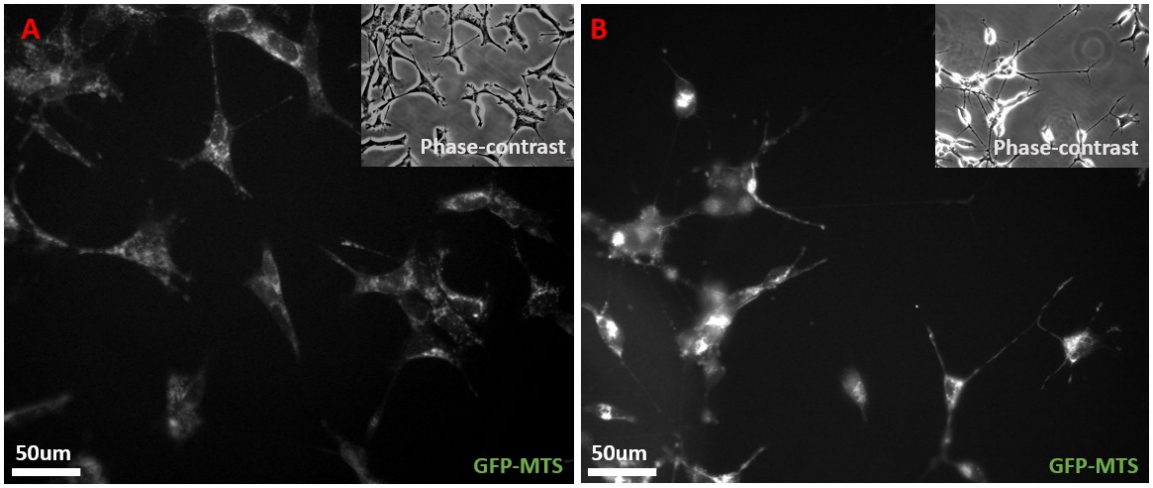

Figure 3.7. GFP-MTS expression is stable throughout differentiation
A) Representative image of undifferentiated SH-SY5Y cells aged 5-days on glass coverslips. B) Differentiated SH-SY5Y cells, aged 10-days in BDNF on glass coverslips (20-days since plating on coverslips). Overall fluorescent intensity levels are consistent between conditions and expression patterns of GFP-MTS remain consistent throughout differentiation. Scale bars: 50µm.

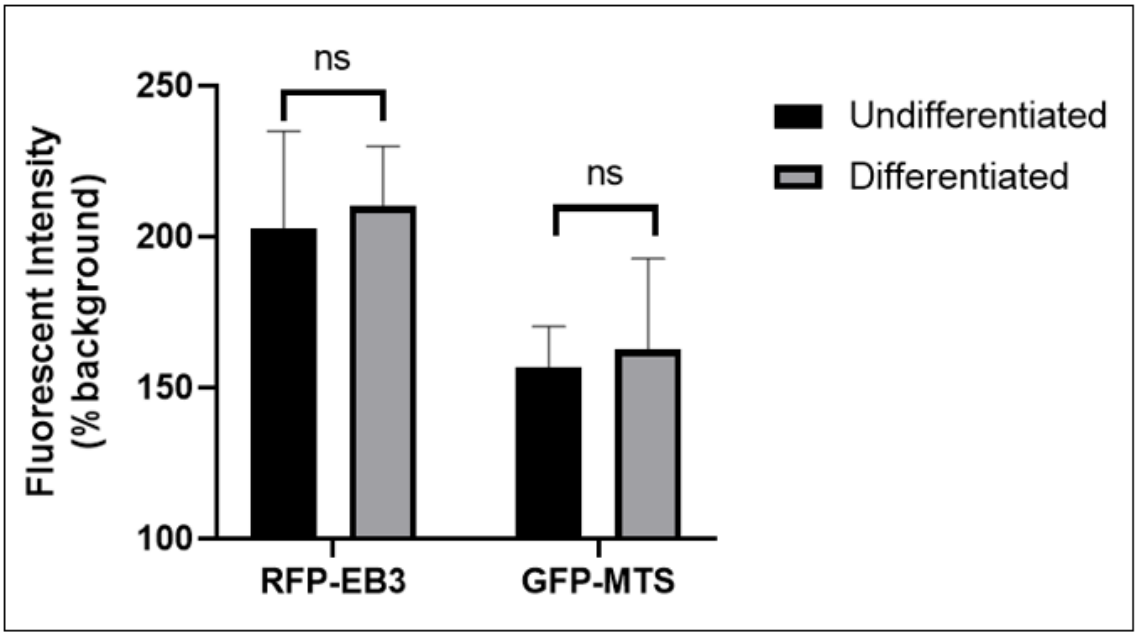

Figure 3.8. Quantification of relative transgene expression levels
Comparison of relative fluorescent intensity expressed as a % of background signal in both RFP-EB3 and GFP-MTS in undifferentiated vs. differentiated SH-SY5Y cells. Graphs show mean ± SEM. Statistical differences were calculated using GraphPad Prism 9. An unpaired *t*-test was performed on each pair. RFP: p=0.544110, n=10 for each group. GFP: p=0.577581, n=10 for each group.

3.2. Cytoskeletal Dynamics

3.2.1. End-Binding Protein 3 Transport

To determine microtubule dynamics in differentiating SH-SY5Y neurites, I recorded dynamic RFP-EB3 comets in differentiating SH-SY5Y cells and quantified their velocities via kymograph analysis throughout the time-course of differentiation. Tracking EB3 is a recognized and validated method used to discern changes in microtubule dynamics, including during neuronal differentiation (Stepanova et al., 2003). The data presented in this section constitutes the ground control and can be used as a baseline for the comparison of data obtained in the future representing EB3 velocity in a microgravity environment.

My first task was to establish a data collection protocol that could mirror the hourly RFP-EB3 recording that will be conducted in microgravity by the MoSL. With help from a technician employed by MetaMorph Software, an automated imaging regimen (journal) was designed wherein fluorescent videos of RFP-EB3 transport would be recorded at 3

locations on a glass coverslip, every 45-minutes, for 12-hours. This journal ran every-night for 15 consecutive nights, fully encapsulating the time-course of RA and BDNF-mediated differentiation.

I then quantified the velocity of EB3 comets in differentiating neurites by generating kymographs (distance-time graphs) in MetaMorph software (See section 2.6. for kymograph generation protocol). A majority of EB3 movement was in the anterograde direction, as indicated by positively sloped lines in the kymograph (Figure 3.9.C.). The average velocity of EB3 comets did not significantly change at any point throughout the course of differentiation (Figure 3.9.D.), with an overall mean velocity of 0.20 ± 0.06 μm/s (n=3394). Previous authors have reported an EB3 comet velocity in differentiating neurons equal to 0.22 ± 0.04 μm/s (Stepanova et al., 2003). This value is comparable to my reported EB3 comet velocity, and as such, I concluded that our transfected SH-SY5Y cell line displays microtubule dynamics comparable to neuronal models. Following SH-SY5Y differentiation in actual microgravity on the MoSL, kymograph analysis will similarly be performed using the procedure outlined in this thesis. EB3 comet velocity may then be compared to the ground-control data generated and analyzed within this framework. Following integration of microgravity-data, statistical analysis for differences in EB3 comet velocity between ground control and microgravity exposure will be conducted via 2-way ANOVA with Tukey's post hoc test.

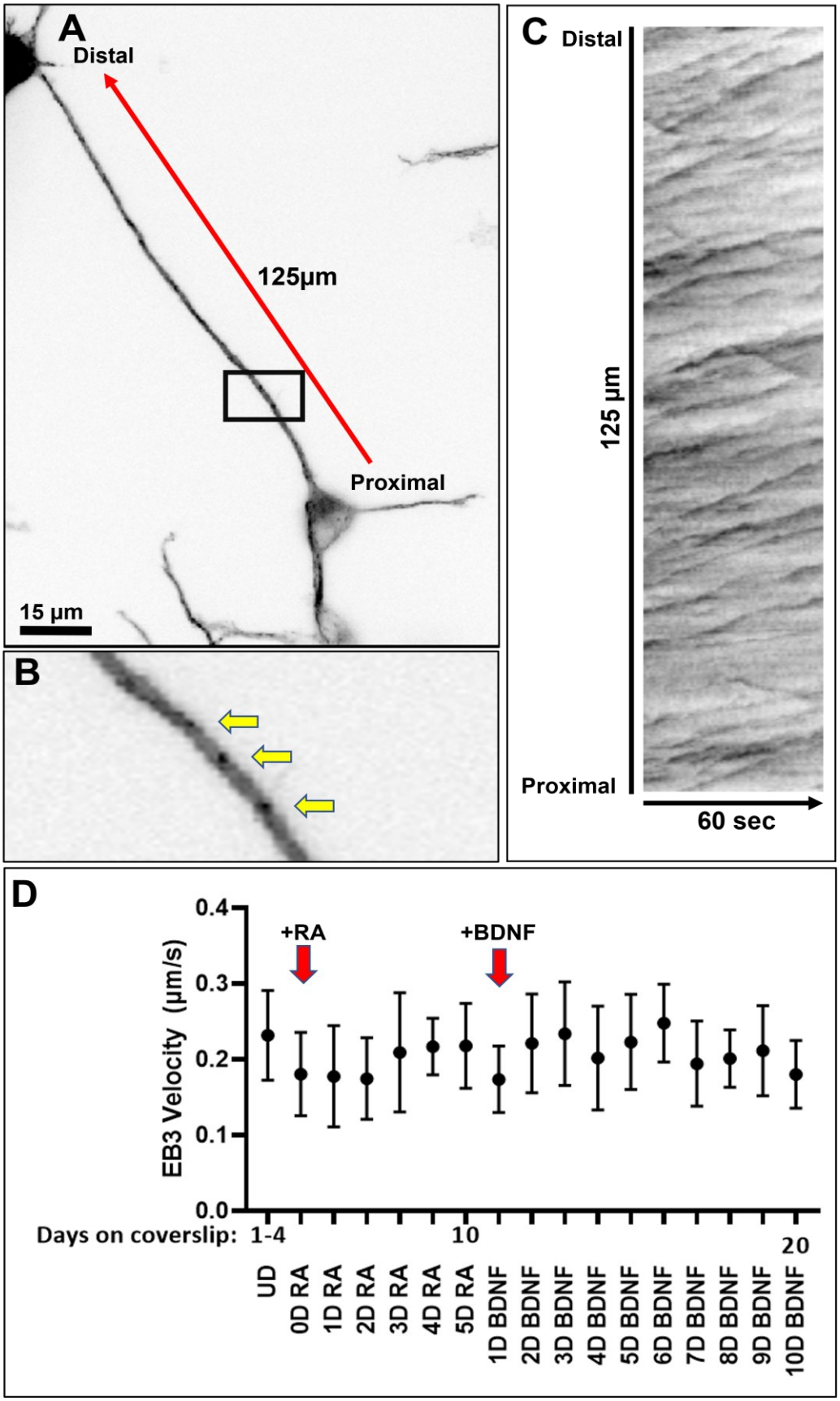
A
Distal
125µm
Proximal
15 µm
B
C
Distal
125 µm
Proximal
60 sec
D
+RA
+BDNF
EB3 Velocity (µm/s)
0.4
0.3
0.2
0.1
0.0
Days on coverslip: 1-4
10
20
UD
0D RA
1D RA
2D RA
3D RA
4D RA
5D RA
1D BDNF
2D BDNF
3D BDNF
4D BDNF
5D BDNF
6D BDNF
7D BDNF
8D BDNF
9D BDNF
10D BDNF

Figure 3.9. EB3 transport and kymograph analysis
A) Video frame from recorded EB3 trafficking in a fully differentiated SH-SY5Y cell. The 125μm neurite was traced and a kymograph representing EB3 transport was generated and quantified. B) Inset highlighting individual EB3 comets. C) Kymograph generated from neurite in A). EB3 comets moving in anterograde are represented by positively sloped lines and EB3 comets moving in retrograde are represented by negatively sloped lines. Total time of recording = 60 seconds. D) Quantification of EB3 comet velocity at 24-hour intervals throughout time course of differentiation. Data presented as mean ± SD. Mean EB3 velocity was equal to 0.20 ± 0.06 μm/s (n=3394).

3.2.2. Neurite Outgrowth and Morphology

To further elucidate the effects of microgravity on microtubule dynamics in neurites, I recorded dynamic neurite outgrowth in differentiating SH-SY5Y cells and quantified outgrowth velocity and the lengths of neurites throughout the time-course of differentiation. Neurite outgrowth during development relies on microtubule elongation, and disruption to microtubule organization impairs neurite outgrowth (discussed in section 1.2.3.). When microtubule organization is disrupted, the velocity of neurite outgrowth is slowed. The number of neurites expressed per cell may also increase, while the mean length of such neurites may be shorter than that of control neurons (Riederer et al., 1997). Thus, changes in quantitative measures of neurite outgrowth may be used as a proxy to identify changes in cytoskeletal organization.

To accomplish this goal, I utilized the MetaMorph journal described in section 3.2.1. A phase-contrast image at 3 separate microscope stage locations with living SH-SY5Y cells was captured every 15-minutes for 12-hours. This journal ran overnight for 15-consecutive nights, fully encapsulating the time-course of RA and BDNF-mediated differentiation. The captured phase-contrast images were converted to a Z-stack and analysed using the TrackPoints function in MetaMorph Software (reviewed in section 2.7.1.). The output of this analysis was exported to an Excel spreadsheet, and the overall rate of neurite outgrowth velocity was calculated. I observed that the neurites of differentiating SH-SY5Y cells advanced at a mean rate of 28.57 ± 13.7 μm/h during RA-mediated differentiation (Figure 3.10.A). Following this, I quantified the fraction of total outgrowth time spent in phases of advancement, retraction, or pause. Growing neurites in SH-SY5Y cells spent approximately 46% of the time advancing, 43% of the time retracting, and the remaining 10% of the time paused (Figure 3.10.B). Previous values of neurite outgrowth in literature haver reported mean rates of outgrowth approximately equal to 25 μm/h, which is comparable to my reported value of 28.57 μm/h (Miller & Suter, 2018).

Thus, I concluded that neurite outgrowth in our transformed SH-SY5Y cell line occurs at a rate comparable to mammalian neurons.

A third analysis of neurite outgrowth was performed wherein the lengths of neurites during each stage of differentiation were quantified. Disruption to microtubule dynamics and organization is known to cause a reduction in neurite length and an increase in the number of short neurites (Riederer et al., 1997). By quantifying the length of neurites in differentiating SH-SY5Y cells, we may compare the lengths of neurites in ground control cells (demonstrated here) versus the length of neurites differentiating in microgravity conditions.

Quantification of neurite length indicated that the bulk of neurite outgrowth occurred within the first-5 days of differentiation, coinciding with RA treatment (Figure 3.11.). Undifferentiated cells (mean length = 26.62 ± 11.23 μm, max length =61.51 μm) grew until reaching a mean length of 82.75 ± 44.04 μm and maximum observed length of 267.81 μm by the end of RA-differentiation. The mean length of neurites did not increase substantially following BDNF-mediated differentiation, where the mean neurite length in BDNF-differentiated neurites was 104.30 μm and maximum observed length was 291.57 μm (Figure 3.11.). Other publications investigating neurite length in SH-SY5Y cells did not grow cells for 21-days (discussed in section 3.1.), thus the length of neurites observed in my experiments was not comparable to those studies. However, there is literature which states that RA mediates the bulk of morphological differentiation, whereas BDNF mediates biochemical differentiation, a trend which was supported by the results of my experiments. (Dwane et al., 2013; Encinas et al., 2002). Following SH-SY5Y differentiation in actual microgravity on the MoSL, quantification of neurite length will be similarly performed using this procedure and integration of microgravity-data into this data set will allow for statistical analysis of differences between neurites generated under microgravity conditions versus ground control. Statistical analysis will be conducted via 2-way ANOVA with Tukey's post hoc test.

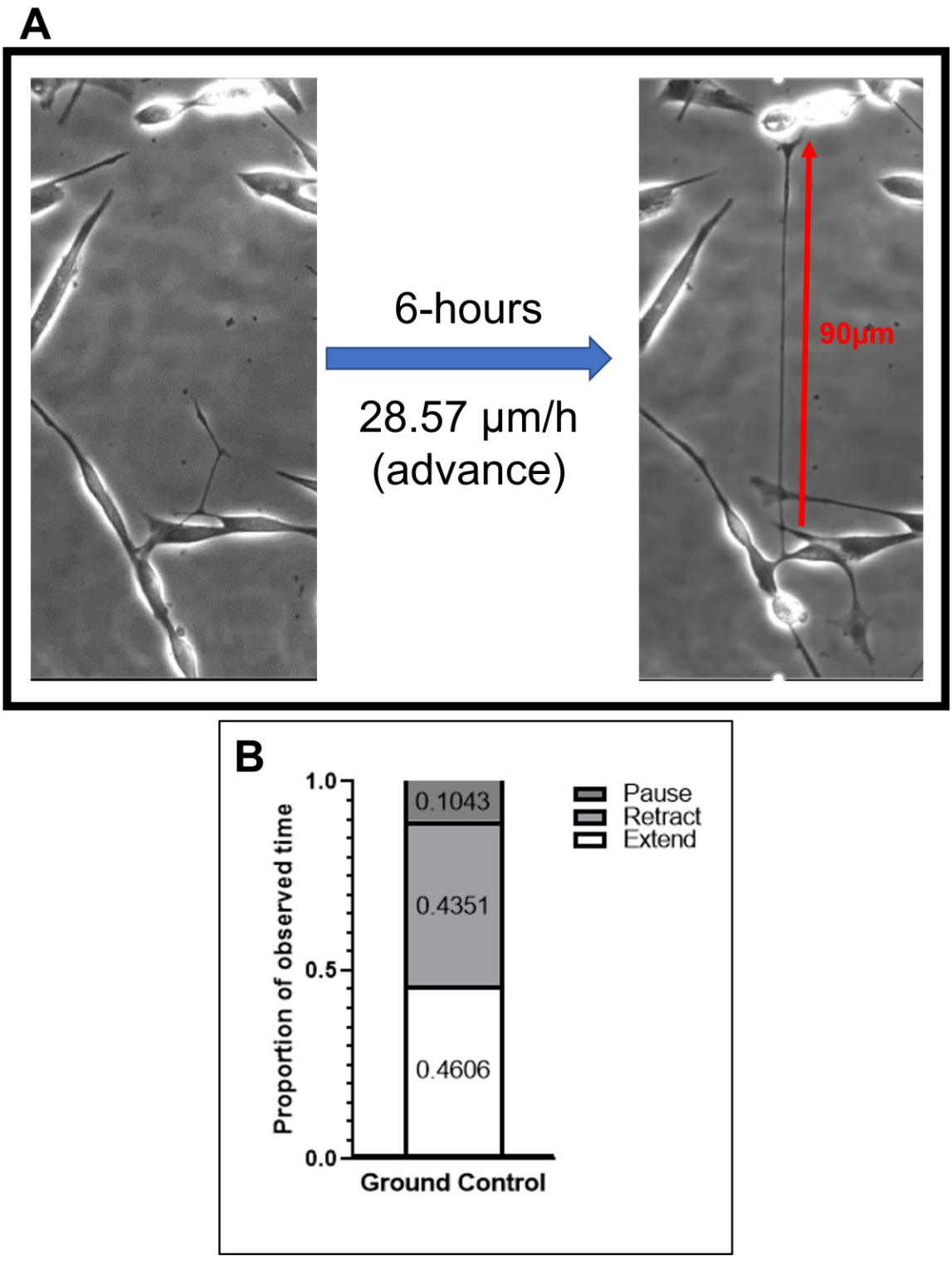

Figure 3.10. Dynamic quantification of neurite outgrowth
A) Phase-contrast image of a neurite before (left) and after (right) completion of a neurite outgrowth event during RA-mediated differentiation. The observed neurite grew at an average rate of 29.1 µm/h during times of advance, reaching its final length of 90 µm after 6-hours. B)

Mean proportion of time spent in each phase of neurite outgrowth (n=20 neurites >30μm in final length).

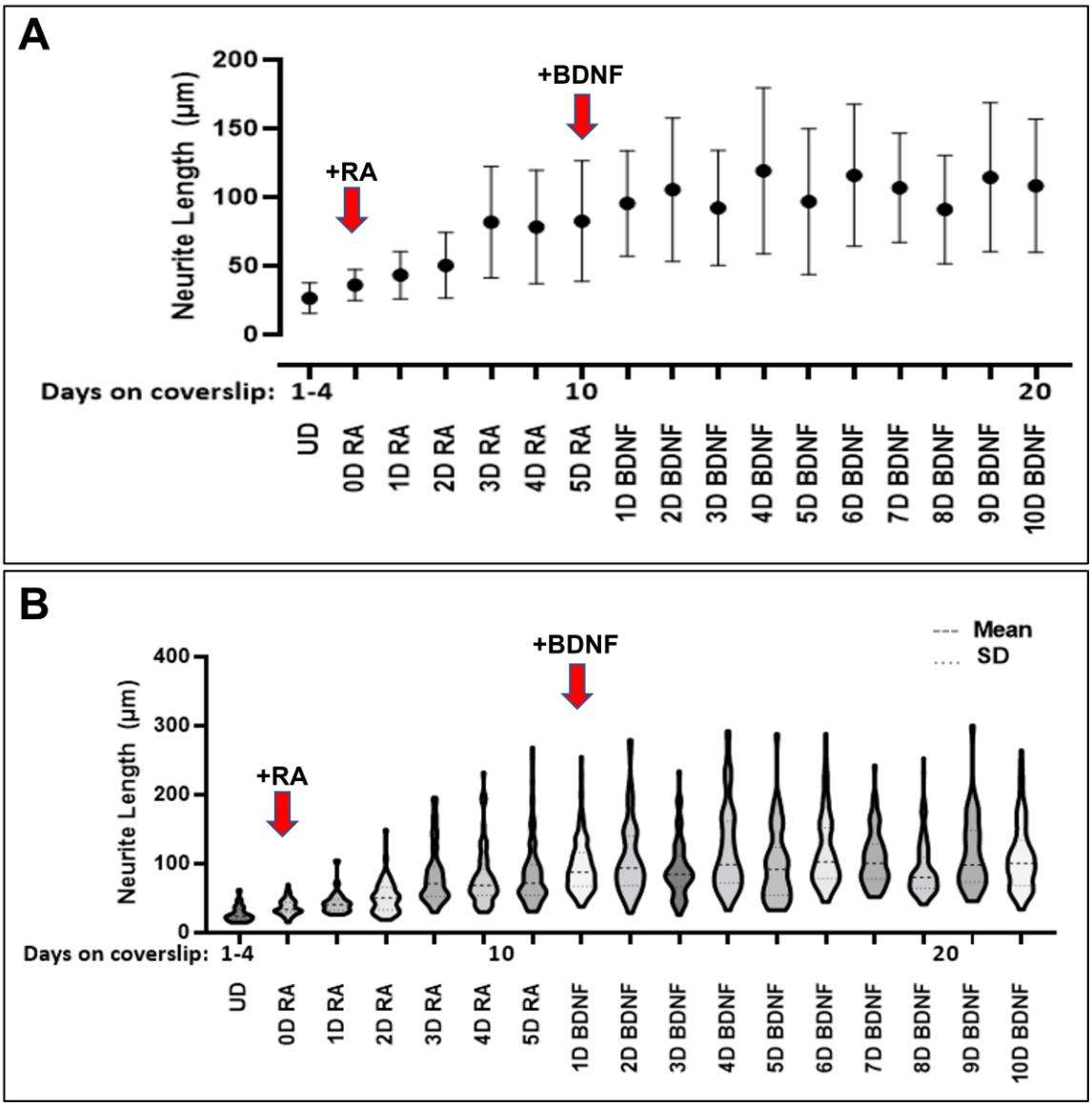

Figure 3.11. Quantification of neurite lengths throughout differentiation
A) Mean neurite length at 24-hour intervals throughout time-course of differentiation. Data presented as mean ± SD, n>50 neurites per group. B) Histogram of distribution of neurite lengths at throughout time-course of differentiation. Wider regions of violin correspond to larger concentration of values. Dashed lines indicate mean, dotted lines indicate SD. n>50 per group in both representations.

3.2.3. Cytoskeletal Immunostaining

To determine the effects of microgravity on cytoskeletal ultrastructure, I visualized and quantified the actin and microtubule cytoskeletons via antibody staining in

differentiated SH-SY5Y cells (ground control) and differentiated SH-SY5Y cells with pharmacologically induced disrupted cytoskeletal organisation (positive control). Using this data, I generated a strategy which will be used to visually and quantitatively assess the level of disorganization to cytoskeletal ultrastructure in microgravity exposed cells.

Following completion of MoSL experimentation in actual microgravity, differentiated SH-SY5Y cells will be fixed and stored in PBS for up to 3-weeks on the ISS before being delivered to our lab on Earth for follow-up immunostaining. To ensure that delaying immunostaining by 3-weeks following fixation did not influence cytoskeletal ultrastructure, I assessed the effect of aging on fixed coverslips stored in isotonic PBS over a 3-week duration. Differentiated cells that were fixed in PFA and stained immediately (Fresh-stain) were compared to cells that were fixed in PFA, stored in isotonic PBS at room temperature in the dark for 3-weeks, and then stained (Aged-stain).

When comparing the actin and microtubule cytoskeletons in cells that were freshly stained versus aged prior to staining, no differences or perturbations to actin or microtubule cytoskeletal structure were observed (Figure 3.12., Figure 3.14.). Quantification of fluorescence intensity in the actin cytoskeleton supported this conclusion, as the corrected total cell fluorescence (CTCF) score was not significantly different between the fresh or aged cell groups (Figure 3.13. E). (See section 2.7.3 for overview of CTCF).

My next goal was to assess whether I could successfully identify disruptions to actin cytoskeletal structure and if so, quantify these disruptions. To accomplish this task, I compared the actin cytoskeleton of untreated SH-SY5Y cells (ground control) to the actin cytoskeleton of cells treated with a pharmacological disruptor of the actin cytoskeleton. By administering 1 μM of the actin polymerization inhibitor latrunculin-A (lat-A) for 30-minutes, extreme disruptions to actin cytoskeletal organization were observed (Figure 3.13.). Cells lost their ability to maintain shape, as indicated by a reduction in the surface area of the cell bodies, and rounded morphology. Characteristic linear actin fibers were observed in ground control cells (Figure 3.12, Figure 3.13. A,C), which were not present in lat-A treated cells (Figure 3.13. B,D). Rather, lat-A treated cells were observed to contain bright spots of fluorescent actin, indicative of F-actin disassembly and sequestering mediated by lat-A (Fujiwara et al., 2018). I then aimed to quantify the differences observed in actin cytoskeletal structure. Similar to previously described results in this section, a CTCF score

representing actin cytoskeletal fluorescent intensity was generated by tracing individual cells from high resolution images. Quantification of actin cytoskeletal CTCF revealed statistically significant differences in CTCF score resultant of treatment (Figure 3.13. E). These results indicate that this quantification method can successfully be utilized to score visually identified differences in actin cytoskeletal structure of our transformed SH-SY5Y cell line. Following data collection in microgravity exposed cells cultured in the MoSL, analysis and quantification of the actin cytoskeleton will similarly be performed on microgravity exposed cells using the procedure outlined here. Integration of microgravity data within the dataset reported in this thesis will allow for follow-up statistical analyses comparing ground control to microgravity, and microgravity to lat-A treated cells. This analysis will allow for a comparative view of the effects of microgravity on the actin cytoskeleton compared to a positive control for complete cytoskeletal disruption. Statistical analyses of these experiments will be performed using an unpaired Student's *t*-test.

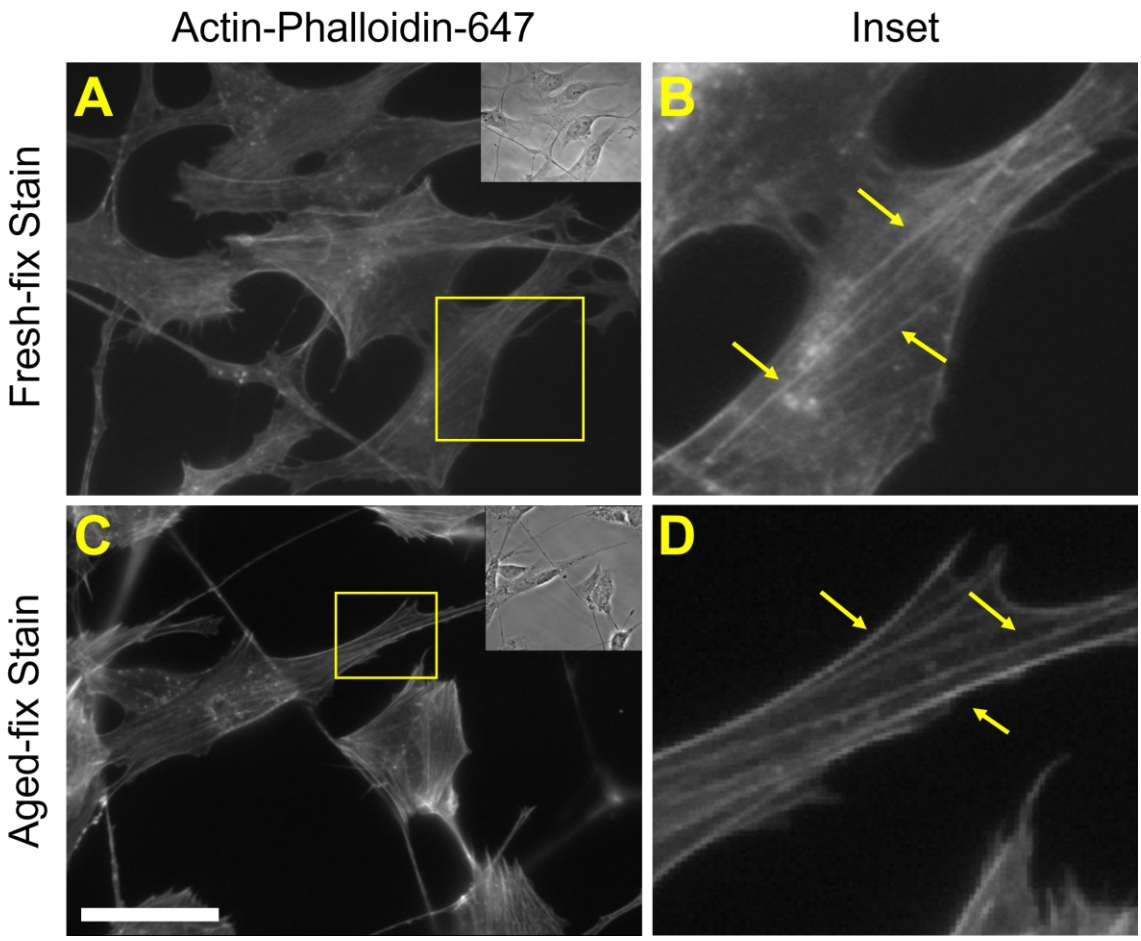

Figure 3.12. Actin cytoskeletal organization is not affected by time between fixation and staining

Visualization of the actin cytoskeleton via Phalloidin-647 staining and imaging at 630X magnification. A) Differentiated SH-SY5Y cells stained immediately following fixation. B) Inset of A). Arrows indicate individual linear F-actin fibers. C) Differentiated SH-SY5Y cells stained following 3-weeks of aging in isotonic PBS. D) Inset of C). Arrows indicate individual linear F-actin fibers. Scale bar: 50μm.

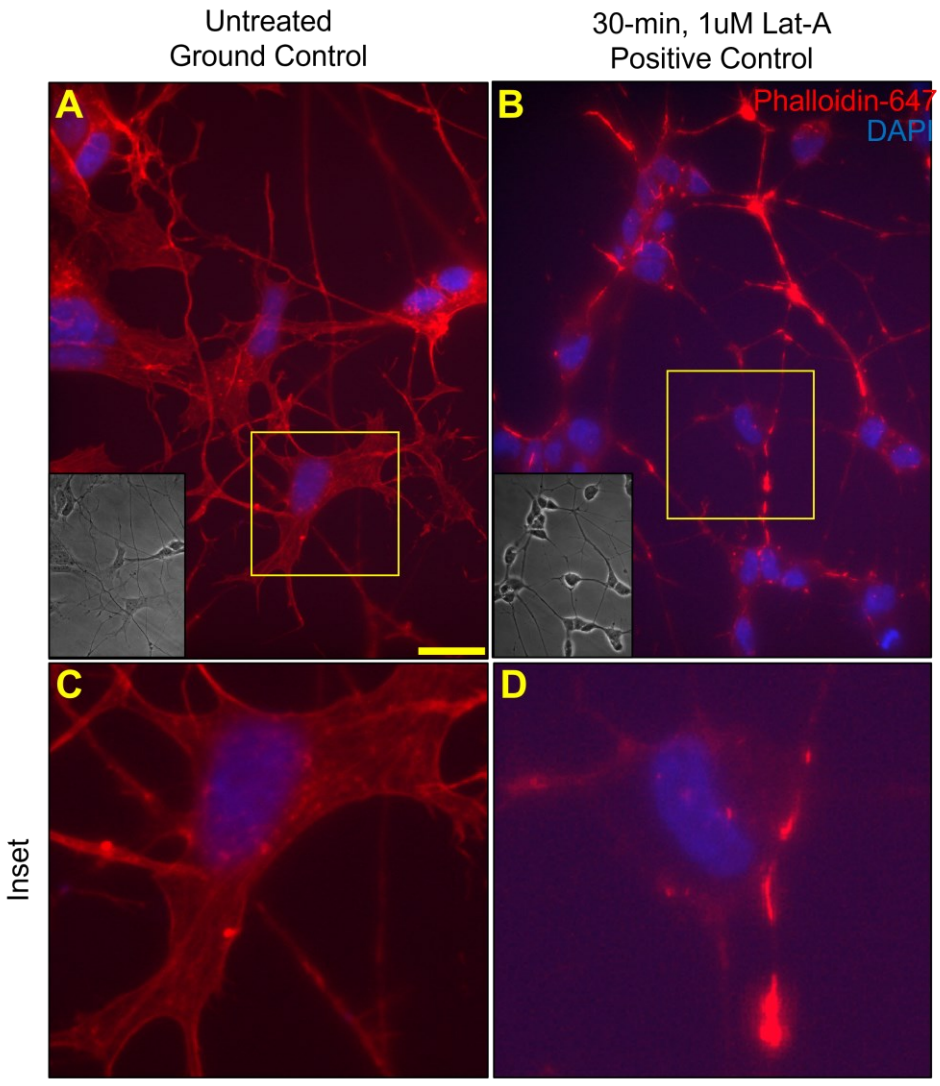
Untreated
Ground Control
30-min, 1uM Lat-A
Positive Control
A
B
Phalloidin-647
DAPI
C
D
Inset

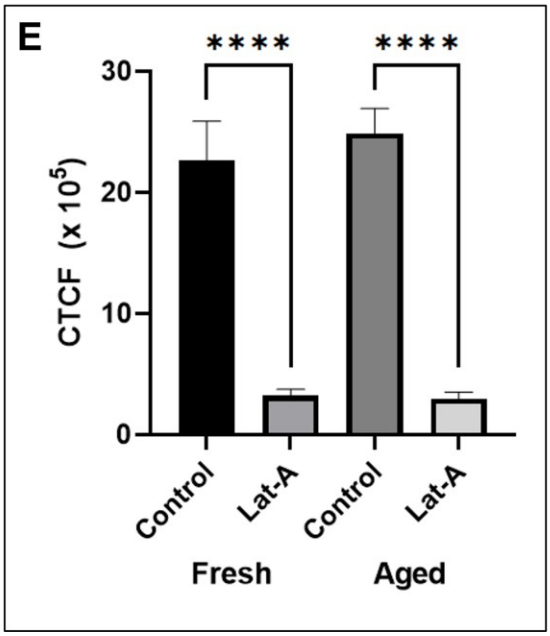
E
****
****
30
20
10
0
CTCF (x 10^5)
Control
Lat-A
Control
Lat-A
Fresh
Aged

Figure 3.13. Effect of Latrunculin-A on the SH-SY5Y actin cytoskeleton
Visualization of the actin cytoskeleton and nuclei via Phalloidin-647 and DAPI staining and imaging at 630X magnification with or without pharmacologically induced actin depolymerization. A) Untreated, differentiated SH-SY5Y cells. C) Inset of A), demonstrating detail of actin cytoskeletal ultrastructure under baseline conditions. B) Latrunculin-A treated, differentiated SH-SY5Y cells. D) Inset of B), demonstrating detail of actin cytoskeletal ultrastructure following depolymerization. Scale bar: 15 µm. E) Analysis of CTCF score in either ground control or lat-A treated cells, with or without 3-week delay in staining post fixation. Data presented as mean ± SEM. n=20 cells per group. ****: $P \leq 0.0001$.

Following quantification of the actin cytoskeleton, I shifted focus to the microtubule cytoskeleton. Here, I aimed to assess whether I could successfully identify disruptions to microtubule cytoskeletal ultrastructure, and if so, generate a methodology for quantification. To accomplish this task, I compared the microtubule cytoskeleton of untreated SH-SY5Y cells (ground control) to the microtubule cytoskeleton of cells treated with a pharmacological disruptor of microtubule organization. By administering 1 µM of the microtubule cytoskeleton depolymerizer, nocodazole for 1-hour prior to fixation, extreme disruptions to microtubule cytoskeleton organization were observed (Figure 3.14. B, D.). A qualitative assessment of microtubule cytoskeletal structure demonstrated that untreated cells displayed long, organized microtubule structures in cell bodies and growth cones with an abundance of neurites expressing dense, linear tubulin networks. Nocodazole treated cells were observed to have a more diffuse tubulin staining pattern, indicative of microtubule depolymerization and tubulin diffusion in the cytoplasm. Noticeably less neurites projected from cell bodies in nocodazole treated cells, which suggests axonal degeneration resultant from a loss of microtubule organization. This is consistent with what has been reported in literature when neurons are treated with microtubule destabilizing drugs (Verstraelen et al., 2017). Skeletonized representations of microtubule ultrastructure were generated to further analyze the effects of microtubule destabilization in SH-SY5Y cells (Figure 3.15). These representations of the microtubule cytoskeleton highlight the transition from a long and straight microtubule cytoskeletal morphology towards one with curved microtubule tips. These curved tips are commonly seen in shrinking microtubules (catastrophe),and indicate a significant amount of the remaining polymerized microtubules in nocodazole treated cells are actively undergoing shrinkage (Aher & Akhmanova, 2018; Gardner et al., 2013). Skeletonized representations illustrate this overall change in morphology. These changes are represented by a transition from linear, angled morphology towards one of with curved and circular morphology (Figure 3.15 C, D). These results indicate that the microtubule cytoskeleton can successfully be qualitatively analyzed in our transformed SH-SY5Y cell line.

Furthermore, the effects observed resulting from nocodazole treatment were consistent with what has been reported in literature in cells exposed to microtubule polymerizing drugs. These results indicate that it will be possible to compare the microtubule cytoskeleton in cells exposed to actual microgravity to either ground control cells, or positive controls for microtubule disorganization.

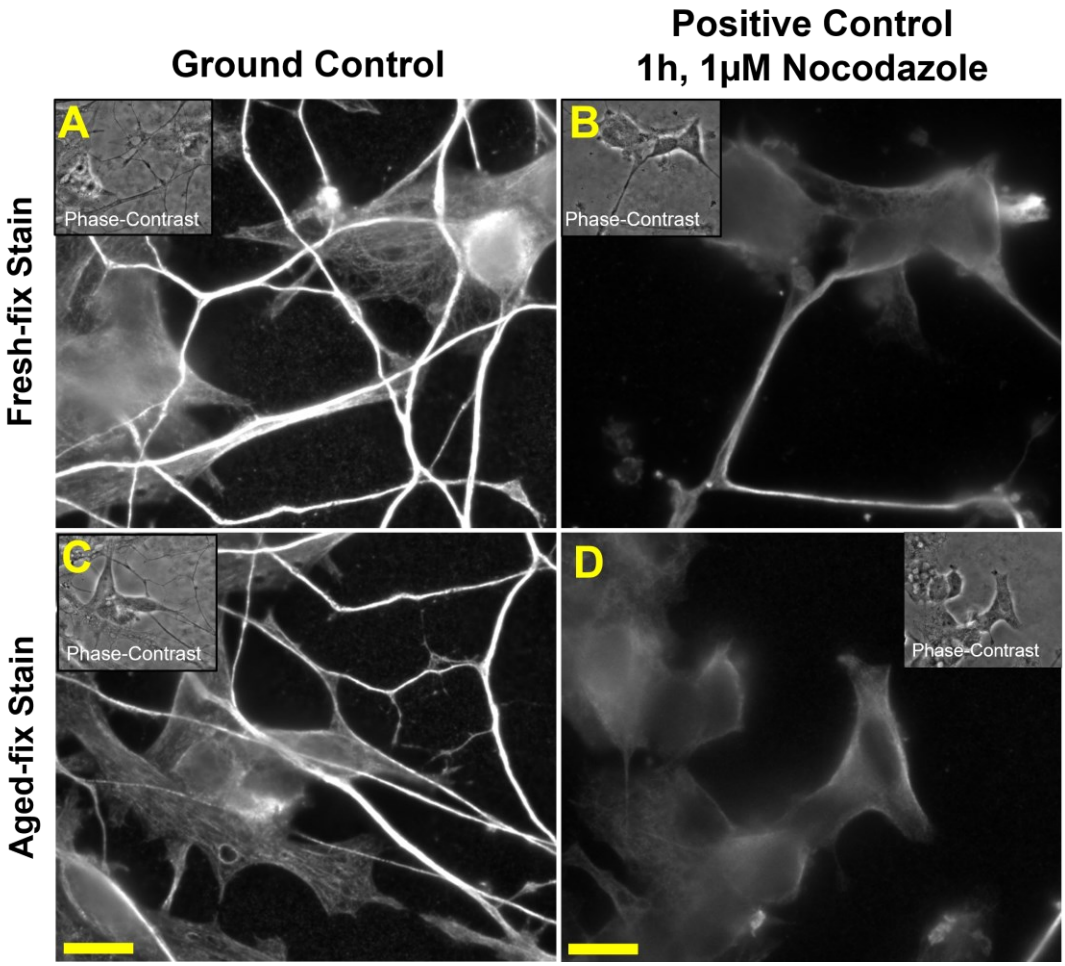

Figure 3.14. Effect of nocodazole on the SH-SY5Y microtubule cytoskeleton
Visualization of the microtubule cytoskeleton via α-Tubulin immunostaining and imaging at 630X magnification. A, C) Fixed, untreated cells stained immediately following fixation (A) or following 3-weeks incubation in isotonic PBS (C). B, D) Fixed cells treated with 1 μM Nocodazole for 1h, stained immediately following fixation (B) or following 3-weeks incubation in isotonic PBS (D). Scale bars: 15μm.

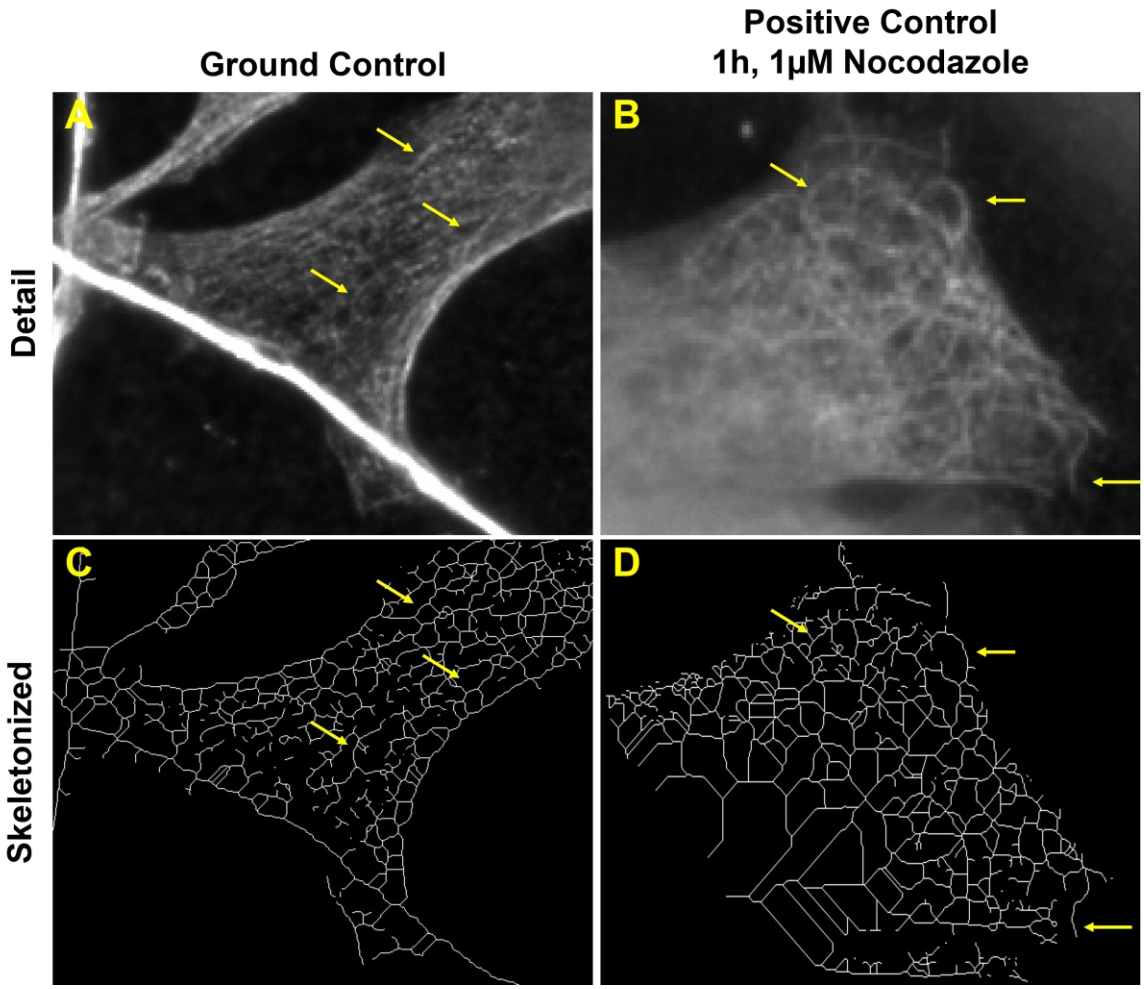

Figure 3.15. Microtubule cytoskeletal ultrastructure
A) Detailed view of microtubule ultrastructure in fixed, untreated differentiated SH-SY5Y cell bodies. B) Detailed view of microtubule ultrastructure in fixed, nocodazole treated differentiated SH-SY5Y cell bodies. C) Skeletonized representation of A. D) Skeletonized representation of B.

3.3. Axonal Transport of Mitochondria

To determine the effects of microgravity on axonal transport of mitochondria, I recorded and analysed the trafficking of fluorescently tagged mitochondria (GFP-MTS) in differentiating SH-SY5Y cells. The regulation of mitochondrial transport is required to maintain proper physiological function of energetically active axons and synapses. Axonal transport is reliant on proper microtubule organization to act as binding sites for the kinesin and dynein motor proteins that facilitate mitochondrial transport, and disruption to microtubule organization can lead to impaired synaptic and axonal energetics (Chada and Hollenbeck, 2004; Morris and Hollenbeck, 1993). Thus, the analysis of mitochondrial transport serves two purposes: 1) It serves as a proxy for evaluation of the effects of

microgravity on microtubule network stability, and 2) identification of disruptions to mitochondrial transport resultant from microgravity may imply the presence of other downstream effects to axonal energetics and health.

To accomplish this task, I collected fluorescent videos of mitochondrial transport using the journal described in section 3.2.1. Two-minute recordings of GFP-MTS were captured at 3 locations on a glass coverslip containing living SH-SY5Y cells every 45-minutes for 12-hours. This journal ran every-night for 15-consecutive nights, fully encapsulating the time-course of RA and BDNF-mediated differentiation. I then quantified mitochondrial transport dynamics by generating kymographs in MetaMorph. Upon qualitative observation of kymographs, I observed that a large fraction of mitochondrial fluorescence was stable (non-moving), indicated by horizontal lines on the kymograph (Figure 3.16. C). These mitochondria were excluded from quantitative analysis so that only observe data representing the dynamic transport of mitochondria would be included. To exclude stable mitochondria, a minimum run length of 1 μm was used as a cut off for analysis of mitochondrial transport events. Other authors have reported that the average run length of mitochondrial trafficking events is within the range of 0.7 - 1.7 μm (Narayanareddy et al., 2014). However, limitations based on MoSL hardware require the use of a 40X dry air objective for this experiment (400X magnification), and identification of short transport events below 1 μm are indistinguishable from non-moving mitochondria at this level of resolution on our microscope (Discussed further in Section 4. 4).

Mitochondrial velocity and run lengths were obtained through tracing kymographs in MetaMorph, and mitochondrial flux was subsequently calculated in an excel spreadsheet. Flux can be thought of as an index of bulk transport, defined as the total distance traveled by mitochondria standardized by the length and duration of each movie (in micrometer-minutes), $\sum_{i=1}^{n} d_i/t$, where d_i are the individual mitochondrial run lengths, l is the length of axon imaged, and t is the duration of the imaging session. The mean flux of mitochondrial transport was found to be 4.80 ± 1.65, with a slight bias towards retrograde transport (Table 3.1. Row 1). The mean velocity of mitochondrial trafficking was 0.15 ± 0.15 μm/s and mean run length 4.65 ± 3.29 μm (Table 3.1.). Because of the exclusion of short run length events in my analysis, there was a wide range in values (i.e., large SDs, large mean run length) for all parameters due to increased statistical weighting of long run length transport events. Thus, I also reported the median velocity (0.09 μm) and velocity range (Table 3.1. Row 3, 4) to provide my analyses with a greater number of

reference points for eventual comparisons with axonal transport under microgravity conditions. Mitochondrial velocity was slower than values reported in literature, which have been reported to be around 0.30 μm/s and as high as 0.60 μm/s as compared to 0.15 μm/s reported here (Gan & Silverman, 2016; Niescier et al., 2016). I hypothesize that this result is due to a possible lack of synaptic activity and axonal signal transduction due to the inability of SH-SY5Y cells to form true synapses (discussed in sections 1.2.2. and 1.2.3.) (Figure A.1.). A lack of mature synapse formation in SH-SY5Y cells would implicate reduced synaptic and axonal energetic requirements, and thus downregulation of signaling pathways which promote mitochondrial transport. This hypothesis also explains the slight retrograde bias observed in flux. Overall, these results indicate that mitochondrial trafficking in SH-SY5Y cells may not represent organelle trafficking dynamics of true neurons. However, differences observed between values reported here and values obtained in the future from microgravity exposed cells may still inform us of changes to microtubule dynamics resulting from microgravity exposure. Following integration of microgravity data, statistical analysis for differences in MTS flux, velocity, and run length will be conducted using multiple unpaired *t*-tests.

Table 3.1. Quantification of mitochondrial transport

	All events	**Anterograde**	**Retrograde**
Flux (min^{-1})	4.80 ± 1.65	1.97 ± 1.23	2.83 ± 2.04
Mean Velocity (μm/s)	0.15 ± 0.15	0.11 ± 0.08	0.22 + 0.19
Median Velocity (μm/s)	0.09	0.09	0.18
Range (μm/s)	0.02 - 0.70	0.02 – 0.35	0.03 – 0.70
Run Length (μm)	4.65 ± 3.29	3.95 ± 2.46	5.58 ± 4.00
n	67	38	29

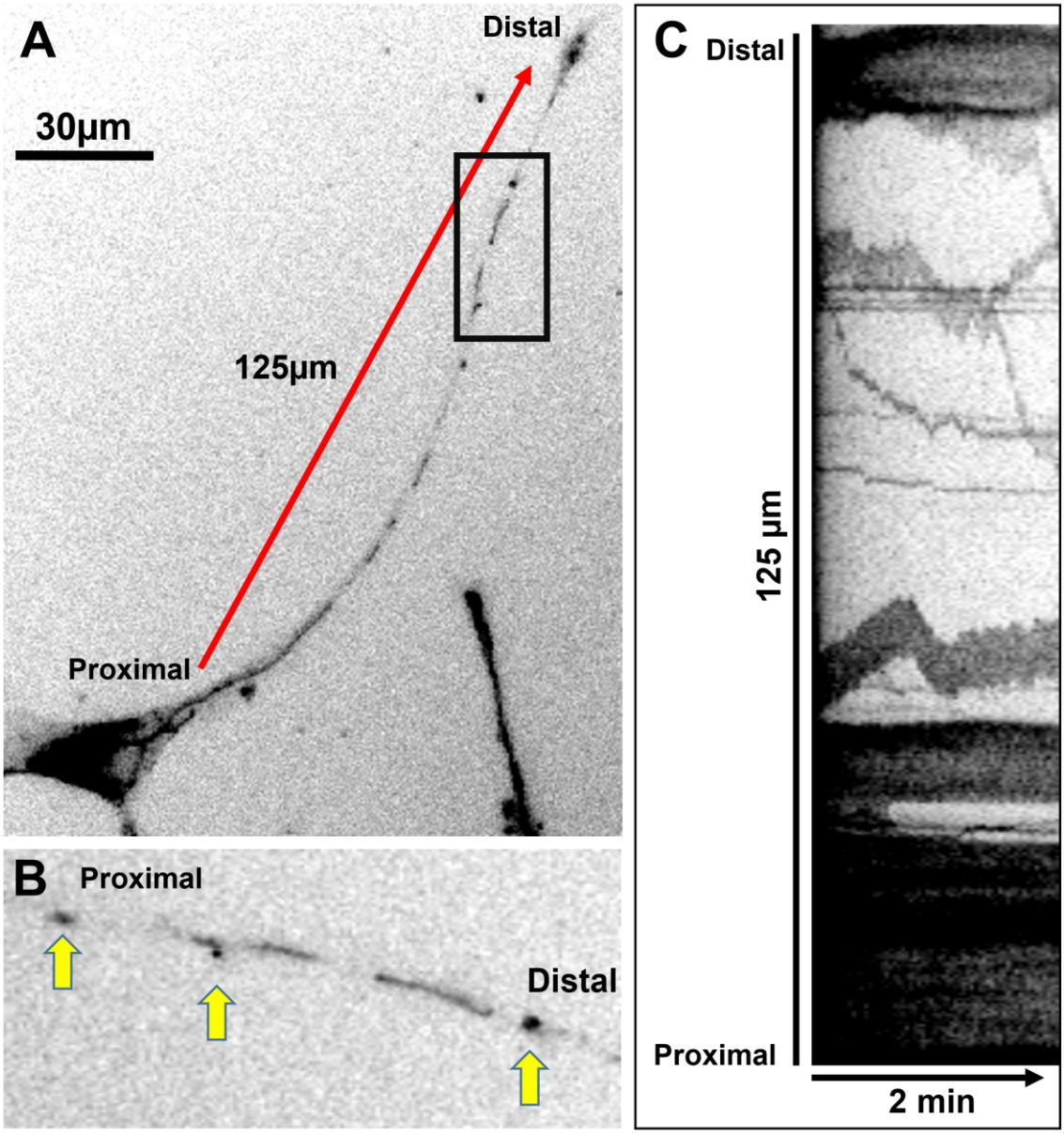

Figure 3.16. Mitochondrial transport and kymograph quantification
A) Video frame from recorded MTS trafficking in a fully differentiated SH-SY5Y cell. The 125 µm neurite was traced and a kymograph representing mitochondrial transport was generated and quantified. Scale bar = 30µm. B) Inset highlighting individual motile mitochondria, rotated 90° clockwise for visibility. C) Kymograph generated from neurite in A). Anterograde movement events are represented by positively sloping lines. Retrograde movement events are represented by negatively sloping lines. Horizontal lines represent stationary mitochondria. Total time of recording = 120 seconds.

3.4. Quantification of Cellular Stress

3.4.1. TIA-1 Stress Granules

To determine the effects of microgravity on cellular stress, I visualized the expression of T cell-Restricted Intracellular Antigen (TIA1) in fixed SH-SY5Y cells with or without treatment of stressful stimulus, and quantified high resolution fluorescent images of TIA1 distribution patterns and SG formation. This quantification method was then used to generate a spectrum wherein the eventual quantification of TIA1 in microgravity exposed cells can be placed within and compared to GC cells. TIA1 is an RNA-binding protein primarily involved in post-transcriptional modification of RNA and is involved in the induction of DNA fragmentation during apoptosis (Fernández-Gómez et al., 2022). It is also a key component of stress granules (SGs), which are stress-related protein aggregates described in section 1.4. In cell culture experiments, immunostaining of stress markers including TIA1 may be performed to visualize and assess SG dynamics following application of an exogenous stressor, such as heat shock. The upregulation of various SG-forming and stress-related proteins has been widely demonstrated in genomic and proteomic experiments during microgravity exposure (Discussed in section 1.4.), implying that the effects of microgravity lead to downstream effects that may be stressful for cells.

To determine the effects of microgravity on TIA1 protein distribution patterns, I stained fully differentiated SH-SY5Y cells for TIA1 with or without immediate previous exposure to a heat shock (HS) stressor (43°C, 2-hours). HS treatment is known to yield robust TIA1 SG formation (Kedersha et al., 1999; Kedersha et al., 2000). As such, I chose HS stress as a positive control for quantification of TIA1 SGs and compared these results to ground control cells. Figure 3.17. A-D) demonstrates TIA1 SG formation prior to and following HS in differentiated SH-SY5Y cells on Earth. Following a stressful stimulus, TIA1 distribution within cells is rearranged from evenly distributed staining patterns towards the formation of multiple bright, speckled SGs and a translocation of protein expression from within the nucleus to the cytoplasm (Kedersha et al., 1999; Kedersha et al., 2000). Thus, I quantified 1) the number of cytoplasmic TIA1 puncta per cell, and 2) the relative nuclear TIA1 immunofluorescence per condition.

Cytoplasmic TIA1 puncta were quantified using ImageJ software as described in section 2.7.4. A nuclear mask was generated and applied to exclude nuclear TIA1 staining

in both control and HS treated cell groups. Following this, a threshold was applied at equal magnitude to images, to subtract background fluorescence and isolate bright TIA1 positive punctae. Statistical analysis revealed significant differences in the number of TIA1 punctae between control and HS treated cells (Figure 3.17. E). A second analysis was performed where the relative fluorescence intensity within the nucleus of control or HS-treated cells was quantified and compared. This analysis revealed statistically significant differences between relative nuclear fluorescence intensity of untreated versus HS-treated SH-SY5Y cells. Furthermore, both quantitative results align with the qualitatively identified increases in TIA1 punctae following HS, and qualitatively identified decreases in TIA1 signal within nuclei following HS (Figure 3.17 A-D), respectively. Thus, I concluded that the transformed SH-SY5Y cell line expresses a normal stress response phenotype, and that this phenotype can be quantified and analyzed using established methods in the field.

Following SH-SY5Y differentiation in actual microgravity on the MoSL, SG analysis and TIA1 redistribution analysis will be performed using these procedures. The values generated from microgravity-exposed cells may then be compared to the controls analyzed within this framework, and the degree of stress-induced TIA1 SG formation may be quantified with respect to a well understood stressor on Earth. Both quantitative and qualitative analysis of stress marker protein expression has never been performed in microgravity exposed cells, making these results significant for being the first of their kind.

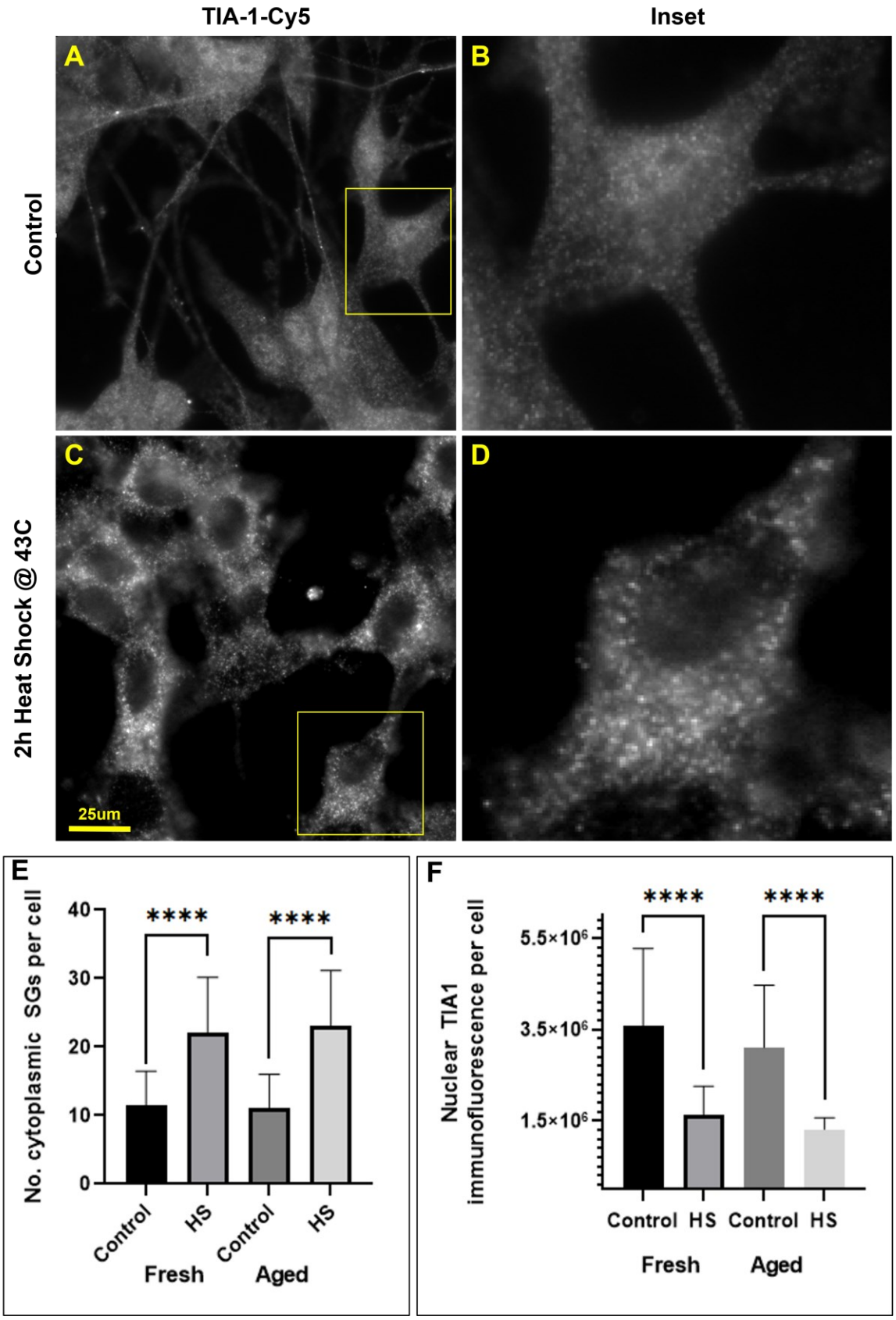
TIA-1-Cy5
Inset
A
B
C
D
Control
2h Heat Shock @ 43C
25um
E
No. cytoplasmic SGs per cell
40
30
20
10
0
****
****
Control
HS
Control
HS
Fresh
Aged
F
Nuclear TIA1 immunofluorescence per cell
5.5×10⁶
3.5×10⁶
1.5×10⁶
****
****
Control
HS
Control
HS
Fresh
Aged

Figure 3.17. TIA1 stress granule analysis
A) ICC of TIA1 in untreated, differentiated SH-SY5Y cells. B) Inset of A). C) ICC of TIA1 in HS treated, differentiated SH-SY5Y cells. Scale bar: 25μm. D) Inset of C). E) Quantification of the number of cytoplasmic puncta per cell positive for SG marker TIA1 in A) or B) (arrows). ****P < 0.0001 by unpaired Student's *t*-test, n=10 cells per group. F) Quantification of total nuclear TIA1 immunofluorescence. ****P < 0.0001 by unpaired Student's *t*-test, n=10 cells per group. Data presented as mean ± SEM.

3.4.2. Mitochondrial Network Analysis

To evaluate the effect of microgravity on mitochondrial network organization, I quantified the mitochondrial network in fully differentiated SH-SY5Y cells using Mitochondrial Network Analysis (MiNA) (Described in Section 2.7.2.). These quantification methods were used to generate a spectrum wherein the eventual quantification of mitochondrial network morphology in microgravity exposed cells can be placed within and compared to GC cells. Observations of increased oxidative stress in microgravity conditions (described in section 1.4.) have led many to presume these observations are resultant of disruptions to mitochondrial physiology. MiNA allows for the quantification of the dynamic mitochondrial network, which is representative of changes in overall mitochondrial morphology resulting from mitochondrial fusion and fission.

To accomplish this goal, I analyzed high resolution images of fixed, differentiated SH-SY5Y cells with or without previous exposure to Carbonyl cyanide-p-trifluoromethoxyphenylhydrazone (FCCP), a strong disruptor of mitochondrial physiology. FCCP is a mitochondrial oxidative uncoupler, which results in severe disruption to mitochondrial physiology that are visually identifiable through observable of mitochondrial morphology. The results of mitochondrial network analysis in FCCP treated cells demonstrates fragmentation and reduced dynamics of mitochondrial network branching (Valente et al., 2017). Conducting MiNA on untreated and FCCP treated cells results in several quantitative outputs which all serve to identify differences in mitochondrial network dynamics. Data representing the mean number of punctate mitochondria per cell, number of networks per cell, branches per mitochondrial network, and branch length per mitochondrial network were obtained in treated and untreated cells, and then statistically analyzed.

Statistical analysis identified a significant increase in punctate mitochondria per cell and number of networks per cell, and a significant decrease in branch length per mitochondrial network following FCCP treatment. The number of branches per

mitochondrial network was not significantly different between conditions (Figure 3.16. C-F). These results indicate that FCCP is indeed capable of inducing fragmentation of the mitochondrial network in our SH-SY5Y cell line, and quantitative analyses confirm these observed differences in mitochondrial network morphology following FCCP treatment, as demonstrated in Figure 3.18 A-B.

Following SH-SY5Y differentiation in actual microgravity on the MoSL, MiNA analysis will similarly be performed using the procedures outlined in this thesis. The values generated from microgravity-exposed cells may then be compared to the controls analyzed within this framework, and the degree of microgravity-induced mitochondrial network dysregulation may be quantified with respect to a well understood control of disrupted mitochondrial physiology on Earth.

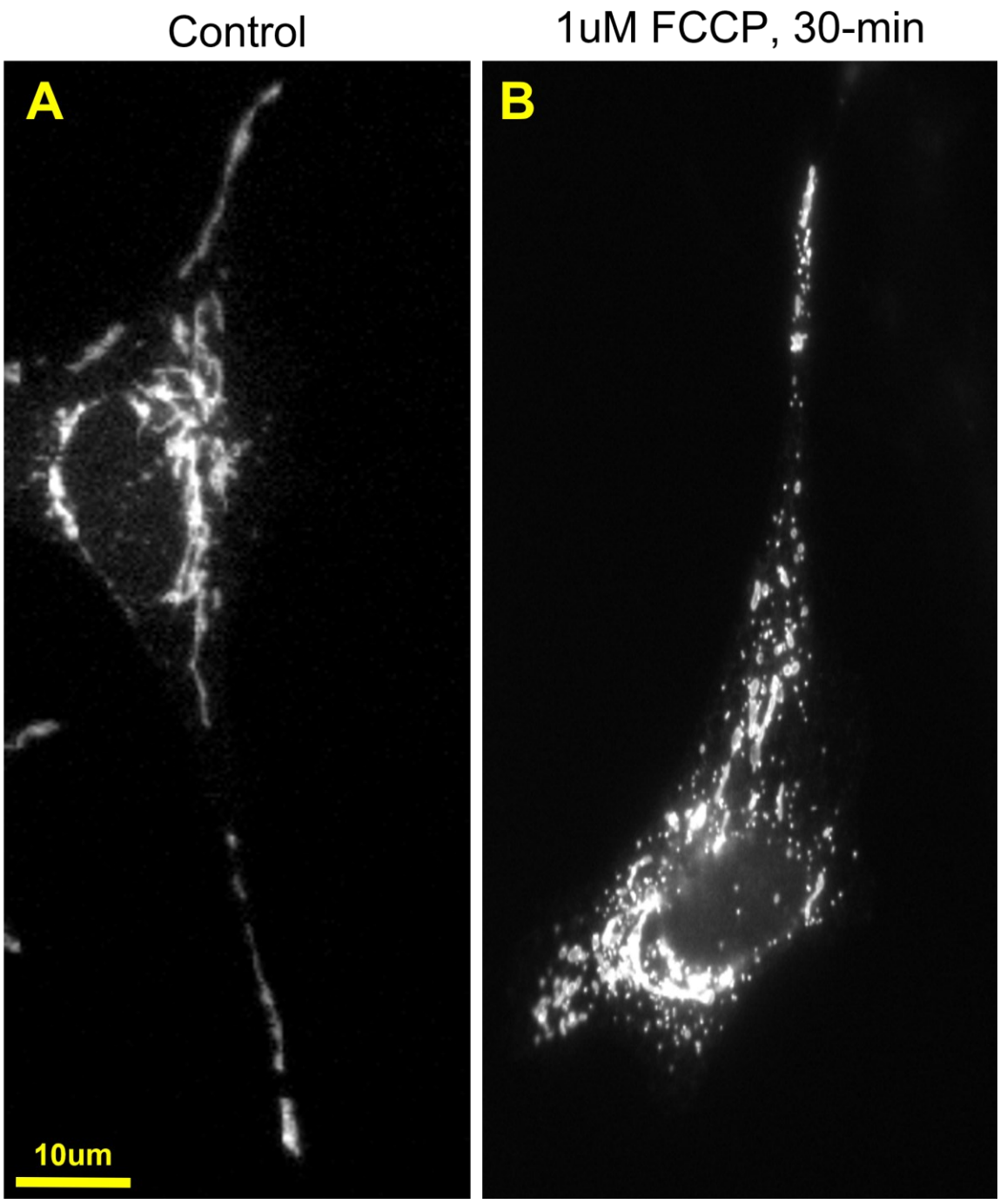
Control
1uM FCCP, 30-min
A
B
10um

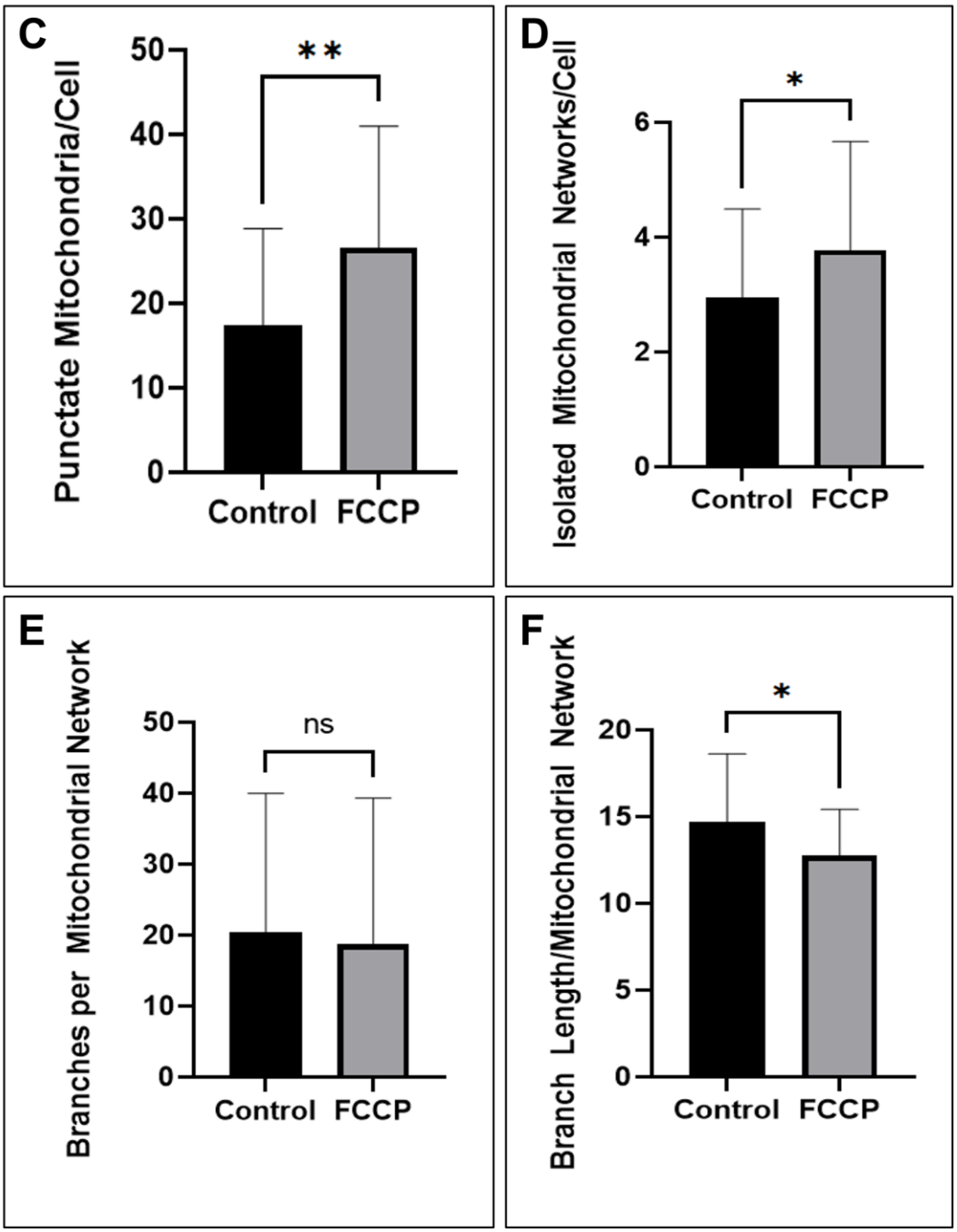

Figure 3.18. Mitochondrial network analysis of differentiated SH-SY5Y cells
A) Visualization of mitochondria and mitochondrial networks in untreated, differentiated SH-SY5Y cells. B) Visualization of mitochondria and mitochondrial networks following 30-minutes FCCP treatment in differentiated SH-SY5Y cells. C) Quantification of the mean number of punctate mitochondria per cell. D) Quantification of the mean number of mitochondrial networks per cell. E) Quantification of the mean branches per mitochondrial network. F) Quantification of the mean branch length per mitochondrial network. All data presented as mean ± SEM. *P<0.05, **P<0.01. n=35 cells per group. All analyses performed using an unpaired Student's *t*-test.

Chapter 4. Discussion

4.1. Summary

Microgravity is one of the unique environmental pressures organisms must face while visiting outer space. To counteract the pressures of the microgravity environment, physiological systems must adapt by utilizing and adjusting their innate homeostatic responses to fit the perceived environment. Because humanity attained the level of technology to reach outer space relatively recently and the cost of conducting research in space is prohibitively expensive, there are major gaps in our understanding of the mechanisms by which physiological systems adapt to microgravity. Among the knowledge we do have, however, is that the cell cytoskeleton is one of the systems that is most affected by microgravity pressures. The cytoskeleton is particularly important in neurons, whose polarisation is both dependent on cytoskeletal structure, and further requires active transport along the cytoskeleton to fulfill subcellular homeostatic needs.

In hopes to characterise the effect of microgravity on the neuronal cytoskeleton, intracellular trafficking, and cell health, this thesis details a strategy of experiments and procedures that will allow for the eventual assessment of the effect of microgravity on said functions. Through collaboration with HNu Photonics and use of the Mobile SpaceLab and BioChips, my research characterises SH-SY5Y cells as a neuron-like model that will be sent to outer space for the purposes of attaining dynamic cytoskeletal data in a neuronal model in outer space. This will lead to the first ever quantification of cytoskeletal dynamics and axonal transport in actual microgravity.

To quantify the effects of microgravity on cytoskeletal organization, I generated a dataset highlighting the ground-control behaviour of SH-SY5Y cells. First, I quantified normal microtubule dynamics in SH-SY5Y cells by tracking EB3 comets in the neurites of differentiating cells. EB3 velocity was constant throughout differentiation, with an average velocity of 0.20 ± 0.06 μm/s. I then quantified the velocity of neurite advancement during outgrowth as a proxy for cytoskeletal dynamics. These experiments demonstrated that neurites advance at a rate of 28.57 ± 13.7 μm/h during periods of RA-mediated differentiation, which is when a majority of outgrowth occurs. Lastly, I developed a semi-quantitative strategy for the comparison of actin and microtubule cytoskeletal

ultrastructure in microgravity-exposed cells to ground control cells that were treated with or without pharmacological-induced disruption to cytoskeletal ultrastructure.

To quantify the effects of microgravity on axonal transport of mitochondria, and by proxy microtubule organization, I quantified mitochondrial transport dynamics in SH-SY5Y cells. Mitochondria in differentiating SH-SY5Y had a mean velocity of 0.15 μm/s and an average run length of 4.65 μm (Table 3.1.). Calculation of mitochondrial transport flux indicated a slight bias towards retrograde over anterograde transport (2.83 retrograde versus 1.97).

Finally, to study the effects of microgravity on cellular health, I focused on cellular stress granules and mitochondrial network morphology to generate a quantitative framework in which these measures can be reliably attained in SH-SY5Y cells, and further, used to create a scale wherein the effects of microgravity on cell health and mitochondrial network dynamics can be weighed.

In the future, the MoSL will travel to outer space and collect data representing many of these experiments for the very first time in microgravity. Using this thesis as an outline, I have generated a strategy to quantify and compare these data to controls on Earth gathered under approximate conditions of how the cells will be cultured in microgravity. The results of these experiments will play a pivotal role in expanding our current understanding of neuronal physiology, cytoskeletal dynamics, and cell health in actual microgravity conditions, and may help uncover sub-cellular mechanisms that could be targeted for therapeutic intervention to better protect the health of astronauts sent on spaceflight missions.

4.2. Expected Experiment Outcomes

In section 1.5., I outlined my experiment goals and hypothesized how microgravity may affect the outcomes of these proposed experiments. These goals were generated based on previously observed effects of microgravity on cell cultures; what makes this thesis unique is that the specific methods chosen to evaluate these effects have never been possible to attempt without the use of the MoSL. Thus, my hypotheses have sound rationale backing them, and I can reasonably expect certain experimental outcomes.

Cytoskeletal structure and organization are disrupted in cellularodels exposed to microgravity. Previous experiments demonstrated irregular actin and microtubule organization, shortening of polymerized microtubules, thinning of F-actin, and irregular expression and distribution of cytoskeletal monomers (Carlsson et al., 2003; Grenon et al., 2013; Hughes-Fulford & Lewis, 1996; Rijken et al., 1992; Ulbrich et al., 2011). I hypothesized that microgravity-induced cytoskeletal disruption will impair (1) neurite outgrowth, (2) EB3 transport dynamics and (3) cytoskeletal ultrastructure. Neurite outgrowth is dependent on microtubule elongation, and disruption to microtubule assembly impairs neurite outgrowth. When neurite outgrowth is impaired on Earth using treatment of microtubule disrupting drugs, the velocity of neurite extension is slowed, and neurites may spend more time in a paused state rather than in active growth (Athamneh et al., 2017; Verstraelen et al., 2017). Furthermore, neurite length is decreased following impaired outgrowth on Earth (Lee, 2022; Thomson, 2021). The experiments outlined in section 3.2. will allow me to quantify the velocity of neurite outgrowth, the relative time spent in each stage of neurite outgrowth, and the lengths of neurites. Because (1) neural differentiation still occurs in simulated microgravity environments, and (2) there is no evidence that microgravity affects the ability of microtubules to polymerize at the biochemical level (i.e., effects observed via nocodazole or taxol treatment), I expect a mild reduction of neurite outgrowth velocity resultant of microgravity-exposure, and a net effect of shortened maximum length of neurites (Pani et al., 2013; Pani et al., 2016). Following this, if microtubule dynamics are mildly disrupted, then a mild reduction in EB3 velocity within differentiating neurites is expected and this result would confirm my predictions. Lastly, because the effects of microgravity on cytoskeletal structure are well documented (priorly discussed in this section), I do not expect qualitative results that differ substantially from the effects listed in this section (irregular actin and microtubule organization, shortened microtubules, etc.). If such disruptions to cytoskeletal organization are observed, my proposed analysis methods in section 3.2 will capture these changes, and my proposed quantitative analyses will score actin and microtubule cytoskeletal organization to an intermediate range of values lying between what was observed in ground control groups and depolymerization controls (Latrunculin-A : Actin, Nocodazole: Tubulin) (Figure 3.13. E).

I hypothesized that microgravity-induced disruption of the microtubule cytoskeleton will impair trafficking of mitochondria. Quantification of axonal trafficking

depends on certain minimum standards of video capture that have never been feasible in microgravity prior to the use of the MoSL, and as such it has never been studied. My hypothesis remains reasonable, because proper microtubule organization is required to serve as the tracks that kinesin and dynein use to transport cargo, and the disruption of microtubule tracks has a net effect of slowing bidirectional axonal transport (Biswas & Das Sarma, 2014). If microgravity is a mild disruptor of microtubule organization, then trafficking of mitochondria may be impaired, but not inhibited (Samson et al., 1979). Based on the quantification methods outlined in section 3.3., these effects will likely manifest as reductions in flux, mean run length, and velocity. Trafficking dynamics are a function of the proper binding of kinesin and dynein motors to microtubules (Abraham et al., 2018). Because axonal trafficking has never been observed in microgravity conditions, any estimation of potential results in these experiments are implied based on the underlying mechanics of microtubule and motor protein binding affinity. However, axonal transport dynamics can also be affected by changes to the expression of various regulatory scaffolding proteins, such as TRAK1/2, Milton, and JIP1 in mitochondrial systems or due to changes in the regulatory systems that modulate the net direction of mitochondrial trafficking (Nirschl et al., 2017). As previously discussed, our SH-SY5Y cell line does not form mature neuronal synapses which may indicate reduced metabolic needs within neurites, therefore resulting in reduced anterograde trafficking of mitochondria. As such, these experiments are novel and interesting, as they will demonstrate the dynamic capture of axonal transport in microgravity for the first time and may inform us of changes to microtubule dynamics but may not shed light on changes to the underlying motor protein or scaffolding dynamics if those systems are poorly represented in the SH-SY5Y model of neuronal systems.

Lastly, I hypothesized that oxidative stress induced from microgravity exposure will (1) impair mitochondrial physiology and (2) result in expression of stress marker proteins. Oxidative stress resultant of simulated microgravity exposure has been observed in neuron-like models, and aberrant alterations to expression of antioxidant factors and stress marker proteins including TIA1 have been observed in actual microgravity (Feger et al., 2016; Kumar et al., 2021; Kwon et al., 2006; Ulbrich et al., 2011). Furthermore, oxidative stress is damaging to mitochondrial physiology and may cause disruptions to mitochondrial morphology and networking dynamics (Valente et al., 2017). The experiments outlined in this thesis will semi-quantitatively assess relative levels of cellular

stress and mitochondrial network morphology via fluorescent intensity analysis of TIA1 distribution and stress granules, and MiNA of mitochondrial networks. Investigation of these outcomes is often done in a fully quantitative format, and as such, there are no qualitative or semi-quantitative experiments in the literature in microgravity conditions that I may draw from to hypothesize the effects of microgravity on these measures. However, the worst outcome of unresolved cellular stress is apoptosis, and while mild levels of apoptosis are seen in cellular systems following microgravity experimentation, the levels observed are not indicative of an inability to resolve an extreme stressor (Lin et al., 2016). Thus, I hypothesize that the effect of microgravity-induced cell stress on stress granule expression and mitochondrial network morphology will be mild, resulting in the values obtained for TIA1 and MiNA quantification to lie in an intermediate range between ground control and heat shock (TIA1) or ground control and FCCP (MiNA).

4.3. Critique of Methodology and Results

In section 3.1., I characterized whether the dually transformed SH-SY5Y cell line exhibited normal parental cell line characteristics. I assessed this via qualitative assessment of cell morphology and long-term survivability of cells in a normal cell culture environment. While I was able to conclude that there were no significant differences between the parental and transgenic cell lines, there are additional experiments that may be required in the future to further support this conclusion. In Figure 3.1. I demonstrated representative images of the transformed SH-SY5Y cell line throughout the differentiation procedure. The morphology and timeline of differentiation was comparable to SH-SY5Y cells in literature but was not compared directly to the parental cell line. A more in-depth analysis should be inclusive of comparison to the parental cell line, not just the cells as compared to literature. To accomplish this, one would need to obtain and thaw a stock of the parental cell line from liquid nitrogen storage, differentiate those cells, and take images of the cells throughout differentiation. Another opportunity to enhance the results in this section is in the assessment of long-term survivability. In Figures 3.2. and 3.3., I demonstrated a timeline of SH-SY5Y cell culture survivability on MoSL hardware and characterized the progression of cell death post-differentiation after 20-days. I concluded that this timeline was inline with literature and was not different from parental cell line characteristics. However, this analysis was based on estimated survivability and qualitative observation. In literature, authors often use a live/dead assay such as trypan

blue to assess viable cells. The lack of this assay was not an oversight, however, as the NASA Ames team approved the use of this cell line based on the data presented without any additional testing required. Following this assessment, the HNu Photonics team decided to place a greater emphasis on higher priority results, and no live/dead assay was performed. In the future, this assay would be a simple addition to strengthen the conclusions made in this section.

In section 3.2., I investigated cytoskeletal dynamics of SH-SY5Y cells in a ground control setting. Here, I presented a strategy to assess disruption to actin and microtubule cytoskeletal systems using a qualitative approach. I concluded that my methodology was able to detect changes to microtubule cytoskeletal structure following administration of the microtubule disruptor nocodazole. One drawback to this approach was a lack of supplementary quantitative analyses to strengthen my assertions. In literature, it is common for cytoskeletal disruptions to be described in a qualitative manner, and my assessment in this report follows typical standards of said literature. In a more thorough analysis, quantitative measures such as microtubule linearity would be provided in addition to qualitative observations. However, computer programs that can generate such quantitative measures often require source imaging in a much higher resolution than that with which my analyses were conducted with. The images used in my analyses are of adequate resolution to investigate changes to cytoskeletal structure, but not *ultra*structure, the likes of which would require access to a facility with super resolution microscopy capabilities. In the future, if access to such microscopy capabilities were granted, then the coverslips utilized in my experiments could be re-imaged, accompanied with coverslips from the BioChip containing SH-SY5Y cells that have been differentiated under microgravity conditions. If such images are captured, there exists a suitable algorithm in MatLab Software that may be applicable to glean quantitative data representing changes to SH-SY5Y cytoskeletal structure, dubbed “FiberScore”. An example of a quantitative assessment using FiberScore following nocodazole treatment is presented in Figure A.4. Similar to the example provided, this algorithm should be able to numerically represent the qualitative changes observed in the cytoskeleton of our SH-SY5Y cell line following nocodazole treatment or long-term microgravity exposure.

In section 3.2. and 3.4., I utilized a quantitative approach to fluorescent intensity distribution analysis termed “Corrected Total Cell Fluorescence” (CTCF). The CTCF protocol (discussed in section 2.7.3.) generates a relative fluorescent intensity score for

isolated cells in an image and corrects for background fluorescence. This analysis was performed to quantify actin cytoskeletal disassembly (section 3.2.3.) and nuclear stress granule intensity (section 3.4.1.). Using CTCF, a statistically significant difference between controls and post-treatment groups was observed in both use cases (actin cytoskeleton disassembly following latrunculin treatment, and stress marker redistribution following heat shock stress). However, it was noted that because of extreme differences between the values prior to, and following treatment conditions in both of these experiments, it is not clear whether the CTCF protocol would be able to capture intermediate differences. To better understand whether CTCF can quantify intermediate effects of actin cytoskeleton disruption and stress marker relocalization, one useful approach would be to apply the CTCF protocol to cells that were treated in a dose-response mannerism. For example, in the case of heat shock, some groups could be included where cells were exposed to heat shock stress for an intermediate range of times (i.e. 30-min, 60-min, 90-min, in addition to the 120-min presented). Then, the CTCF protocol could be applied, and the sensitivity of the protocol may be assessed. Therefore, if the effects of microgravity on cellular stress and/or actin cytoskeletal organization are mild, we would know beforehand whether the proposed quantitative scoring algorithm is appropriate for assessing mild changes.

4.4. Setbacks and Complications

This thesis was originally intended to include data obtained from microgravity-exposed cells cultured in the MoSL. Unfortunately, due to the unforeseen circumstances of the CoViD-19 pandemic, factors outside of my control such as spaceflight launch delays, and supply chain shipment delays have resulted in an inability to complete these experiments before the completion of my graduate program. Coordination of space flight missions and research is a delicate task with many moving parts behind the scenes, and I appreciate the immense amount of work that my colleagues and collaborators at Simon Fraser University, HNu Photonics, and NASA have contributed to the planning and progress of this project thus far. Current projections place the MoSL's inclusion on SpaceX27, scheduled for January 2023, thereafter this project can be completed and published.

Other complications in project design and data collection were generated in the necessity to analyze SH-SY5Y cells in an approximation of normal cell culture techniques

that will closely resemble the conditions of the MoSL in actual microgravity. One such complication is the uncertainty in precise launch date and subsequent MoSL integration to a power source on the ISS. The initiation of differentiation and experiment procedures cannot begin until the MoSL has been integrated into an ISS EXPRESS rack, where power and data storage capacity can be supplied to the MoSL. Thus, SH-SY5Y cells must remain in an undifferentiated state for an uncertain amount of time, potentially for a maximum of 5-days within MoSL hardware. Cells exhibit normal proliferative activity during this time, and visible surface area between cells is progressively reduced as cells proliferate, leading to clumps and growth within proximity of each other. This waiting period was also integrated into cell culture conditions on Earth so that ground control experiments could closely mirror microgravity-experiments. This ultimately hinders data collection, as the imaging and analysis protocols for neurite outgrowth and axonal trafficking depend upon being able to observe unobstructed neurites and their extensions into empty space. Neurite-expressing cells preferentially grow neurites in the direction of other cells based on chemically sensed axon guidance factors, and the process becomes difficult to visualize if cells are in close proximity, resulting in neurite overlap and growth overtop cell bodies (Aberle, 2019). Traditional differentiation experiments using SH-SY5Y cells analyse neurites in equidistantly spaced cells, where individual neurites are visible and unobstructed (Dwane et al., 2013).

Another complication in project design was due to limitations in availability of replicate BioChips (polycarbonate glass slides that cells affix to, discussed in section 2.9.). Current MoSL hardware permits the loading of two BioChips, which is equivalent to eight wells (four per BioChip) of independently plated SH-SY5Y populations. Of those eight wells, only four will be available for immunological staining in the post-flight experimentation stage of the project. The other four coverslips would be treated with either taxol or nocodazole prior to the completion of the experiments, which will likely impact the results and expression of any potential proteins of interest (Figure 4.1.). Thus, the limited number of coverslips was a key consideration when designing post-flight immunostaining experiments. Post-transfection, SH-SY5Y cells expressed two fluorophores, taking up the red (RFP-EB3) and green (GFP-MTS) colour filters on our microscope. In the context of fluorescence microscopy, these colour channels are now unavailable to use for the staining and expression of alternate protein markers in any of the transformed cells. It was collectively decided that three coverslips would be stained for actin or tubulin in the far-

red channel with one replicate, and further, that all three will be co-stained with DAPI in the blue channel. The last remaining coverslip would be stained for TIA1 and DAPI, using the far-red and blue channels respectively. Attempting to utilize more than four different protein fluorophores in a single population of cells would likely result in signal bleed through and was not considered a viable strategy. Alternative ideas to increase protein visualization and obtain more data were considered, such as quantum dots. Quantum dots are nanoscale crystals that are excitable by wavelengths in the ultraviolet spectrum and demonstrate highly specific emission spectra, which would solve the problem of bleed through when using traditional fluorophores (Barroso, 2011). However, this approach was deemed prohibitively expensive and impractical, and was not pursued further. Ultimately, this meant that alternative experiments, such as labelling additional stress markers, neuronal markers, markers for DNA damage, or markers of cell viability were not considered. If future flights or changes to MoSL hardware permit more flexibility in utilizing replicate coverslips, these ideas may be revisited at that time.

Another complication was identified in detection, but not expression of the stably expressed GFP-MTS construct in our SH-SY5Y cell line. To mimic the data collection regimen and quality that will be provided by the MoSL, an upper limit in imaging magnification was placed on the collection of dynamic data (neurite outgrowth, RFP and GFP recordings). In practical terms, this meant that images were captured on our microscope with a 40X dry air objective rather than a higher magnification oil objective. Immersion oils have a similar refractive value to the glass slides and coverslips the SH-SY5Y cells are grown on, thus reducing the distortion that occurs with higher levels of magnification. Mitochondria are small organelles with complex and dynamic morphologies. As such, detection of fine details in mitochondrial morphology and movement is empowered by having the ability to use oil immersion techniques. In these experiments, it was not possible to resolve the fine details of mitochondrial morphology and transport dynamics using the air objective, and allowances had to be made in the quantification of mitochondrial transport. Mitochondrial transport run lengths have been reported to be as low as 0.7 μm (Narayanareddy et al., 2014). In the 40X air conditions, a short run length, regardless of velocity, was indistinguishable from a stationary mitochondrion. When a higher magnification 63X, 1.2NA oil objective was used, these short run lengths were visible and quantifiable. Figure 3.18. demonstrates an example of high-resolution visualization of mitochondria in our cell line via oil immersion microscopy.

Additionally, a video of high-resolution mitochondrial transport has been included in Appendix B. In conclusion, my quantification of axonal transport of mitochondria is acknowledged to represent the movement of only long run length trafficking events and may not necessarily represent the dynamics of the bulk of mitochondrial transport. This conjecture limits the usefulness of these experiments in extrapolating conclusions mitochondrial trafficking in actual neurons but are still useful in the context of observing changes to microtubule dynamics and characterizing whether axonal transport is affected by microgravity exposure.

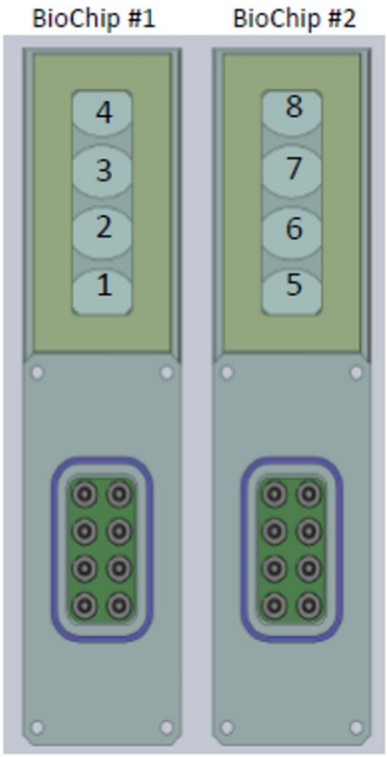

Well number	Proposed
1 & 5	Untreated
2 & 6	Untreated
3 & 7	Nocodazole
4 & 8	Taxol

Figure 4.1. Proposed post-differentiation treatment plan of BioChip wells
The 8 wells containing fully differentiated cultures of SH-SY5Y cells will be divided into groups of 4 wells with no treatment, two wells treated with nocodazole, and 2 wells treated with Taxol. Post-flight immunostaining is limited to untreated wells.

4.5. Potential Mechanisms of Microgravity Sensing and Other Downstream Effects

The current understanding of the effects of microgravity on the cell cytoskeleton and its associated processes are in large part based on non-dynamic types of information. This information is traditionally obtained by methods that are more accessible in microgravity conditions, and include fixed-cell imaging, immunoblot analyses, and proteomic and genomic expression experiments. While the usefulness of such experiments is not in question, it is a fact these types of experiments by themselves are not sufficient to fill every gap in the knowledge. Dynamic data, such as neurite outgrowth, EB3 transport, and axonal transport of organelles that can be obtained via experimentation on living cells as described in this thesis may be exceedingly useful to help elucidate underlying mechanisms of physiologic responses to microgravity. For example, the mechanisms by which cells initially sense microgravity, or how the cytoskeleton becomes disorganized are not known. Elucidating these mechanisms, and the inner workings of other steps within downstream pathways may help us gain a better understanding of the overall physiological response to microgravity in neurons and elucidate potential therapeutic targets in organisms. Here, I review previous research and proposed mechanisms of gravity sensing (gravisensing) in neurons. I then explore how the mechanics of gravisensing may directly affect neuronal cytoskeletal organisation, and further, how cytoskeletal disruption can lead to other negative downstream effects including impaired neuronal morphology, axonal degeneration, mitophagy, and cell stress. Finally, I will propose a unified pathway of neuronal dysfunction in microgravity based on these discussions and consider how the experiments proposed in this thesis may help elucidate the mechanisms underlying each step in this pathway.

4.5.1. Mechanics of Gravisensing

The mechanism by which the cytoskeleton converts change in mechanical force into electrical and chemical signals in the context of microgravity is not fully known. Normally, both specialized and non-specialized mammalian cells have innate mechanosensing ability due to the tensegrity architecture of the actin and microtubule cytoskeletons. Tensegrity is an engineering design principle that is applicable when a set of compression elements is opposed and balanced by a continuous tensile force, creating a pre-stress that stabilizes the entire structure (Grimm et al., 2011; Gardiner, 2021). In eukaryotes, this

pre-stress is elicited from multiple sources such as Earth's constant gravitational field or the pull of cell-cell and cell-extracellular matrix (ECM) adhesions. When cells experience increased mechanical loading, one mechanism to counteract this loading is activation of the "cytoskeletal strengthening" pathway. During this pathway integrin-mediated cell-ECM adhesions are enhanced through increased expression of cytoskeletal proteins and other related stabilizing complexes. (Bachir et al., 2017). Following cytoskeletal strengthening, cells are able to withstand increased amounts of mechanical pressure.

There are two hypotheses that are thought to play primary roles in activation of the cytoskeletal strengthening pathways. The first is through increased detection of free focal adhesion proteins. Mechanical stress such as shear and compression can cause cell detachment from ECM, which is mediated by various factors including integrin binding affinity. The increase in cell detachment leaves a footprint containing free focal adhesion proteins, and increased levels of these detached proteins can activate downstream pathways that lead to cytoskeletal strengthening and subsequent increases in integrin binding affinity. Integrin binding affinity can be modulated via presence of cations and leads to increased focal adhesion strength and quantity. Cytoskeletal strengthening also occurs due to increased translation and interaction with proteins such as vinculin (Bachir et al., 2017; Choquet et al., 1997; Fuhrmann & Engler, 2015; Gardiner, 2021). Vinculin stimulates actin polymerization and is a part of the focal adhesion complex, which nucleates actin filaments and acts as a crosslinker between the actin cytoskeleton, the plasma membrane, and the extracellular matrix (Bachir et al., 2017). Due to Vinculin's role as an intermediary protein between the actin cytoskelon and the focal adhesion complex, it has emerged as an interesting target for those studying the mechanics of gravisensing and microgravity.

A second possible mechanism for mechanical signal transduction in gravisensing is via mechano-sensitive ion channels (MSCs). MSCs are expressed in a variety of specialized as well as non-specialized cell types, including neurons (Cho et al., 2002; O'Hagan et al., 2004; Gaub et al., 2019; Sharif-Naeini, 2020). One of the main mechanisms proposed for MSC activation is direct linkage to the cytoskeleton (Hayakawa et al., 2008). In this model, tension in the cytoskeleton causes a conformational change in MSCs to an open state, followed by Ca^{2+} influx, and activation of downstream pathways involved in cell migration and cytoskeletal morphogenesis (Doyle and Lee, 2005; Munevar et al., 2004; Naruse et al., 1998; Tanaka et al., 2005). Further proof for this model is that

MSCs show a loss of mechanosensitivity when examined in a cytoskeleton free membrane (Zhang et al., 2000).

In microgravity, it is hypothesized that these pathways work in the opposite direction. That is to say, the unloading of mechanical pre-stress elicited by Earth's gravitational field is sensed, and cytoskeletal strengthening pathways are downregulated as a result. In this context, decreased cell-cell and cell-ECM interactions mediated by integrin and other focal adhesion proteins occurs less frequently following microgravity exposure. Less cell detachment and presence of fewer free focal adhesion proteins may inactivate or downregulate the homeostatic baseline of cytoskeletal strengthening pathways, resulting in a new baseline of pre-stress that is elicited on cells based solely on osmotic and hydrostatic pressures within tissues. Thus, cytoskeletal strength is regulated in accordance with a lower homeostatic baseline, which may explain why cytoskeletal disruptions are observed without complete ablation of structure and organization. In the alternate mechanism, if MSCs are involved in gravisensing, then microgravity may result in a net decrease in cytoskeleton-induced conformational change in MSC structure to the open state, thus attenuating activity of pathways downstream of MSC activation, such as cell migration and cytoskeletal reorganization. Therefore, cytoskeletal-based behaviours and functions which rely on proper cytoskeletal organization including neurite outgrowth and axon stability may be affected. Unfortunately, providing conclusive evidence of this model relies on conducting electrophysiological manipulation of MSCs combined with simultaneous manipulations of the cytoskeleton, a difficult task based on current technological barriers which is even more difficult in space (Hayakawa et al., 2008). Furthermore, the physiological function of many MSCs is not yet understood even on Earth, and a "force-sensing domain" has not yet been identified in MSC molecular structure (Árnadóttir & Chalfie, 2010; Gantenbein et al., 2018; Haswell et al., 2011; Wuest,).

4.5.2. Downstream Effects of Neuronal Cytoskeletal Disruption

In chapter one, I explored how neurons are reliant on regulation of cytoskeletal dynamics in the actin and microtubule networks to differentiate, maintain polarization, and regulate intracellular trafficking. I also explored how both short and long-term microgravity exposure is known to disrupt cytoskeletal dynamics in various cell lines including neurons. Some of these effects include reductions in the expression of actin and microtubule

subunits, reductions in expression of cytoskeleton-associated proteins, shortened microtubule polymer lengths, and major disruptions of both the actin and microtubule cytoskeletal networks. Following these disruptions, it is reasonable to expect that neuronal functions which are reliant on proper cytoskeletal organisation may also become impaired in microgravity.

To start off, I will consider how microgravity's effects on the actin cytoskeletal may sensitize neurons to axonal degeneration. It is already known that disruption to F-actin organisation is linked to increased susceptibility to axonal degeneration in neurons in normal cell culture conditions. These effects are likely due to the reliance of axonal structure on the presence of the membrane-associated periodic skeleton (MPS). The MPS is highly expressed throughout axons, where it is thought to support the extreme physical and structural conditions that axons must resist during their lifespans (Xu et al., 2013). The MPS is a supramolecular protein structure consisting of periodic, equidistantly spaced transverse F-actin rings separated by αII/βII-spectrin tetramer "spacers" extended along the length of the axon (Xu et al., 2013) (Figure 1.2.). The structure and function of the MPS has caused many to suggest that it may be necessary for the structural stability of the axon, but studies have shown that destruction of the MPS is not sufficient to cause axonal destruction (Zhong et al., 2014; Valakh et al., 2015; Qu et al., 2017). Rather, it has been shown that in situations where the axon may encounter degenerative stimuli, pharmacological stabilization of F-actin can prevent axonal fragmentation (Unsain et al., 2018). Thus, in a situation where F-actin polymerization or MPS structure is compromised due to environmental effect (such as microgravity), the axon becomes susceptible to degeneration, and neurons may exhibit physiology similar to early-stage neurodegenerative disorders such as AD, ALS, or PD (Salvadores et al., 2017; Unsain et al., 2018).

Similar experiments conducted on the microtubule cytoskeleton have shown that dysfunctional microtubule organization and dynamics are causative in many neurological diseases, and controlled disruption to microtubules or their associated proteins is sufficient to generate cell lines with disease phenotypes that mimic neurological disease in vivo (Franker & Hoogenraad, 2013; Matamoros & Baas, 2016; Millecamps & Julien, 2013; Sorbara et al., 2014). The disruption of microtubule-dependent function such as axonal transport is also implicated in several neurodegenerative disorders including ALS, AD, and PD. Because the axon is largely devoid of biosynthetic machinery, it relies on

anterograde axonal transport to supply axon terminals with cargos such as mitochondria, synaptic vesicle precursors (SVP), dense core vesicles (DCV), and other Golgi-derived proteins and lipids. Retrograde transport from distal portions of the neuron is of equal importance to prevent accumulation of toxic aggregates by clearing recycled or misfolded proteins (Hinckelman et al., 2013; Millecamps and Julien, 2013), as well as supporting synapse-cell body communication by signaling endosomes ferrying trophic signals (Olenick et al., 2019). Defects in transport can disrupt all these functions, are sufficient to induce neurodegeneration, and in extreme cases progressive neuronal cell death is observed (Perlson et al., 2010).

A third effect downstream of cytoskeletal disruption I will consider is disruption to mitochondrial physiology and cell stress. Mitochondrial dynamics are dependent on interaction with both the actin and microtubule cytoskeletal networks, and changes in cytoskeletal dynamics can regulate the balance of mitochondrial fission and fusion (Milner et al., 2000). Miro, the Ca^{2+} binding GTPase, is anchored to the outer mitochondrial membrane, where it interacts with scaffolding proteins such as Milton, thus mediating mitochondrial association to microtubules and transport proteins and regulation of mitochondrial motility (Moore & Holzbaur, 2018). The neuronal phenotypes observed for Miro and Milton mutations indicate that the active translocation of mitochondria along microtubules is critically important for neuronal health, especially during neuronal differentiation and neurite outgrowth (Lewis et al., 2016; Misgeld & Schwarz, 2017; Moore & Holzbaur, 2018). The actin cytoskeleton is also involved in mitochondrial motility and anchoring at the synapse. Various myosin motors facilitate mitochondrial dynamics, and research in drosophila motor neurons indicates that Myosin V and VI localize to axonal mitochondria and anchor mitochondria to actin filaments (Pathak et al., 2010; Moore & Holzbaur, 2018). Pharmacological disruption of the cytoskeleton results in disruptions to mitochondrial physiology and morphology, likely initiated through disturbances of the mitochondrial membrane (Michaletti et al., 2017). One factor of disrupted mitochondrial physiology is reduced expression of antioxidant factors such as CoQ10, COX5a, COX6C and CYB5A (Nguyen et al., 2021). The reduced expression of mitochondrial antioxidants hinders cell's ability to clear ROS and is directly responsible for increased mitochondrial and cellular oxidative stress (Bhatti et al., 2017; Oyewole & Birch-Machin, 2015). As discussed in section 1.4., increases in oxidative stress and ROS results in cellular and molecular damage, and the upregulation of cellular stress pathways is subsequently

observed (Kalmar & Greensmith, 2009; Oyewole & Birch-Machin, 2015). Oxidative stress has also been observed to underlie axonal degeneration in diseases such as X-linked adrenoleukodystrophy (X-ALD) and may also play a role in the mechanisms behind other neurodegenerative processes such as in AD or PD (Galea et al., 2012). Because there exists strong evidence of mitochondria playing a role in microgravity-mediated increases in oxidative stress (discussed in section 1.4.), a connection between mitochondrial dysfunction and neurodegenerative phenotypes may also exist or be amplified because of microgravity conditions (Asghari Adib et al., 2018). However, such experiments have yet to be conducted, and the results of experiments in this thesis may be informative as to whether a potential link exists in this space.

4.5.3. Summary and Proposed Unified Pathway

Based on the discussed mechanisms underlying neuronal and cellular function in microgravity environments, there is a great deal of observed overlap between physiological pathways that are influenced by these mechanisms, which often result in neuronal dysfunction. Neuronal physiology may be impaired by changes to any one of the following: cytoskeletal systems, exposure to cellular stress, and mitochondrial dysfunction. Furthermore, all these effects are known to be affected in some way by both simulated and actual microgravity, as discussed throughout this thesis. In this section, I will summarize the potential links between microgravity exposure leading to dysfunctional neuronal physiology, and outline each potential step within this pathway, highlighting sites of crossover and overlap (Figure 4.2.).

The experiments in this thesis target a variety of points in this proposed pathway. For example, visualization of the cytoskeleton and neurite outgrowth analysis can be informative of cytoskeletal dynamics and changes to neuronal morphology. Impaired axonal transport of mitochondria can inform us of cytoskeletal dynamics, as well as the potential for impaired synaptic and axonal energetics. In Figure 4.2., I indicate portions of my proposed pathway where my thesis' experiments may come into play to help elucidate mechanisms underlying the link between microgravity and neuronal dysfunction.

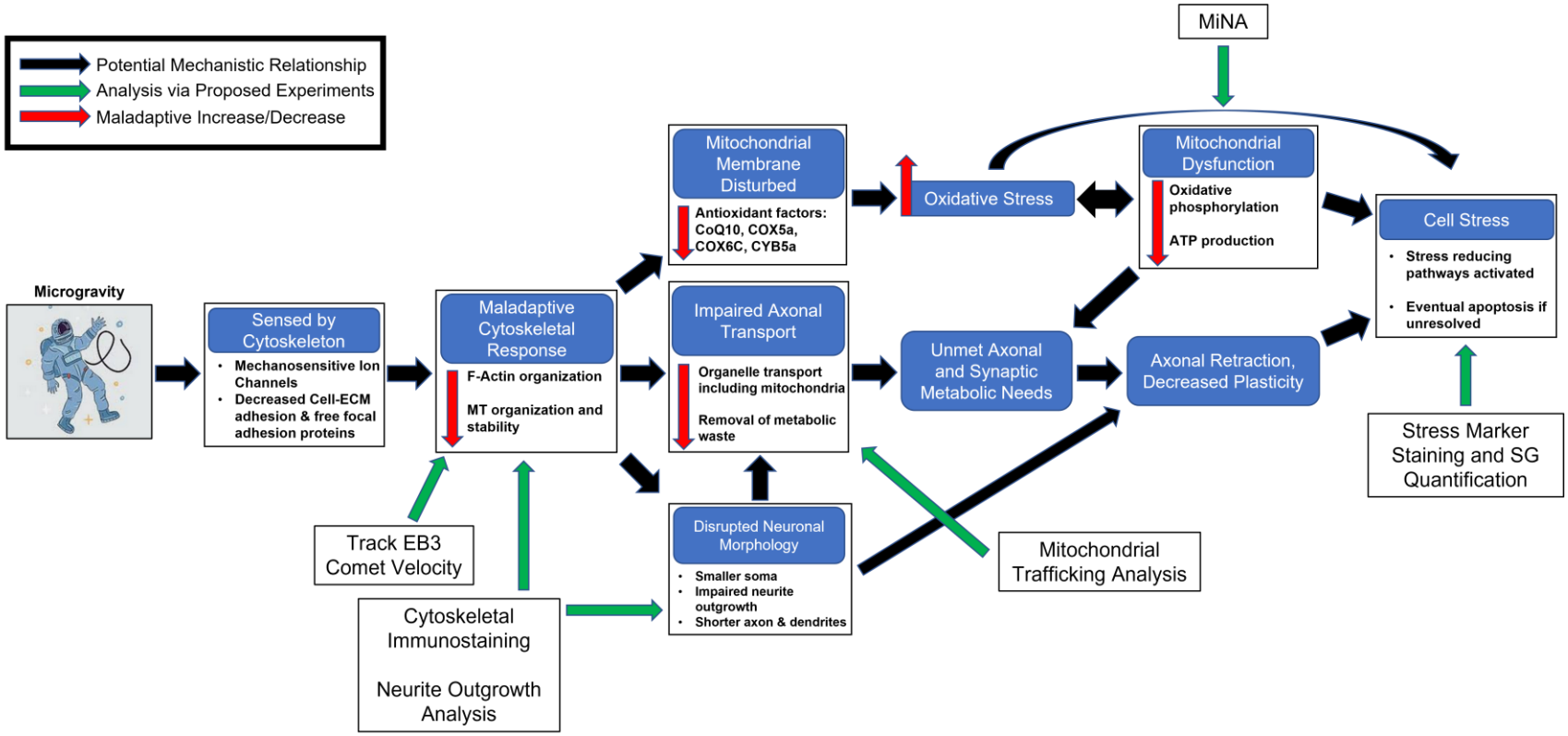

Figure 4.2. Proposed mechanism of neuronal dysfunction resulting from long-term microgravity exposure
Space microgravity causes cytoskeletal reorganization, which may affect a multitude of parallel downstream pathways, including mitochondrial and neuronal physiology. The effects of the dysfunction in these pathways overlap at times, and similar effects can be observed resulting from events occurring in separate pathways. Ultimately, the cell must cope with dysfunctional sub-cellular systems and may do so by upregulating proteins involved in cellular stress response pathways. Failure to ameliorate long-term cell stress may result in apoptosis of cultured cells. Experiments proposed in this thesis may help to elucidate mechanisms underlying the proposed pathways represented here (green arrows).

4.6. Future Directions and Applications

Following completion of data collection onboard the ISS in the MoSL, there exist several potential consequences for the future of MoSL and microgravity research, depending on the results. First, the results of these experiments may validate the MoSL as a platform for cell and tissue biology experimentation in low earth orbit, and thus it may become a permanent fixture on the ISS for future experiments. There are several parameters in the MoSL that will be monitored and evaluated both during and after the spaceflight mission relating to the MoSL's ability to keep cells alive, differentiate cells, acquire images, and retain high quality samples of fixed cells following experiment completion. Each parameter is graded based on either quality of data (for biological components) or number of replicates (for hardware components) based on numerous quantitative benchmarks (Figure 4.3.). These benchmarks are evaluated, and graded as acceptable, marginal, or unacceptable, as per Figure 4.3. If any parameter is deemed unacceptable following experiment completion, it may affect the final evaluation of MoSL as a cell culture platform depending on the rationale for failure. In such an event, adjustments to hardware or cell culture strategy may be required. In terms of biological parameters, MoSL will be evaluated for the number of replicate BioChips (up to four replicates with surviving cells post-launch), viability of cells (% of cells with neurites, % of cells with unhealthy morphology/rounded cell bodies), RA differentiation (% increase in neurite to cell body ratio) and BDNF differentiation (% increase in neurite to cell body ratio post-RA). In terms of hardware parameters, MoSL will be evaluated for the number of wells (up to four per BioChip) where phase contrast image acquisition was successful, the number of wells where fluorescent video acquisition was successful (for both GFP and RFP), and the sample fixation quality (number of replicates preserved in PFA, and number of subcellular markers preserved for labelling). A table of specific criteria of success for each aforementioned parameter is available in figure 4.3. Results other than those presented in Figure 4.3. may support/not support the hypotheses presented in this thesis, but those results will not be used to evaluate the success of the MoSL. For example, validation of the MoSL is not dependent on whether EB3 velocity is increased or decreased, but rather, on whether videos of EB3 transport were able to be collected, and if these videos were of sufficient quality to analyze. This principle applies to all other experiments presented here.

	Acceptable		Marginal	Unacceptable		Affected Specific Aims
Criterion	**Excellent**	**Good**	**Marginal**	**Poor**	**Failure**	
Flight/On-Orbit						
Number of replicates	4 replicates from each BioChip	3 replicates from each BioChip	2 replicates from each BioChip	1 replicate from each BioChip	0 replicates from each BioChip	1-3
Cell viability Post-Launch	>95% elongated cell bodies (~10 μM) with short neurites (healthy morphology), 0% rounded cell bodies (unhealthy morphology)	75-95% elongated cell bodies with short neurites, 10-25% rounded cell bodies	50-74% elongated cell bodies with short neurites, 25-50% rounded cell bodies	25-49% elongated cell bodies with short neurites, 51-75% rounded cell bodies	0-24% elongated cell bodies with short neurites, 76-100% rounded cell bodies	1-3
RA differentiation	>20% increase in neurite-cell body ratio post-recovery	10-20% increase in neurite- cell body ratio post-recovery	5-10% increase in neurite-cell body ratio post-recovery	0-5% increase in neurite-cell body ratio post-recovery	<0% increase in neurite-cell body ratio post-recovery	1-3
BDNF-differentiation	>10% increase in neurite-cell body ratio post-RA	1-10% increase in neurite-cell body ratio post-RA	0-1% increase in neurite-cell body ratio post-RA	-0-10% decrease in neurite-cell body ratio post-RA	>10% decrease in neurite-cell body ratio post-RA	1-3
Image Acquisition Microtubules	4 wells per BioChip, 28 ± 2D, 16-96 videos per BioChip per day (1 min per video) (pending EVT)	3 wells per BioChip, 25± 2D, 12-72 videos per BioChip per day (1 min per video) (pending EVT)	2 wells per BioChip, 21 ± 2D, 8-48 videos per BioChip per day (1 min per video) (pending EVT)	1 well per BioChip, 14 ± 2D, 4-24 videos per BioChip per day (1 min per video) (pending EVT)	0 wells	1-3
Phase Contrast Image Acquisition	4 wells per BioChip, 28 ± 2D, 96-960 images per BioChip per day (pending EVT)	3 wells per BioChip, 25 ± 2D, 72-720 images per BioChip per day (pending EVT)	2 wells per BioChip, 21 ± 2D, 48-480 images per BioChip per day (pending EVT)	1 well per BioChip, 14 ± 2D, 24-240 images per BioChip per day (pending EVT)	0 wells	1-3
Mitochondria Trafficking Video Acquisition	4 wells per BioChip, 28 ± 2D, 16-96 videos per BioChip per day (3-5 min per video) (pending EVT)	3 wells per BioChip, 25 ± 2D, 12-72 videos per BioChip per day (3-5 min per video) (pending EVT)	2 wells per BioChip, 21 ± 2D, 8-48 videos per BioChip per day (3-5 min per video) (pending EVT)	1 well per BioChip, 14 ± 2D, 4-24 videos per BioChip per day(3-5 min per video) (pending EVT)	0 wells	1-3
Sample Fixation Quality (Paraformaldehyde)	4 replicates from each BioChip, able to label 4 subcellular markers. (pending EVT)	3 replicates from each BioChip, able to label 3 subcellular markers. (pending EVT)	2 replicates from each Biochip, able to label 2 subcellular markers. (pending EVT)	0-1 replicates from each BioChip		3

Figure 4.3. Outline of MoSL Success Critieria
Table illustrating success criteria for biological and hardware parameters of MoSL and related experiments in microgravity.

If the MoSL is indeed validated as a platform for cell biology in low earth orbit, this research will have far reaching implications towards understanding the effects of microgravity on neuroplasticity, which may lead to future drug targets and therapeutic interventions to attenuate the deleterious effects of long-term microgravity exposure on human physiology. Microgravity has been proposed as an ideal environment for pre-clinical trials in the drug development process due to the nature of cell cultures in the absence of gravity (Johnson, 2018). In general, cell cultures have a higher propensity to form three-dimensional (3D) matrices, rather than the standard two-dimensional (2D) cell cultures observed on Earth. These 3D cultures are thought to better mimic complex biological functionality of cells *in vivo* than 2D cultures, which are not observed *in vivo* (Jensen & Teng, 2020). This principle is especially true in the case of neuronal systems, as true neurons develop in incredibly dense environments with tremendous overlap between neurons and their projections in a small, enclosed 3D space. With the MoSL as a permanent fixture on the ISS, preclinical drug trials can be performed with a model system that may better represent *in vivo* cell culture and help to address one of the major problems in drug development, which is a lack of translation between successful cell culture trials and drug efficacy in preliminary clinical trials (Mehta, 2017).

In the context of neuronal systems, enhanced drug discovery models are imperative for development of drugs targeting neurodegenerative diseases. Neurodegenerative diseases such as Alzheimer's Disease (AD) have historically demonstrated poor results in clinical human trials, despite promising pre-clinical and animal trial results (Mehta, 2017). Because abnormal aggregates of cytoskeletal proteins and dysfunction of cytoskeleton-related processes are commonly observed in a variety of neurodegenerative diseases, having a better understanding of these sub-cellular mechanisms is a crucial step towards understanding the etiology of these diseases. If real-time, dynamic changes and aberrations to microtubule cytoskeletal structure can be observed using MoSL technology, then follow up experiments using microtubule and microtubule associated protein targeting drug candidates may be possible using MoSL technology. A potential outline of possible experiments is as follows: BioChips with cultured neurons or neuron-like cells are seeded on BioChip wells and maintained as normal in microgravity conditions until a maladaptive cytoskeletal phenotype sets in (the time it takes for these effects to occur may be determined in experiments described in this thesis). The microfluidic system of the MoSL can then administer the target drug at various

concentrations directly through the cell culture media in three of the four BioChip wells, leaving one well as a control group (this design is then replicated depending on number of available BioChips). Fluorescent videos of some select fluorescently tagged protein (in this example, microtubules) are obtained and analyzed on Earth. Following the experiment, cells are fixed and returned to Earth for follow-up assays (proteomics, transcriptomics, genomics, immunostaining, etc.). This basic experimental outline could be applied to a variety of cellular systems and candidate pharmaceuticals, thus further enhancing the quality and diversity of obtainable data in this field. One specific pharmaceutical candidate is the use of low-dose microtubule stabilizers as a therapy for the effects of space flight on microtubule organization. Recently, microtubule stabilizers such as paclitaxel and dictyostatin have been investigated as potentially beneficial in combating microtubule effects of neurodegenerative diseases such as AD and PD. These drugs are purported to cross the blood brain barrier and directly stabilize microtubules within the brain, helping to prevent spontaneous microtubule collapse and reduce the neurodegenerative phenotype (Brunden et al., 2017; Cross et al., 2021). If the experiments proposed in this thesis do indeed disrupt the stability of microtubules in SH-SY5Y cells, then follow-up experiments in space could investigate whether these microtubule stabilizing drugs exhibit similar therapeutic effects *in vitro* in a microgravity environment. Additionally, using the MoSL for drug discovery programs answers one of the most common criticisms of spaceflight and microgravity research; how does spending all this effort and money help the general population on Earth? By developing better methods to test candidate pharmaceuticals on systems that are difficult to replicate and study on Earth's conditions, we are directly answering that criticism – with better models to study human disease and treatment of those diseases comes a better understanding of disease and treatments with higher efficacy for those on Earth who may suffer from these diseases.

Lastly, I will end this section with a few thoughts about human society in the distant future. In the introduction, I discussed how life on Earth evolved under the context of a constant, unchanging gravitational force. As a thought experiment, suppose humans lived and evolved over thousands of years in a low-gravity environment. What kind of traits might be selected for with respect to cytoskeletal systems and their related processes?

One possible adaptation could be alterations to the expression levels of genes associated with microtubule stabilization. The first view I will take is that of decreased

expression of microtubule destabilizing proteins. This could potentially occur via genetic mutations affecting protein structure in the transcription factors and activating proteins that interact with enhancers and promoters for microtubule associated proteins. For example, consider microtubule-severing enzymes, which are ATPases that use the energy of ATP hydrolysis to extract tubulin subunits from the microtubule lattice, causing microtubule fragmentation. Spastin is an example of one such enzyme, whose expression is mediated by the transcription factor 'Knot' (Errico, 2002; Hersh & Carroll, 2005). If the *knot* gene were to undergo mutation leading to a reduced binding affinity of Knot to promoter regions of the *spastin* gene, then Spastin protein might be under expressed and thus a net decrease in microtubule-severing activity may occur. Interestingly, overexpression of Spastin is one of the major factors in Hereditary Spastic Paraplegia (HSP), a neurodegenerative disorder (Errico, 2002). Thus, it may be plausible that in a population evolving in a scenario where cytoskeletal stability is selected for, microtubule-severing enzymes are under expressed compared to modern humans.

Another perspective can be taken at the opposite spectrum, where we may see an increased expression of molecules involved in the stabilization of cytoskeletal structures. For example, end-stabilizing proteins such as EB1, XMAP215, CLASP, and CLIP170 are known to increase stabilization of growing microtubules (Goodson & Jonasson, 2018). Similarly to the previous scenario, a situation where transcription factors of these proteins more strongly activate transcriptional machinery leading to increased transcription and translation of end-stabilizing proteins might result in an increase in microtubule stability. Interestingly, microtubule stabilizing agents are considered useful in modern medicine to counteract microtubule defects often observed in neurological disorders such as AD, PD, and ALS (Varidaki et al., 2018). Therefore, in a population evolving under the pressure of reduced cytoskeletal stability, mutations leading to increases in cytoskeletal stability might be positively selected for.

Despite it being plausible that these genetic mutations could be advantageous for an individual living in a microgravity environment, it should also be noted that simply stabilizing the cytoskeleton is not without consequence. The cytoskeleton exists in a state of dynamic instability, and cytoskeletal remodeling is extremely important in many cellular processes. If the cytoskeleton were overly stabilized, adverse side effects might be expected, which could cause any of the proposed mutations to be harmful rather than adaptive, depending on severity. For example, microtubule stabilizing drugs are commonly

used as cancer treatments due to their anti-mitotic properties (Bates & Eastman, 2016; Risinger et al., 2009). An individual with a mutation causing increased microtubule stability may also experience reduced mitotic rates, which could potentially impact development during embryotic development and early life. It is unknown what an individual with such a mutation might look like, but if such an individual in a population from the distant future did exist, one characteristic we might see is reduced overall mass due to lower mitotic rates during development. Ultimately, these ideas are simply a narrow-viewed molecular perspective of what a future population evolving under low gravity conditions may look like. Guided by novel scientific developments such as the MoSL, the true future of the human race contains limitless potential.

4.7. Conclusions and Future Directions

Although the work presented in this thesis remains incomplete for the time being, I was successful in generating a series of experiments which have been validated for use in our transfected SH-SY5Y cell line that will eventually be sent to outer space cultured in MoSL hardware. My results indicate that our transformed cell line expresses properly localizing RFP-EB3 and GFP-MTS. These markers do not experience significant changes in expression throughout the proposed 21-day experiment duration, and fluorophore bleaching has not been observed when cells are recorded in periodic intervals. These cells differentiated and express neuron-like morphology and neuron-specific protein markers. Cells exhibit cytoskeletal and trafficking dynamics that are quantifiable under the specific parameters of MoSL hardware, and results of such quantifications indicate that these dynamics are comparable to actual neuronal systems. Post-flight analysis, consisting of actin and microtubule cytoskeletal immunostaining, mitochondrial network analysis, and TIA1 stress granule analysis was successfully conducted in fixed, fully differentiated SH-SY5Y cells, resulting in generation of a framework for semi-quantitative analysis that was validated for use in these cells. This framework will allow for the quantification and integration of data collected from microgravity-exposed cells at a future date, and subsequent comparison to control data presented in this thesis. Using the expected results from these experiments, I hypothesized what a potential unified model for neuronal dysfunction resulting from microgravity exposure could look like and presented possible pathways linking the various sub-cellular neuronal systems that have

previously demonstrated changes resultant of microgravity exposure. The results of these experiments may validate portions of my conjectures and identify avenues in follow up experiments that may or may not be worthwhile. Furthermore, identifying and validating the potential mechanisms underlying neuronal dysfunction in microgravity may help develop therapeutic strategies which alleviate the long-term effects of microgravity on neuronal cells, and other associated cellular systems.

The capture and analysis of cytoskeletal dynamics and axonal transport have never been performed in a microgravity environment, and through collaboration with HNu Photonics and the use of their MoSL hardware, the first analysis of such data will be performed and published based on the framework generated in this thesis. On the basis of these analyses, the MoSL can be assessed for its validity in use as a low orbit cell culture platform. success in this mission may open the hatch for follow-up experiments using this framework and MoSL across cell biology.

In conclusion, it is not yet known if my hypotheses concerning the effects of microgravity on cytoskeletal disruption, axonal transport, neurite outgrowth, and cell stress will be supported. However, I have successfully determined that these hypotheses are answerable based on results from ground control experiments, and data obtained in the near future from microgravity-based experiments may give conclusive answers as to whether my hypotheses will be or will not be supported.

References

Aberle, H. (2019). Axon Guidance and Collective Cell Migration by Substrate-Derived Attractants. Frontiers In Molecular Neuroscience, 12. doi: 10.3389/fnmol.2019.00148

Abraham, Z., Hawley, E., Hayosh, D., Webster-Wood, V., & Akkus, O. (2018). Kinesin and Dynein Mechanics: Measurement Methods and Research Applications. Journal Of Biomechanical Engineering, 140(2). doi: 10.1115/1.4037886

Agholme, L., Lindström, T., Kågedal, K., Marcusson, J., & Hallbeck, M. (2010). An In Vitro Model for Neuroscience: Differentiation of SH-SY5Y Cells into Cells with Morphological and Biochemical Characteristics of Mature Neurons. Journal Of Alzheimer's Disease, 20(4), 1069-1082. doi: 10.3233/jad-2010-091363

Aher, A., & Akhmanova, A. (2018). Tipping microtubule dynamics, one protofilament at a time. Current Opinion In Cell Biology, 50, 86-93. doi: 10.1016/j.ceb.2018.02.015

Ahuja, R., Pinyol, R., Reichenbach, N., Custer, L., Klingensmith, J., Kessels, M., & Qualmann, B. (2007). Cordon-Bleu Is an Actin Nucleation Factor and Controls Neuronal Morphology. Cell, 131(2), 337-350. doi: 10.1016/j.cell.2007.08.030

Akhmanova, A., & Hoogenraad, C. (2005). Microtubule plus-end-tracking proteins: mechanisms and functions. Current Opinion In Cell Biology, 17(1), 47-54. doi: 10.1016/j.ceb.2004.11.001

Alao, J., & Sunnerhagen, P. (2008). Rad3 and Sty1 function in Schizosaccharomyces pombe: an integrated response to DNA damage and environmental stress?. Molecular Microbiology, 68(2), 246-254. doi: 10.1111/j.1365-2958.2008.06147.x

Anderson, P., & Kedersha, N. (2006). RNA granules. Journal Of Cell Biology, 172(6), 803-808. doi: 10.1083/jcb.200512082

Árnadóttir, J., & Chalfie, M. (2010). Eukaryotic Mechanosensitive Channels. Annual Review Of Biophysics, 39(1), 111-137. doi: 10.1146/annurev.biophys.37.032807.125836

Arnal, I., Metoz, F., DeBonis, S., & Wade, R. (1996). Three-dimensional structure of functional motor proteins on microtubules. Current Biology, 6(10), 1265-1270. doi: 10.1016/s0960-9822(02)70712-4

Asadi, M., Sadat Moslehian, M., Sabaie, H., Jalaiei, A., Ghafouri-Fard, S., Taheri, M., & Rezazadeh, M. (2021). Stress Granules and Neurodegenerative Disorders: A Scoping Review. Frontiers In Aging Neuroscience, 13. doi: 10.3389/fnagi.2021.650740

Asghari Adib, E., Smithson, L., & Collins, C. (2018). An axonal stress response pathway: degenerative and regenerative signaling by DLK. Current Opinion In Neurobiology, 53, 110-119. doi: 10.1016/j.conb.2018.07.002

Athamneh, A., He, Y., Lamoureux, P., Fix, L., Suter, D., & Miller, K. (2017). Neurite elongation is highly correlated with bulk forward translocation of microtubules. Scientific Reports, 7(1). doi: 10.1038/s41598-017-07402-6

Aulas, A., Lyons, S., Fay, M., Anderson, P., & Ivanov, P. (2018). Nitric oxide triggers the assembly of “type II” stress granules linked to decreased cell viability. Cell Death &Amp; Disease, 9(11). doi: 10.1038/s41419-018-1173-x

Bachir, A., Horwitz, A., Nelson, W., & Bianchini, J. (2017). Actin-Based Adhesion Modules Mediate Cell Interactions with the Extracellular Matrix and Neighboring Cells. Cold Spring Harbor Perspectives In Biology, 9(7), a023234. doi: 10.1101/cshperspect.a023234

Baines, A. (2010). The spectrin–ankyrin–4.1–adducin membrane skeleton: adapting eukaryotic cells to the demands of animal life. Protoplasma, 244(1-4), 99-131. doi: 10.1007/s00709-010-0181-1

Barkus, R., Klyachko, O., Horiuchi, D., Dickson, B., & Saxton, W. (2008). Identification of an Axonal Kinesin-3 Motor for Fast Anterograde Vesicle Transport that Facilitates Retrograde Transport of Neuropeptides. Molecular Biology Of The Cell, 19(1), 274-283. doi: 10.1091/mbc.e07-03-0261

Barlan, K., & Gelfand, V. (2017). Microtubule-Based Transport and the Distribution, Tethering, and Organization of Organelles. Cold Spring Harbor Perspectives In Biology, 9(5), a025817. doi: 10.1101/cshperspect.a025817

Barroso, M. (2011). Quantum Dots in Cell Biology. Journal Of Histochemistry &Amp; Cytochemistry, 59(3), 237-251. doi: 10.1369/0022155411398487

Bates, D., & Eastman, A. (2016). Microtubule destabilising agents: far more than just antimitotic anticancer drugs. British Journal Of Clinical Pharmacology, 83(2), 255-268. doi: 10.1111/bcp.13126

Beck, M., Moreels, M., Quintens, R., Abou-El-Ardat, K., EL-SaghHre, H., & Tabury, K. et al. (2014). Chronic exposure to simulated space conditions predominantly affects cytoskeleton remodeling and oxidative stress response in mouse fetal fibroblasts. International Journal Of Molecular Medicine, 34(2), 606-615. doi: 10.3892/ijmm.2014.1785

Bennett, V., & Baines, A. (2001). Spectrin and Ankyrin-Based Pathways: Metazoan Inventions for Integrating Cells Into Tissues. Physiological Reviews, 81(3), 1353-1392. doi: 10.1152/physrev.2001.81.3.1353

Bentley, M., & Banker, G. (2016). The cellular mechanisms that maintain neuronal polarity. Nature Reviews Neuroscience, 17(10), 611-622. doi: 10.1038/nrn.2016.100

Bhatti, J., Bhatti, G., & Reddy, P. (2017). Mitochondrial dysfunction and oxidative stress in metabolic disorders — A step towards mitochondria based therapeutic strategies. Biochimica Et Biophysica Acta (BBA) - Molecular Basis Of Disease, 1863(5), 1066-1077. doi: 10.1016/j.bbadis.2016.11.010

Biswas, K., & Das Sarma, J. (2014). Effect of Microtubule Disruption on Neuronal Spread and Replication of Demyelinating and Nondemyelinating Strains of Mouse Hepatitis Virus In Vitro. Journal Of Virology, 88(5), 3043-3047. doi: 10.1128/jvi.02545-13

Bloomfield, S., Martinez, D., Boudreaux, R. & Mantri, A. Microgravity Stress: Bone and Connective Tissue. Comprehensive Physiology 645-686 (2016). doi:10.1002/cphy.c130027

Brooks, A., Harkins, R., Wang, P., Qian, H., Liu, P., & Rubanyi, G. (2004). Transcriptional silencing is associated with extensive methylation of the CMV promoter following adenoviral gene delivery to muscle. The Journal Of Gene Medicine, 6(4), 395-404. doi: 10.1002/jgm.516

Brown, A., Dahl, A., & Chapman, D. (1976). Limitation on the Use of the Horizontal Clinostat as a Gravity Compensator. Plant Physiology, 58(2), 127-130. doi: 10.1104/pp.58.2.127

Brugg, B., Reddy, D., & Matus, A. (1993). Attenuation of microtubule-associated protein 1B expression by antisense oligodeoxynucleotides inhibits initiation of neurite outgrowth. Neuroscience, 52(3), 489-496. doi: 10.1016/0306-4522(93)90401-z

Brunden, K., Lee, V., Smith, A., Trojanowski, J., & Ballatore, C. (2017). Altered microtubule dynamics in neurodegenerative disease: Therapeutic potential of microtubule-stabilizing drugs. *Neurobiology Of Disease*, *105*, 328-335. doi: 10.1016/j.nbd.2016.12.021

Buck, K., & Zheng, J. (2002). Growth Cone Turning Induced by Direct Local Modification of Microtubule Dynamics. The Journal Of Neuroscience, 22(21), 9358-9367. doi: 10.1523/jneurosci.22-21-09358.2002

Buravkova, L., & Romanov, Y. (2001). The role of cytoskeleton in cell changes under condition of simulated microgravity. Acta Astronautica, 48(5-12), 647-650. doi: 10.1016/s0094-5765(01)00023-6

Campellone, K., & Welch, M. (2010). A nucleator arms race: cellular control of actin assembly. Nature Reviews Molecular Cell Biology, 11(4), 237-251. doi: 10.1038/nrm2867

Cappelletti, G. et al. Linking microtubules to Parkinson's disease: the case of parkin. Biochemical Society Transactions 43, 292-296 (2015).

Carlsson, S., Bertilaccio, M., Ballabio, E., & Maier, J. (2003). Endothelial stress by gravitational unloading: effects on cell growth and cytoskeletal organization. Biochimica Et Biophysica Acta (BBA) - Molecular Cell Research, 1642(3), 173-179. doi: 10.1016/j.bbamcr.2003.08.003

Chaaban, S., & Brouhard, G. (2017). A microtubule bestiary: structural diversity in tubulin polymers. Molecular Biology Of The Cell, 28(22), 2924-2931. doi: 10.1091/mbc.e16-05-0271

Chada, S., & Hollenbeck, P. (2004). Nerve Growth Factor Signaling Regulates Motility and Docking of Axonal Mitochondria. Current Biology, 14(14), 1272-1276. doi: 10.1016/j.cub.2004.07.027

Chesarone, M., & Goode, B. (2009). Actin nucleation and elongation factors: mechanisms and interplay. Current Opinion In Cell Biology, 21(1), 28-37. doi: 10.1016/j.ceb.2008.12.001

Chen, C., Peng, Y., Yen, Y., Bhan, P., Muthaiyan Shanmugam, M., Klopfenstein, D., & Wagner, O. (2018). Insights on UNC-104-dynein/dynactin interactions and their implications on axonal transport in Caenorhabditis elegans. Journal Of Neuroscience Research, 97(2), 185-201. doi: 10.1002/jnr.24339

Chen, H., Vermulst, M., Wang, Y., Chomyn, A., Prolla, T., McCaffery, J., & Chan, D. (2010). Mitochondrial Fusion Is Required for mtDNA Stability in Skeletal Muscle and Tolerance of mtDNA Mutations. Cell, 141(2), 280-289. doi: 10.1016/j.cell.2010.02.026

Chen, Y., Pallant, C., Sampson, C., Boiti, A., Johnson, S., & Brazauskas, P. et al. (2020). Rapid Lentiviral Vector Producer Cell Line Generation Using a Single DNA Construct. Molecular Therapy - Methods &Amp; Clinical Development, 19, 47-57. doi: 10.1016/j.omtm.2020.08.011

Chen, Z., Luo, Q., Lin, C., Kuang, D., & Song, G. (2016). Simulated microgravity inhibits osteogenic differentiation of mesenchymal stem cells via depolymerizing F-actin to impede TAZ nuclear translocation. Scientific Reports, 6(1). doi: 10.1038/srep30322

Chesarone, M., DuPage, A., & Goode, B. (2009). Unleashing formins to remodel the actin and microtubule cytoskeletons. Nature Reviews Molecular Cell Biology, 11(1), 62-74. doi: 10.1038/nrm2816

Chowdhury, P., & Soulsby, N. (2002). Lipid peroxidation in rat brain is increased by simulated weightlessness and decreased by a soy-protein diet. Annals Of Clinical And Laboratory Science, 32(2).

Ciccia, A., & Elledge, S. (2010). The DNA Damage Response: Making It Safe to Play with Knives. Molecular Cell, 40(2), 179-204. doi: 10.1016/j.molcel.2010.09.019

Cho, H., Shin, J., Shin, C., Lee, S., & Oh, U. (2002). Mechanosensitive Ion Channels in Cultured Sensory Neurons of Neonatal Rats. The Journal Of Neuroscience, 22(4), 1238-1247. doi: 10.1523/jneurosci.22-04-01238.2002

Choquet, D., Felsenfeld, D., & Sheetz, M. (1997). Extracellular Matrix Rigidity Causes Strengthening of Integrin–Cytoskeleton Linkages. Cell, 88(1), 39-48. doi: 10.1016/s0092-8674(00)81856-5

Coles, C., & Bradke, F. (2015). Coordinating Neuronal Actin–Microtubule Dynamics. Current Biology, 25(15), R677-R691. doi: 10.1016/j.cub.2015.06.020

Conde, C., & Cáceres, A. (2009). Microtubule assembly, organization and dynamics in axons and dendrites. Nature Reviews Neuroscience, 10(5), 319-332. doi: 10.1038/nrn2631

Cooper GM. The Cell: A Molecular Approach. 2nd edition. Sunderland (MA): Sinauer Associates; 2000. Intermediate Filaments. Available from: https://www.ncbi.nlm.nih.gov/books/NBK9834/

Cross, D., Huber, B., Silverman, M., Cline, M., Gill, T., & Cross, C. et al. (2021). Intranasal Paclitaxel Alters Alzheimer's Disease Phenotypic Features in 3xTg-AD Mice. *Journal Of Alzheimer's Disease*, *83*(1), 379-394. doi: 10.3233/jad-210109

Crucian, B., Stowe, R., Pierson, D. & Sams, C. Immune System Dysregulation Following Short- vs Long-Duration Spaceflight. Aviation, Space, and Environmental Medicine 79, 835-843 (2008).

de Medeiros, L., De Bastiani, M., Rico, E., Schonhofen, P., Pfaffenseller, B., & Wollenhaupt-Aguiar, B. et al. (2019). Cholinergic Differentiation of Human Neuroblastoma SH-SY5Y Cell Line and Its Potential Use as an In vitro Model for Alzheimer's Disease Studies. Molecular Neurobiology, 56(11), 7355-7367. doi: 10.1007/s12035-019-1605-3

Dehmelt, L., Smart, F., Ozer, R., & Halpain, S. (2003). The Role of Microtubule-Associated Protein 2c in the Reorganization of Microtubules and Lamellipodia during Neurite Initiation. The Journal Of Neuroscience, 23(29), 9479-9490. doi: 10.1523/jneurosci.23-29-09479.2003

Doherty, G., & McMahon, H. (2008). Mediation, Modulation, and Consequences of Membrane-Cytoskeleton Interactions. Annual Review Of Biophysics, 37(1), 65-95. doi: 10.1146/annurev.biophys.37.032807.125912

Dominguez, R., & Holmes, K. (2011). Actin Structure and Function. Annual Review Of Biophysics, 40(1), 169-186. doi: 10.1146/annurev-biophys-042910-155359

Dotti, C., Sullivan, C., & Banker, G. (1988). The establishment of polarity by hippocampal neurons in culture. The Journal Of Neuroscience, 8(4), 1454-1468. doi: 10.1523/jneurosci.08-04-01454.1988

Doyle, A., & Lee, J. (2005). Cyclic changes in keratocyte speed and traction stress arise from Ca2+-dependent regulation of cell adhesiveness. Journal Of Cell Science, 118(2), 369-379. doi: 10.1242/jcs.01590

Dutcher, S. (2001). The tubulin fraternity: alpha to eta. Current Opinion In Cell Biology, 13(1), 49-54. doi: 10.1016/s0955-0674(00)00173-3

Dwane, S., Durack, E., & Kiely, P. (2013). Optimising parameters for the differentiation of SH-SY5Y cells to study cell adhesion and cell migration. BMC Research Notes, 6(1). doi: 10.1186/1756-0500-6-366

Encinas, M., Iglesias, M., Liu, Y., Wang, H., Muhaisen, A., & Ceña, V. et al. (2002). Sequential Treatment of SH-SY5Y Cells with Retinoic Acid and Brain-Derived Neurotrophic Factor Gives Rise to Fully Differentiated, Neurotrophic Factor-Dependent, Human Neuron-Like Cells. Journal Of Neurochemistry, 75(3), 991-1003. doi: 10.1046/j.1471-4159.2000.0750991.x

Errico, A. (2002). Spastin, the protein mutated in autosomal dominant hereditary spastic paraplegia, is involved in microtubule dynamics. Human Molecular Genetics, 11(2), 153-163. doi: 10.1093/hmg/11.2.153

Eyer, J., & Peterson, A. (1994). Neurofilament-deficient axons and perikaryal aggregates in viable transgenic mice expressing a neurofilament-β-galactosidase fusion protein. Neuron, 12(2), 389-405. doi: 10.1016/0896-6273(94)90280-1

Feger, B., Thompson, J., Dubois, L., Kommaddi, R., Foster, M., & Mishra, R. et al. (2016). Microgravity induces proteomics changes involved in endoplasmic reticulum stress and mitochondrial protection. Scientific Reports, 6(1). doi: 10.1038/srep34091

Fernández-Gómez, A., Velasco, B., & Izquierdo, J. (2022). Dynamics of T-Cell Intracellular Antigen 1-Dependent Stress Granules in Proteostasis and Welander Distal Myopathy under Oxidative Stress. Cells, 11(5), 884. doi: 10.3390/cells11050884

Fitts, R., Riley, D. & Widrick, J. Physiology of a Microgravity Environment Invited Review: Microgravity and skeletal muscle. Journal of Applied Physiology 89, 823-839 (2000).

Firestein, B., Brenman, J., Aoki, C., Sanchez-Perez, A., El-Husseini, A., & Bredt, D. (1999). Cypin. Neuron, 24(3), 659-672. doi: 10.1016/s0896-6273(00)81120-4

Fletcher, D., & Mullins, R. (2010). Cell mechanics and the cytoskeleton. Nature, 463(7280), 485-492. doi: 10.1038/nature08908

Florian, S., & Mitchison, T. (2016). Anti-Microtubule Drugs. Methods In Molecular Biology, 403-421. doi: 10.1007/978-1-4939-3542-0_25

Flynn, K. (2013). The cytoskeleton and neurite initiation. Bioarchitecture, 3(4), 86-109. doi: 10.4161/bioa.26259

Flynn, K., Hellal, F., Neukirchen, D., Jacob, S., Tahirovic, S., & Dupraz, S. et al. (2012). ADF/Cofilin-Mediated Actin Retrograde Flow Directs Neurite Formation in the Developing Brain. Neuron, 76(6), 1091-1107. doi: 10.1016/j.neuron.2012.09.038

Franker, M., & Hoogenraad, C. (2013). Microtubule-based transport – basic mechanisms, traffic rules and role in neurological pathogenesis. Journal Of Cell Science. doi: 10.1242/jcs.115030

Friede, R., & Samorajski, T. (1970). Axon caliber related to neurofilaments and microtubules in sciatic nerve fibers of rats and mice. The Anatomical Record, 167(4), 379-387. doi: 10.1002/ar.1091670402

Fuhrmann, A., & Engler, A. (2015). The Cytoskeleton Regulates Cell Attachment Strength. Biophysical Journal, 109(1), 57-65. doi: 10.1016/j.bpj.2015.06.003

Fujiwara, I., Zweifel, M., Courtemanche, N., & Pollard, T. (2018). Latrunculin A Accelerates Actin Filament Depolymerization in Addition to Sequestering Actin Monomers. Current Biology, 28(19), 3183-3192.e2. doi: 10.1016/j.cub.2018.07.082

Fulda, S., Gorman, A., Hori, O., & Samali, A. (2010). Cellular Stress Responses: Cell Survival and Cell Death. International Journal Of Cell Biology, 2010, 1-23. doi: 10.1155/2010/214074

Gaboyard, S., Blanchard, M., Travo, C., Viso, M., Sans, A., & Lehouelleur, J. (2002). Weightlessness affects cytoskeleton of rat utricular hair cells during maturation in vitro. Neuroreport, 13(16), 2139-2142. doi: 10.1097/00001756-200211150-00030

Galea, E., Launay, N., Portero-Otin, M., Ruiz, M., Pamplona, R., & Aubourg, P. et al. (2012). Oxidative stress underlying axonal degeneration in adrenoleukodystrophy: A paradigm for multifactorial neurodegenerative diseases?. Biochimica Et Biophysica Acta (BBA) - Molecular Basis Of Disease, 1822(9), 1475-1488. doi: 10.1016/j.bbadis.2012.02.005

Gallo, G. (2013). Mechanisms Underlying the Initiation and Dynamics of Neuronal Filopodia. International Review Of Cell And Molecular Biology, 95-156. doi: 10.1016/b978-0-12-407704-1.00003-8

Gan, K., & Silverman, M. (2016). Imaging organelle transport in primary hippocampal neurons treated with amyloid-β oligomers. Methods In Cell Biology, 425-451. doi: 10.1016/bs.mcb.2015.06.012

Gardiner, J. (2021). Cytoskeletal Tensegrity in Microgravity. Life, 11(10), 1091. doi: 10.3390/life11101091

Gardner, M., Zanic, M., & Howard, J. (2013). Microtubule catastrophe and rescue. Current Opinion In Cell Biology, 25(1), 14-22. doi: 10.1016/j.ceb.2012.09.006

Gaub, B., Kasuba, K., Mace, E., Strittmatter, T., Laskowski, P., & Geissler, S. et al. (2019). Neurons differentiate magnitude and location of mechanical stimuli. Proceedings Of The National Academy Of Sciences, 117(2), 848-856. doi: 10.1073/pnas.1909933117

Georges, P., Hadzimichalis, N., Sweet, E., & Firestein, B. (2008). The Yin–Yang of Dendrite Morphology: Unity of Actin and Microtubules. Molecular Neurobiology, 38(3), 270-284. doi: 10.1007/s12035-008-8046-8

Gittes, F., Mickey, B., Nettleton, J., & Howard, J. (1993). Flexural rigidity of microtubules and actin filaments measured from thermal fluctuations in shape. Journal Of Cell Biology, 120(4), 923-934. doi: 10.1083/jcb.120.4.923

Goldberg, J., Currais, A., Prior, M., Fischer, W., Chiruta, C., & Ratliff, E. et al. (2018). The mitochondrial ATP synthase is a shared drug target for aging and dementia. Aging Cell, 17(2), e12715. doi: 10.1111/acel.12715

Goldie, B., Barnett, M., & Cairns, M. (2014). BDNF and the maturation of posttranscriptional regulatory networks in human SH-SY5Y neuroblast differentiation. Frontiers In Cellular Neuroscience, 8. doi: 10.3389/fncel.2014.00325

Goldstein, L., & Yang, Z. (2000). Microtubule-Based Transport Systems in Neurons: The Roles of Kinesins and Dyneins. Annual Review Of Neuroscience, 23(1), 39-71. doi: 10.1146/annurev.neuro.23.1.39

Gómez, X., Sanon, S., Zambrano, K., Asquel, S., Bassantes, M., & Morales, J. et al. (2021). Key points for the development of antioxidant cocktails to prevent cellular stress and damage caused by reactive oxygen species (ROS) during manned space missions. Npj Microgravity, 7(1). doi: 10.1038/s41526-021-00162-8

Goodson, H., & Jonasson, E. (2018). Microtubules and Microtubule-Associated Proteins. Cold Spring Harbor Perspectives In Biology, 10(6), a022608. doi: 10.1101/cshperspect.a022608

Goswami, N., White, O., Blaber, A., Evans, J., van Loon, J., & Clement, G. (2021). Human physiology adaptation to altered gravity environments. Acta Astronautica, 189, 216-221. doi: 10.1016/j.actaastro.2021.08.023

Grenon, S., Jeanne, M., Aguado-Zuniga, J., Conte, M., & Hughes-Fulford, M. (2013). Effects of Gravitational Mechanical Unloading in Endothelial Cells: Association between Caveolins, Inflammation and Adhesion Molecules. Scientific Reports, 3(1). doi: 10.1038/srep01494

Grimm, D., Wise, P., Lebert, M., Richter, P., & Baatout, S. (2011). How and why does the proteome respond to microgravity?. Expert Review Of Proteomics, 8(1), 13-27. doi: 10.1586/epr.10.105

Grosse, J., Wehland, M., Pietsch, J., Ma, X., Ulbrich, C., & Schulz, H. et al. (2011). Short-term weightlessness produced by parabolic flight maneuvers altered gene expression patterns in human endothelial cells. The FASEB Journal, 26(2), 639-655. doi: 10.1096/fj.11-194886

Guedes-Dias, P., & Holzbaur, E. (2019). Axonal transport: Driving synaptic function. Science, 366(6462). doi: 10.1126/science.aaw9997

Haswell, E., Phillips, R., & Rees, D. (2011). Mechanosensitive Channels: What Can They Do and How Do They Do It?. Structure, 19(10), 1356-1369. doi: 10.1016/j.str.2011.09.005

Hawkins, T., Mirigian, M., Selcuk Yasar, M., & Ross, J. (2010). Mechanics of microtubules. Journal Of Biomechanics, 43(1), 23-30. doi: 10.1016/j.jbiomech.2009.09.005

Hayakawa, K., Tatsumi, H., & Sokabe, M. (2008). Actin stress fibers transmit and focus force to activate mechanosensitive channels. Journal Of Cell Science, 121(4), 496-503. doi: 10.1242/jcs.022053

Heiman, M., & Shaham, S. (2010). Twigs into branches: how a filopodium becomes a dendrite. Current Opinion In Neurobiology, 20(1), 86-91. doi: 10.1016/j.conb.2009.10.016

Hersh, B., & Carroll, S. (2005). Direct regulation of knot gene expression by Ultrabithorax and the evolution of cis-regulatory elements in Drosophila. Development, 132(7), 1567-1577. doi: 10.1242/dev.01737

Hinckelmann, M., Zala, D., & Saudou, F. (2013). Releasing the brake: restoring fast axonal transport in neurodegenerative disorders. Trends In Cell Biology, 23(12), 634-643. doi: 10.1016/j.tcb.2013.08.007

Hirokawa, N. (1998). Kinesin and Dynein Superfamily Proteins and the Mechanism of Organelle Transport. Science, 279(5350), 519-526. doi: 10.1126/science.279.5350.519

Hirokawa, N., & Takemura, R. (2005). Molecular motors and mechanisms of directional transport in neurons. Nature Reviews Neuroscience, 6(3), 201-214. doi: 10.1038/nrn1624

Hirokawa, N., Noda, Y., Tanaka, Y., & Niwa, S. (2009). Kinesin superfamily motor proteins and intracellular transport. Nature Reviews Molecular Cell Biology, 10(10), 682-696. doi: 10.1038/nrm2774

Hirokawa, N., & Tanaka, Y. (2015). Kinesin superfamily proteins (KIFs): Various functions and their relevance for important phenomena in life and diseases. Experimental Cell Research, 334(1), 16-25. doi: 10.1016/j.yexcr.2015.02.016

Hirokawa, N., Nitta, R., & Okada, Y. (2009). The mechanisms of kinesin motor motility: lessons from the monomeric motor KIF1A. Nature Reviews Molecular Cell Biology, 10(12), 877-884. doi: 10.1038/nrm2807

Hirokawa, N., Niwa, S., & Tanaka, Y. (2010). Molecular Motors in Neurons: Transport Mechanisms and Roles in Brain Function, Development, and Disease. Neuron, 68(4), 610-638. doi: 10.1016/j.neuron.2010.09.039

Hollenbeck, P. (1993). Products of endocytosis and autophagy are retrieved from axons by regulated retrograde organelle transport. Journal Of Cell Biology, 121(2), 305-315. doi: 10.1083/jcb.121.2.305

Horch, H. (2004). Local Effects of BDNF on Dendritic Growth. Reviews In The Neurosciences, 15(2). doi: 10.1515/revneuro.2004.15.2.117

Horiguchi, K., Hanada, T., Fukui, Y., & Chishti, A. (2006). Transport of PIP3 by GAKIN, a kinesin-3 family protein, regulates neuronal cell polarity. Journal Of Cell Biology, 174(3), 425-436. doi: 10.1083/jcb.200604031

Hsu, C., Li, H., Hung, Y., Leu, Y., Wu, W., & Wang, F. et al. (2010). Targeted methylation of CMV and E1A viral promoters. Biochemical And Biophysical Research Communications, 402(2), 228-234. doi: 10.1016/j.bbrc.2010.09.131

Hu, X., Ballo, L., Pietila, L., Viesselmann, C., Ballweg, J., & Lumbard, D. et al. (2011). BDNF-Induced Increase of PSD-95 in Dendritic Spines Requires Dynamic Microtubule Invasions. Journal Of Neuroscience, 31(43), 15597-15603. doi: 10.1523/jneurosci.2445-11.2011

Hughes-Fulford, M., & Lewis, M. (1996). Effects of Microgravity on Osteoblast Growth Activation. Experimental Cell Research, 224(1), 103-109. doi: 10.1006/excr.1996.0116

Hughes-Fulford, M. (2003). Function of the cytoskeleton in gravisensing during spaceflight. Advances In Space Research, 32(8), 1585-1593. doi: 10.1016/s0273-1177(03)90399-1

Hughes-Fulford, M. (2004). Signal Transduction and Mechanical Stress. Science's STKE, 2004(249). doi: 10.1126/stke.2492004re12

Hyman, A., Salser, S., Drechsel, D., Unwin, N., & Mitchison, T. (1992). Role of GTP hydrolysis in microtubule dynamics: information from a slowly hydrolyzable analogue, GMPCPP. Molecular Biology Of The Cell, 3(10), 1155-1167. doi: 10.1091/mbc.3.10.1155

ISS Expedition Three Science Operations Weekly Science Status Report 29 Aug 2001. (2001). Retrieved 13 April 2022, from http://spaceref.com/news/viewsr.html?pid=3571

Iwase, S., Nishimura, N., Tanaka, K., & Mano, T. (2020). Effects of Microgravity on Human Physiology. Beyond LEO - Human Health Issues For Deep Space Exploration [Working Title]. doi: 10.5772/intechopen.90700

Jaworski, J., Kapitein, L., Gouveia, S., Dortland, B., Wulf, P., & Grigoriev, I. et al. (2009). Dynamic Microtubules Regulate Dendritic Spine Morphology and Synaptic Plasticity. Neuron, 61(1), 85-100. doi: 10.1016/j.neuron.2008.11.013

Jean, D. & Baas, P. It cuts two ways: microtubule loss during Alzheimer disease. The EMBO Journal 32, 2900-2902 (2013).

Jensen, C., & Teng, Y. (2020). Is It Time to Start Transitioning From 2D to 3D Cell Culture?. Frontiers In Molecular Biosciences, 7. doi: 10.3389/fmolb.2020.00033

Jing, Z., Yin, H., Wang, P., Gao, J., & Yuan, L. (2016). Centlein, a novel microtubule-associated protein stabilizing microtubules and involved in neurite formation. Biochemical And Biophysical Research Communications, 472(2), 360-365. doi: 10.1016/j.bbrc.2016.02.079

Johnson, M. (2018). Tissue Chips in Space a Big Leap for Research. Retrieved 4 July 2022, from https://www.nasa.gov/tissue-chips

Kalinski, A., Kar, A., Craver, J., Tosolini, A., Sleigh, J., & Lee, S. et al. (2019). Deacetylation of Miro1 by HDAC6 blocks mitochondrial transport and mediates axon growth inhibition. Journal Of Cell Biology, 218(6), 1871-1890. doi: 10.1083/jcb.201702187

Kalmar, B., & Greensmith, L. (2009). Induction of heat shock proteins for protection against oxidative stress. Advanced Drug Delivery Reviews, 61(4), 310-318. doi: 10.1016/j.addr.2009.02.003

Kametani, F. & Hasegawa, M. Reconsideration of Amyloid Hypothesis and Tau Hypothesis in Alzheimer's Disease. (2021).

Kanai, Y., Okada, Y., Tanaka, Y., Harada, A., Terada, S., & Hirokawa, N. (2000). KIF5C, a Novel Neuronal Kinesin Enriched in Motor Neurons. The Journal Of Neuroscience, 20(17), 6374-6384. doi: 10.1523/jneurosci.20-17-06374.2000

Kann, O., & Kovács, R. (2007). Mitochondria and neuronal activity. American Journal Of Physiology-Cell Physiology, 292(2), C641-C657. doi: 10.1152/ajpcell.00222.2006

Kapitein, L., & Hoogenraad, C. (2015). Building the Neuronal Microtubule Cytoskeleton. Neuron, 87(3), 492-506. doi: 10.1016/j.neuron.2015.05.046

Karki, R., Mariani, M., Andreoli, M., He, S., Scambia, G., Shahabi, S., & Ferlini, C. (2013). βIII-Tubulin: biomarker of taxane resistance or drug target?. Expert Opinion On Therapeutic Targets, 17(4), 461-472. doi: 10.1517/14728222.2013.766170

Kazemi, L., Rahbarghazi, R., Salehi, R., Abedelahi, A., Niari, S., Karimipour, M., & Nasrabadi, H. (2020). Superior Synaptogenic Effect of Electrospun PLGA-PEG Nanofibers Versus PLGA Nanofibers on Human Neural SH-SY5Y Cells in a Three-Dimensional Culture System. Journal Of Molecular Neuroscience, 70(12), 1967-1976. doi: 10.1007/s12031-020-01596-7

Kedersha, N., Gupta, M., Li, W., Miller, I., & Anderson, P. (1999). RNA-Binding Proteins Tia-1 and Tiar Link the Phosphorylation of Eif-2α to the Assembly of Mammalian Stress Granules. Journal Of Cell Biology, 147(7), 1431-1442. doi: 10.1083/jcb.147.7.1431

Kedersha, N., Cho, M., Li, W., Yacono, P., Chen, S., & Gilks, N. et al. (2000). Dynamic Shuttling of Tia-1 Accompanies the Recruitment of mRNA to Mammalian Stress Granules. Journal Of Cell Biology, 151(6), 1257-1268. doi: 10.1083/jcb.151.6.1257

Kenwood, B., Weaver, J., Bajwa, A., Poon, I., Byrne, F., & Murrow, B. et al. (2014). Identification of a novel mitochondrial uncoupler that does not depolarize the plasma membrane. Molecular Metabolism, 3(2), 114-123. doi: 10.1016/j.molmet.2013.11.005

Ketschek, A., & Gallo, G. (2010). Nerve Growth Factor Induces Axonal Filopodia through Localized Microdomains of Phosphoinositide 3-Kinase Activity That Drive the Formation of Cytoskeletal Precursors to Filopodia. Journal Of Neuroscience, 30(36), 12185-12197. doi: 10.1523/jneurosci.1740-10.2010

Kim, T., & Eberwine, J. (2010). Mammalian cell transfection: the present and the future. Analytical And Bioanalytical Chemistry, 397(8), 3173-3178. doi: 10.1007/s00216-010-3821-6

Kimura Arimura Fukata, T., Watanabe, H., Iwamatsu, A., & Kaibuchi, K. (2005). Tubulin and CRMP-2 complex is transported via Kinesin-1. Journal Of Neurochemistry, 93(6), 1371-1382. doi: 10.1111/j.1471-4159.2005.03063.x

Komarova, Y., Lansbergen, G., Galjart, N., Grosveld, F., Borisy, G., & Akhmanova, A. (2005). EB1 and EB3 Control CLIP Dissociation from the Ends of Growing Microtubules. Molecular Biology Of The Cell, 16(11), 5334-5345. doi: 10.1091/mbc.e05-07-0614

Korobova, F., & Svitkina, T. (2008). Arp2/3 Complex Is Important for Filopodia Formation, Growth Cone Motility, and Neuritogenesis in Neuronal Cells. Molecular Biology Of The Cell, 19(4), 1561-1574. doi: 10.1091/mbc.e07-09-0964

Korobova, F., & Svitkina, T. (2010). Molecular Architecture of Synaptic Actin Cytoskeleton in Hippocampal Neurons Reveals a Mechanism of Dendritic Spine Morphogenesis. Molecular Biology Of The Cell, 21(1), 165-176. doi: 10.1091/mbc.e09-07-0596

Kumar, A., Tahimic, C., Almeida, E., & Globus, R. (2021). Spaceflight Modulates the Expression of Key Oxidative Stress and Cell Cycle Related Genes in Heart. International Journal Of Molecular Sciences, 22(16), 9088. doi: 10.3390/ijms22169088

Kwon, O., Sartor, M., Tomlinson, C., Millard, R., Olah, M., Sankovic, J., & Banerjee, R. (2006). Effect of simulated microgravity on oxidation-sensitive gene expression in PC12 cells. Advances In Space Research, 38(6), 1168-1176. doi: 10.1016/j.asr.2006.02.059

Lalli, G., & Schiavo, G. (2002). Analysis of retrograde transport in motor neurons reveals common endocytic carriers for tetanus toxin and neurotrophin receptor p75NTR. Journal Of Cell Biology, 156(2), 233-240. doi: 10.1083/jcb.200106142

Lasser, M., Tiber, J., & Lowery, L. (2018). The Role of the Microtubule Cytoskeleton in Neurodevelopmental Disorders. Frontiers In Cellular Neuroscience, 12. doi: 10.3389/fncel.2018.00165

Lazarov, O. Axonal Transport, Amyloid Precursor Protein, Kinesin-1, and the Processing Apparatus: Revisited. Journal of Neuroscience 25, 2386-2395 (2005).

Leondaritis, G., & Eickholt, B. (2015). Short Lives with Long-Lasting Effects: Filopodia Protrusions in Neuronal Branching Morphogenesis. PLOS Biology, 13(9), e1002241. doi: 10.1371/journal.pbio.1002241

Lenaz, G. (1998). Role of mitochondria in oxidative stress and ageing. Biochimica Et Biophysica Acta (BBA) - Bioenergetics, 1366(1-2), 53-67. doi: 10.1016/s0005-2728(98)00120-0

Leterrier, C. (2021). A Pictorial History of the Neuronal Cytoskeleton. The Journal Of Neuroscience, 41(1), 11-27. doi: 10.1523/jneurosci.2872-20.2020

Lee, J., Escher, B., Scholz, S., & Schlichting, R. (2022). Inhibition of neurite outgrowth and enhanced effects compared to baseline toxicity in SH-SY5Y cells. Archives Of Toxicology, 96(4), 1039-1053. doi: 10.1007/s00204-022-03237-x

Lewis, M. (2002). The Cytoskeleton, apoptosis, and gene expression in T lymphocytes and other mammalian cells exposed to altered gravity. Cell Biology And Biotechnology In Space, 77-128. doi: 10.1016/s1569-2574(02)08016-4

Lewis, M., Reynolds, J., Cubano, L., Hatton, J., Lawless, B., & Piepmeier, E. (1998). Spaceflight alters microtubules and increases apoptosis in human lymphocytes (Jurkat). The FASEB Journal, 12(11), 1007-1018. doi: 10.1096/fasebj.12.11.1007

Lewis, T., Turi, G., Kwon, S., Losonczy, A., & Polleux, F. (2016). Progressive Decrease of Mitochondrial Motility during Maturation of Cortical Axons In Vitro and In Vivo. Current Biology, 26(19), 2602-2608. doi: 10.1016/j.cub.2016.07.064

Li, J., Zhang, S., Chen, J., Du, T., Wang, Y., & Wang, Z. (2009). Modeled microgravity causes changes in the cytoskeleton and focal adhesions, and decreases in migration in malignant human MCF-7 cells. Protoplasma, 238(1-4), 23-33. doi: 10.1007/s00709-009-0068-1

Li, Y., Ghavampur, S., Bondallaz, P., Will, L., Grenningloh, G., & Pu¨schel, A. (2009). Rnd1 Regulates Axon Extension by Enhancing the Microtubule Destabilizing Activity of SCG10. Journal Of Biological Chemistry, 284(1), 363-371. doi: 10.1074/jbc.m808126200

Lichtenstein, N., Geiger, B., & Kam, Z. (2003). Quantitative analysis of cytoskeletal organization by digital fluorescent microscopy. Cytometry, 54A(1), 8-18. doi: 10.1002/cyto.a.10053

Liu, X., Rizzo, V. & Puthanveettil, S. Pathologies of axonal transport in neurodegenerative diseases. Translational Neuroscience 3, (2012).

Lin, S., Gou, G., Hsia, C., Ho, C., Huang, K., & Wu, Y. et al. (2016). Simulated Microgravity Disrupts Cytoskeleton Organization and Increases Apoptosis of Rat Neural Crest Stem Cells Via UpregulatingCXCR4Expression and RhoA-ROCK1-p38 MAPK-p53 Signaling. Stem Cells And Development, 25(15), 1172-1193. doi: 10.1089/scd.2016.0040

Lin, X., Zhang, K., Wei, D., Tian, Y., Gao, Y., Chen, Z., & Qian, A. (2020). The Impact of Spaceflight and Simulated Microgravity on Cell Adhesion. International Journal Of Molecular Sciences, 21(9), 3031. doi: 10.3390/ijms21093031

López de Silanes, I., Galbán, S., Martindale, J., Yang, X., Mazan-Mamczarz, K., & Indig, F. et al. (2005). Identification and Functional Outcome of mRNAs Associated with RNA-Binding Protein TIA-1. Molecular And Cellular Biology, 25(21), 9520-9531. doi: 10.1128/mcb.25.21.9520-9531.2005

Lowery, L., & Vactor, D. (2009). The trip of the tip: understanding the growth cone machinery. Nature Reviews Molecular Cell Biology, 10(5), 332-343. doi: 10.1038/nrm2679

Luo, Y., Na, Z., & Slavoff, S. (2018). P-Bodies: Composition, Properties, and Functions. Biochemistry, 57(17), 2424-2431. doi: 10.1021/acs.biochem.7b01162

Lyon, C. (1970). Choice of Rotation Rate for the Horizontal Clinostat. Plant Physiology, 46(3), 355-358. doi: 10.1104/pp.46.3.355

MacAskill, A., Rinholm, J., Twelvetrees, A., Arancibia-Carcamo, I., Muir, J., & Fransson, A. et al. (2009). Miro1 Is a Calcium Sensor for Glutamate Receptor-Dependent Localization of Mitochondria at Synapses. Neuron, 61(4), 541-555. doi: 10.1016/j.neuron.2009.01.030

Maday, S., Twelvetrees, A., Moughamian, A., & Holzbaur, E. (2014). Axonal Transport: Cargo-Specific Mechanisms of Motility and Regulation. Neuron, 84(2), 292-309. doi: 10.1016/j.neuron.2014.10.019

Maillet, A., Beaufrere, B., Di Nardo, P., Elia, M., & Pichard, C. (2001). Weightlessness as an accelerated model of nutritional disturbances. Current Opinion In Clinical Nutrition And Metabolic Care, 4(4), 301-306. doi: 10.1097/00075197-200107000-00010

Manzey, D., Lorenz, B. & Poljakov, V. Mental performance in extreme environments: results from a performance monitoring study during a 438-day spaceflight. Ergonomics 41, 537-559 (1998).

Marijan, D., Tse, R., Elliott, K., Chandhok, S., Luo, M., Lacroix, E., & Audas, T. (2019). Stress-specific aggregation of proteins in the amyloid bodies. FEBS Letters, 593(22), 3162-3172. doi: 10.1002/1873-3468.13597

Martino, F., Perestrelo, A., Vinarský, V., Pagliari, S., & Forte, G. (2018). Cellular Mechanotransduction: From Tension to Function. Frontiers In Physiology, 9. doi: 10.3389/fphys.2018.00824

Matamoros, A., & Baas, P. (2016). Microtubules in health and degenerative disease of the nervous system. Brain Research Bulletin, 126, 217-225. doi: 10.1016/j.brainresbull.2016.06.016

McCormick, C., & Khaperskyy, D. (2017). Translation inhibition and stress granules in the antiviral immune response. Nature Reviews Immunology, 17(10), 647-660. doi: 10.1038/nri.2017.63

McIntosh, J. (2016). Mitosis. Cold Spring Harbor Perspectives In Biology, 8(9), a023218. doi: 10.1101/cshperspect.a023218

Mehta, D., Jackson, R., Paul, G., Shi, J., & Sabbagh, M. (2017). Why do trials for Alzheimer's disease drugs keep failing? A discontinued drug perspective for 2010-2015. Expert Opinion On Investigational Drugs, 26(6), 735-739. doi: 10.1080/13543784.2017.1323868

Merten, O., Hebben, M., & Bovolenta, C. (2016). Production of lentiviral vectors. Molecular Therapy - Methods &Amp; Clinical Development, 3, 16017. doi: 10.1038/mtm.2016.17

Meyers, V., Zayzafoon, M., Douglas, J., & McDonald, J. (2005). RhoA and Cytoskeletal Disruption Mediate Reduced Osteoblastogenesis and Enhanced Adipogenesis of Human Mesenchymal Stem Cells in Modeled Microgravity. Journal Of Bone And Mineral Research, 20(10), 1858-1866. doi: 10.1359/jbmr.050611

Michaletti, A., Gioia, M., Tarantino, U., & Zolla, L. (2017). Effects of microgravity on osteoblast mitochondria: a proteomic and metabolomics profile. Scientific Reports, 7(1). doi: 10.1038/s41598-017-15612-1

Millecamps, S., & Julien, J. (2013). Axonal transport deficits and neurodegenerative diseases. Nature Reviews Neuroscience, 14(3), 161-176. doi: 10.1038/nrn3380

Miller, K., & Sheetz, M. (2004). Axonal mitochondrial transport and potential are correlated. Journal Of Cell Science, 117(13), 2791-2804. doi: 10.1242/jcs.01130

Miller, K., & Suter, D. (2018). An Integrated Cytoskeletal Model of Neurite Outgrowth. Frontiers In Cellular Neuroscience, 12. doi: 10.3389/fncel.2018.00447

Milner, D., Mavroidis, M., Weisleder, N., & Capetanaki, Y. (2000). Desmin Cytoskeleton Linked to Muscle Mitochondrial Distribution and Respiratory Function. Journal Of Cell Biology, 150(6), 1283-1298. doi: 10.1083/jcb.150.6.1283

Misgeld, T., & Schwarz, T. (2017). Mitostasis in Neurons: Maintaining Mitochondria in an Extended Cellular Architecture. Neuron, 96(3), 651-666. doi: 10.1016/j.neuron.2017.09.055

Monici, M., Fusi, F., Paglierani, M., Marziliano, N., Cogoli, A., Pratesi, R., & Bernabei, P. (2006). Modeled gravitational unloading triggers differentiation and apoptosis in preosteoclastic cells. Journal Of Cellular Biochemistry, 98(1), 65-80. doi: 10.1002/jcb.20747

Moore, A., & Holzbaur, E. (2018). Mitochondrial-cytoskeletal interactions: dynamic associations that facilitate network function and remodeling. Current Opinion In Physiology, 3, 94-100. doi: 10.1016/j.cophys.2018.03.003

Moritz, B., Becker, P., & Göpfert, U. (2015). CMV promoter mutants with a reduced propensity to productivity loss in CHO cells. Scientific Reports, 5(1). doi: 10.1038/srep16952

Morris, R., & Hollenbeck, P. (1993). The regulation of bidirectional mitochondrial transport is coordinated with axonal outgrowth. Journal Of Cell Science, 104(3), 917-927. doi: 10.1242/jcs.104.3.917

Morris, R., & Hollenbeck, P. (1995). Axonal transport of mitochondria along microtubules and F-actin in living vertebrate neurons. Journal Of Cell Biology, 131(5), 1315-1326. doi: 10.1083/jcb.131.5.1315

Munevar, S., Wang, Y., & Dembo, M. (2004). Regulation of mechanical interactions between fibroblasts and the substratum by stretch-activated Ca2+ entry. Journal Of Cell Science, 117(1), 85-92. doi: 10.1242/jcs.00795

Nabavi, N., Khandani, A., Camirand, A., & Harrison, R. (2011). Effects of microgravity on osteoclast bone resorption and osteoblast cytoskeletal organization and adhesion. Bone, 49(5), 965-974. doi: 10.1016/j.bone.2011.07.036

Nakata, T., Niwa, S., Okada, Y., Perez, F., & Hirokawa, N. (2011). Preferential binding of a kinesin-1 motor to GTP-tubulin–rich microtubules underlies polarized vesicle transport. Journal Of Cell Biology, 194(2), 245-255. doi: 10.1083/jcb.201104034

Nangaku, M., Sato-Yoshitake, R., Okada, Y., Noda, Y., Takemura, R., Yamazaki, H., & Hirokawa, N. (1994). KIF1B, a novel microtubule plus end-directed monomeric motor protein for transport of mitochondria. Cell, 79(7), 1209-1220. doi: 10.1016/0092-8674(94)90012-4

Narayanareddy, B., Vartiainen, S., Hariri, N., O'Dowd, D., & Gross, S. (2014). A Biophysical Analysis of Mitochondrial Movement: Differences Between Transport in Neuronal Cell Bodies Versus Processes. Traffic, 15(7), 762-771. doi: 10.1111/tra.12171

Naruse, K., Yamada, T., & Sokabe, M. (1998). Involvement of SA channels in orienting response of cultured endothelial cells to cyclic stretch. American Journal Of Physiology-Heart And Circulatory Physiology, 274(5), H1532-H1538. doi: 10.1152/ajpheart.1998.274.5.h1532

Nassef, M., Kopp, S., Wehland, M., Melnik, D., Sahana, J., & Krüger, M. et al. (2019). Real Microgravity Influences the Cytoskeleton and Focal Adhesions in Human Breast Cancer Cells. International Journal Of Molecular Sciences, 20(13), 3156. doi: 10.3390/ijms20133156

Nguyen, H., Tran, P., Kim, K., & Yang, S. (2021). The effects of real and simulated microgravity on cellular mitochondrial function. Npj Microgravity, 7(1). doi: 10.1038/s41526-021-00171-7

Niescier, R., Kwak, S., Joo, S., Chang, K., & Min, K. (2016). Dynamics of Mitochondrial Transport in Axons. Frontiers In Cellular Neuroscience, 10. doi: 10.3389/fncel.2016.00123

Nirschl, J., Ghiretti, A., & Holzbaur, E. (2017). The impact of cytoskeletal organization on the local regulation of neuronal transport. Nature Reviews Neuroscience, 18(10), 585-597. doi: 10.1038/nrn.2017.100

Nishimura, T., Kato, K., Yamaguchi, T., Fukata, Y., Ohno, S., & Kaibuchi, K. (2004). Role of the PAR-3–KIF3 complex in the establishment of neuronal polarity. Nature Cell Biology, 6(4), 328-334. doi: 10.1038/ncb1118

Nixon, R., & Shea, T. (1992). Dynamics of neuronal intermediate filaments: A developmental perspective. Cell Motility And The Cytoskeleton, 22(2), 81-91. doi: 10.1002/cm.970220202

Oakley, B. (2000). An abundance of tubulins. Trends In Cell Biology, 10(12), 537-542. doi: 10.1016/s0962-8924(00)01857-2

O'Hagan, R., Chalfie, M., & Goodman, M. (2004). The MEC-4 DEG/ENaC channel of Caenorhabditis elegans touch receptor neurons transduces mechanical signals. Nature Neuroscience, 8(1), 43-50. doi: 10.1038/nn1362

Ohara, O., Gahara, Y., Miyake, T., Teraoka, H., & Kitamura, T. (1993). Neurofilament deficiency in quail caused by nonsense mutation in neurofilament-L gene. Journal Of Cell Biology, 121(2), 387-395. doi: 10.1083/jcb.121.2.387

Ohno, N., Kidd, G., Mahad, D., Kiryu-Seo, S., Avishai, A., Komuro, H., & Trapp, B. (2011). Myelination and Axonal Electrical Activity Modulate the Distribution and Motility of Mitochondria at CNS Nodes of Ranvier. Journal Of Neuroscience, 31(20), 7249-7258. doi: 10.1523/jneurosci.0095-11.2011

Okamoto, K.-I., Nagai, T., Miyawaki, A., and Hayashi, Y. (2004). Rapid and persistent modulation of actin dynamics regulates postsynaptic reorganization underlying bidirectional plasticity. Nat. Neurosci. 7, 1104–1112. doi: 10.1038/nn1311

Orr, A., Helmke, B., Blackman, B., & Schwartz, M. (2006). Mechanisms of Mechanotransduction. Developmental Cell, 10(1), 11-20. doi: 10.1016/j.devcel.2005.12.006

Oyewole, A., & Birch-Machin, M. (2015). Mitochondria-targeted antioxidants. The FASEB Journal, 29(12), 4766-4771. doi: 10.1096/fj.15-275404

Panchal, K., & Tiwari, A. (2021). Miro (Mitochondrial Rho GTPase), a key player of mitochondrial axonal transport and mitochondrial dynamics in neurodegenerative diseases. Mitochondrion, 56, 118-135. doi: 10.1016/j.mito.2020.10.005

Pani, G., Samari, N., Quintens, R., de Saint-Georges, L., Meloni, M., & Baatout, S. et al. (2013). Morphological and Physiological Changes in Mature In Vitro Neuronal Networks towards Exposure to Short-, Middle- or Long-Term Simulated Microgravity. Plos ONE, 8(9), e73857. doi: 10.1371/journal.pone.0073857

Pani, G., Verslegers, M., Quintens, R., Samari, N., de Saint-Georges, L., & van Oostveldt, P. et al. (2016). Combined Exposure to Simulated Microgravity and Acute or Chronic Radiation Reduces Neuronal Network Integrity and Survival. PLOS ONE, 11(5), e0155260. doi: 10.1371/journal.pone.0155260

Pathak, D., Sepp, K., & Hollenbeck, P. (2010). Evidence That Myosin Activity Opposes Microtubule-Based Axonal Transport of Mitochondria. Journal Of Neuroscience, 30(26), 8984-8992. doi: 10.1523/jneurosci.1621-10.2010

Pchitskaya, E., Rakovskaya, A., Chigray, M., & Bezprozvanny, I. (2022). Cytoskeleton Protein EB3 Contributes to Dendritic Spines Enlargement and Enhances Their Resilience to Toxic Effects of Beta-Amyloid. International Journal Of Molecular Sciences, 23(4), 2274. doi: 10.3390/ijms23042274

Pedrotti, B., & Islam, K. (1995). Microtubule associated protein 1B (MAP1B) promotes efficient tubulin polymerisation in vitro. FEBS Letters, 371(1), 29-31. doi: 10.1016/0014-5793(95)00842-w

Perlson, E., Maday, S., Fu, M., Moughamian, A., & Holzbaur, E. (2010). Retrograde axonal transport: pathways to cell death?. Trends In Neurosciences, 33(7), 335-344. doi: 10.1016/j.tins.2010.03.006

Pilling, A., Horiuchi, D., Lively, C., & Saxton, W. (2006). Kinesin-1 and Dynein Are the Primary Motors for Fast Transport of Mitochondria inDrosophilaMotor Axons. Molecular Biology Of The Cell, 17(4), 2057-2068. doi: 10.1091/mbc.e05-06-0526

Qu, L., Chen, H., Liu, X., Bi, L., Xiong, J., Mao, Z., & Li, Y. (2010). Protective Effects of Flavonoids Against Oxidative Stress Induced by Simulated Microgravity in SH-SY5Y Cells. Neurochemical Research, 35(9), 1445-1454. doi: 10.1007/s11064-010-0205-4

Qu, L., Yang, T., Yuan, Y., Zhong, P., & Li, Y. (2006). Protein nitration increased by simulated weightlessness and decreased by melatonin and quercetin in PC12 cells. Nitric Oxide, 15(1), 58-63. doi: 10.1016/j.niox.2005.12.006

Qu, Y., Hahn, I., Webb, S., Pearce, S., & Prokop, A. (2017). Periodic actin structures in neuronal axons are required to maintain microtubules. Molecular Biology Of The Cell, 28(2), 296-308. doi: 10.1091/mbc.e16-10-0727

Richter, K., Haslbeck, M., & Buchner, J. (2010). The Heat Shock Response: Life on the Verge of Death. Molecular Cell, 40(2), 253-266. doi: 10.1016/j.molcel.2010.10.006

Riederer, B. (2007). Microtubule-associated protein 1B, a growth-associated and phosphorylated scaffold protein. Brain Research Bulletin, 71(6), 541-558. doi: 10.1016/j.brainresbull.2006.11.012

Riederer, B., Pellier, V., Antonsson, B., Di Paolo, G., Stimpson, S., & Lütjens, R. et al. (1997). Regulation of microtubule dynamics by the neuronal growth-associated protein SCG10. Proceedings Of The National Academy Of Sciences, 94(2), 741-745. doi: 10.1073/pnas.94.2.741

Rijken, P., de Groot, R., Kruijer, W., de Laat, S., Verkleij, A., & Boonstra, J. (1992). Identification of specific gravity sensitive signal transduction pathways in human A431 carcinoma cells. Advances In Space Research, 12(1), 145-152. doi: 10.1016/0273-1177(92)90277-5

Risinger, A., Giles, F., & Mooberry, S. (2009). Microtubule dynamics as a target in oncology. Cancer Treatment Reviews, 35(3), 255-261. doi: 10.1016/j.ctrv.2008.11.001

Rösner, H., Wassermann, T., Möller, W., & Hanke, W. (2006). Effects of altered gravity on the actin and microtubule cytoskeleton of human SH-SY5Y neuroblastoma cells. Protoplasma, 229(2-4), 225-234. doi: 10.1007/s00709-006-0202-2

Roy, S. (2014). Seeing the unseen: The hidden world of slow axonal transport. Neuroscientist, Vol. 20, pp. 71–81. https://doi.org/10.1177/1073858413498306

Ruane, P., Gumy, L., Bola, B., Anderson, B., Wozniak, M., Hoogenraad, C., & Allan, V. (2016). Tumour Suppressor Adenomatous Polyposis Coli (APC) localisation is regulated by both Kinesin-1 and Kinesin-2. Scientific Reports, 6(1). doi: 10.1038/srep27456

Rubinstein, L., Schreurs, A., Torres, S., Steczina, S., Lowe, M., & Kiffer, F. et al. (2021). Overexpression of catalase in mitochondria mitigates changes in hippocampal cytokine expression following simulated microgravity and isolation. Npj Microgravity, 7(1). doi: 10.1038/s41526-021-00152-w

Şahin, M., Öncü, G., Yılmaz, M., Özkan, D., & Saybaşılı, H. (2021). Transformation of SH-SY5Y cell line into neuron-like cells: Investigation of electrophysiological and biomechanical changes. Neuroscience Letters, 745, 135628. doi: 10.1016/j.neulet.2021.135628

Salvadores, N., Sanhueza, M., Manque, P., & Court, F. (2017). Axonal Degeneration during Aging and Its Functional Role in Neurodegenerative Disorders. Frontiers In Neuroscience, 11. doi: 10.3389/fnins.2017.00451

Schaefer, A., Kabir, N., & Forscher, P. (2002). Filopodia and actin arcs guide the assembly and transport of two populations of microtubules with unique dynamic parameters in neuronal growth cones. Journal Of Cell Biology, 158(1), 139-152. doi: 10.1083/jcb.200203038

Schaefer, A., Schoonderwoert, V., Ji, L., Mederios, N., Danuser, G., & Forscher, P. (2008). Coordination of Actin Filament and Microtubule Dynamics during Neurite Outgrowth. Developmental Cell, 15(1), 146-162. doi: 10.1016/j.devcel.2008.05.003

Schelski, M., & Bradke, F. (2017). Neuronal polarization: From spatiotemporal signaling to cytoskeletal dynamics. Molecular And Cellular Neuroscience, 84, 11-28. doi: 10.1016/j.mcn.2017.03.008

Schwamborn, J., & Püschel, A. (2004). The sequential activity of the GTPases Rap1B and Cdc42 determines neuronal polarity. Nature Neuroscience, 7(9), 923-929. doi: 10.1038/nn1295

Schwarzenberg, M., Pippia, P., Meloni, M., Cossu, G., Cogoli-Greuter, M., & Cogoli, A. (1999). Signal transduction in T lymphocytes — A comparison of the data from space, the free fall machine and the random positioning machine. Advances In Space Research, 24(6), 793-800. doi: 10.1016/s0273-1177(99)00075-7

Sharp, D., Yu, W., Ferhat, L., Kuriyama, R., Rueger, D., & Baas, P. (1997). Identification of a Microtubule-associated Motor Protein Essential for Dendritic Differentiation. Journal Of Cell Biology, 138(4), 833-843. doi: 10.1083/jcb.138.4.833

Sharif-Naeini, R. (2020). Role of mechanosensitive ion channels in the sensation of pain. Journal Of Neural Transmission, 127(4), 407-414. doi: 10.1007/s00702-020-02182-2

Sharp, D., Yu, W., Ferhat, L., Kuriyama, R., Rueger, D., & Baas, P. (1997). Identification of a Microtubule-associated Motor Protein Essential for Dendritic Differentiation. Journal Of Cell Biology, 138(4), 833-843. doi: 10.1083/jcb.138.4.833

Shen, M. & Frishman, W. Effects of Spaceflight on Cardiovascular Physiology and Health. Cardiology in Review 27, 122-126 (2019).

Singh, R., Rajput, M., & Singh, R. (2021). Simulated microgravity triggers DNA damage and mitochondria-mediated apoptosis through ROS generation in human promyelocytic leukemic cells. Mitochondrion, 61, 114-124. doi: 10.1016/j.mito.2021.09.006

Smith, B., Daugherty-Clarke, K., Goode, B., & Gelles, J. (2013). Pathway of actin filament branch formation by Arp2/3 complex revealed by single-molecule imaging. Proceedings Of The National Academy Of Sciences, 110(4), 1285-1290. doi: 10.1073/pnas.1211164110

Soulsby, M., Philips, B., & Chowdhury, P. (2004). Brief communication: Effects of soy-protein diet on elevated brain lipid peroxide levels induced by simulated weightlessness. Annals Of Clinical And Laboratory Science, 34(1).

Sorbara, C., Wagner, N., Ladwig, A., Nikić, I., Merkler, D., & Kleele, T. et al. (2014). Pervasive Axonal Transport Deficits in Multiple Sclerosis Models. Neuron, 84(6), 1183-1190. doi: 10.1016/j.neuron.2014.11.006

Stein, T. (2002). Space flight and oxidative stress. Nutrition, 18(10), 867-871. doi: 10.1016/s0899-9007(02)00938-3

Straube, A., & Merdes, A. (2007). EB3 Regulates Microtubule Dynamics at the Cell Cortex and Is Required for Myoblast Elongation and Fusion. Current Biology, 17(15), 1318-1325. doi: 10.1016/j.cub.2007.06.058

Stepanova, T., Slemmer, J., Hoogenraad, C., Lansbergen, G., Dortland, B., & De Zeeuw, C. et al. (2003). Visualization of Microtubule Growth in Cultured Neurons via the Use of EB3-GFP (End-Binding Protein 3-Green Fluorescent Protein). The Journal Of Neuroscience, 23(7), 2655-2664. doi: 10.1523/jneurosci.23-07-02655.2003

Strollo, F., Masini, M., Pastorino, M., Ricci, F., Vadrucci, S., Cogoli-Greuter, M., & Uva, B. (2004). Microgravity-induced alterations in cultured testicular cells. Journal Of Gravitational Physiology, 11(2).

Sui, H., & Downing, K. (2010). Structural Basis of Interprotofilament Interaction and Lateral Deformation of Microtubules. Structure, 18(8), 1022-1031. doi: 10.1016/j.str.2010.05.010

Sweeney, H., & Holzbaur, E. (2018). Motor Proteins. Cold Spring Harbor Perspectives In Biology, 10(5), a021931. doi: 10.1101/cshperspect.a021931

Takahashi, K., Takahashi, H., Furuichi, T., Toyota, M., Furutani-Seiki, M., & Kobayashi, T. et al. (2021). Gravity sensing in plant and animal cells. Npj Microgravity, 7(1). doi: 10.1038/s41526-020-00130-8

Takemura, R., Okabe, S., Umeyama, T., Kanai, Y., Cowan, N., & Hirokawa, N. (1992). Increased microtubule stability and alpha tubulin acetylation in cells transfected with microtubule-associated proteins MAP1B, MAP2 or tau. Journal Of Cell Science, 103(4), 953-964. doi: 10.1242/jcs.103.4.953

Tan, X., Xu, A., Zhao, T., Zhao, Q., Zhang, J., & Fan, C. et al. (2018). Simulated microgravity inhibits cell focal adhesions leading to reduced melanoma cell proliferation and metastasis via FAK/RhoA-regulated mTORC1 and AMPK pathways. Scientific Reports, 8(1). doi: 10.1038/s41598-018-20459-1

Tanaka, T., Naruse, K., & Sokabe, M. (2005). Effects of mechanical stresses on the migrating behavior of endothelial cells. Biomechanics At Micro- And Nanoscale Levels, 75-87. doi: 10.1142/9789812569301_0007

Tanaka, Y., Kanai, Y., Okada, Y., Nonaka, S., Takeda, S., Harada, A., & Hirokawa, N. (1998). Targeted Disruption of Mouse Conventional Kinesin Heavy Chain kif5B, Results in Abnormal Perinuclear Clustering of Mitochondria. Cell, 93(7), 1147-1158. doi: 10.1016/s0092-8674(00)81459-2

Teng, J., Takei, Y., Harada, A., Nakata, T., Chen, J., & Hirokawa, N. (2001). Synergistic effects of MAP2 and MAP1B knockout in neuronal migration, dendritic outgrowth, and microtubule organization. Journal Of Cell Biology, 155(1), 65-76. doi: 10.1083/jcb.200106025

Tian, G., & Cowan, N. (2013). Tubulin-Specific Chaperones. Methods In Cell Biology, 155-171. doi: 10.1016/b978-0-12-407757-7.00011-6

Tian, Y., Ma, X., Yang, C., Su, P., Yin, C., & Qian, A. (2017). The Impact of Oxidative Stress on the Bone System in Response to the Space Special Environment. International Journal Of Molecular Sciences, 18(10), 2132. doi: 10.3390/ijms18102132

Thomson, A., Schuhmann, T., de Graaf, T., Sack, A., Rutten, B., & Kenis, G. (2021). The Effects of Serum Removal on Gene Expression and Morphological Plasticity Markers in Differentiated SH-SY5Y Cells. Cellular And Molecular Neurobiology. doi: 10.1007/s10571-021-01062-x

Torres-Espín, A., Santos, D., González-Pérez, F., del Valle, J., & Navarro, X. (2014). Neurite-J: An Image-J plug-in for axonal growth analysis in organotypic cultures. Journal Of Neuroscience Methods, 236, 26-39. doi: 10.1016/j.jneumeth.2014.08.005

Ulbrich, C., Pietsch, J., Grosse, J., Wehland, M., Schulz, H., & Saar, K. et al. (2011). Differential Gene Regulation under Altered Gravity Conditions in Follicular Thyroid Cancer Cells: Relationship between the Extracellular Matrix and the Cytoskeleton. Cellular Physiology And Biochemistry, 28(2), 185-198. doi: 10.1159/000331730

Unsain, N., Bordenave, M., Martinez, G., Jalil, S., von Bilderling, C., & Barabas, F. et al. (2018). Author Correction: Remodeling of the Actin/Spectrin Membrane-associated Periodic Skeleton, Growth Cone Collapse and F-Actin Decrease during Axonal Degeneration. Scientific Reports, 8(1). doi: 10.1038/s41598-018-23781-w

Unsain, N., Stefani, F., & Cáceres, A. (2018). The Actin/Spectrin Membrane-Associated Periodic Skeleton in Neurons. Frontiers In Synaptic Neuroscience, 10. doi: 10.3389/fnsyn.2018.00010

Uva, B., Masini, M., Sturla, M., Prato, P., Passalacqua, M., & Giuliani, M. et al. (2002). Clinorotation-induced weightlessness influences the cytoskeleton of glial cells in culture. Brain Research, 934(2), 132-139. doi: 10.1016/s0006-8993(02)02415-0

Uva, B., Strollo, F., Ricci, F., Pastorino, M., Mason, J., & Masini, M. (2005). Morpho-functional alterations in testicular and nervous cells submitted to modelled microgravity. Journal Of Endocrinological Investigation, 28.

Viswanadha, R., Sale, W., & Porter, M. (2017). Ciliary Motility: Regulation of Axonemal Dynein Motors. Cold Spring Harbor Perspectives In Biology, 9(8), a018325. doi: 10.1101/cshperspect.a018325

Vulevic, B., & Correia, J. (1997). Thermodynamic and structural analysis of microtubule assembly: the role of GTP hydrolysis. Biophysical Journal, 72(3), 1357-1375. doi: 10.1016/s0006-3495(97)78782-4

Wang, J., Zhang, J., Bai, S., Wang, G., Mu, L., & Sun, B. et al. (2009). Simulated microgravity promotes cellular senescence via oxidant stress in rat PC12 cells. Neurochemistry International, 55(7), 710-716. doi: 10.1016/j.neuint.2009.07.002

Wang, L. et al. Early processing variations in selective attention to the color and direction of moving stimuli during 30 days head-down bed rest. Acta Astronautica 92, 29-37 (2013).

Wang, S., & Good, T. (2001). Effect of culture in a rotating wall bioreactor on the physiology of differentiated neuron-like PC12 and SH-SY5Y cells. Journal Of Cellular Biochemistry, 83(4), 574-584. doi: 10.1002/jcb.1252

Wang, X., & Schwarz, T. (2009). The Mechanism of Ca2+-Dependent Regulation of Kinesin-Mediated Mitochondrial Motility. Cell, 136(1), 163-174. doi: 10.1016/j.cell.2008.11.046

Wang, X., Du, J., Wang, D., Zeng, F., Wei, Y., & Wang, F. et al. (2016). Effects of simulated microgravity on human brain nervous tissue. Neuroscience Letters, 627, 199-204. doi: 10.1016/j.neulet.2016.06.004

Westermann, S., & Weber, K. (2003). Post-translational modifications regulate microtubule function. Nature Reviews Molecular Cell Biology, 4(12), 938-948. doi: 10.1038/nrm1260

Winans, A., Collins, S., & Meyer, T. (2016). Waves of actin and microtubule polymerization drive microtubule-based transport and neurite growth before single axon formation. Elife, 5. doi: 10.7554/elife.12387

Witte, H., Neukirchen, D., & Bradke, F. (2008). Microtubule stabilization specifies initial neuronal polarization. Journal Of Cell Biology, 180(3), 619-632. doi: 10.1083/jcb.200707042

Wolozin, B. (2012). Regulated protein aggregation: stress granules and neurodegeneration. Molecular Neurodegeneration, 7(1), 56. doi: 10.1186/1750-1326-7-56

Valakh, V., Frey, E., Babetto, E., Walker, L., & DiAntonio, A. (2015). Cytoskeletal disruption activates the DLK/JNK pathway, which promotes axonal regeneration and mimics a preconditioning injury. Neurobiology Of Disease, 77, 13-25. doi: 10.1016/j.nbd.2015.02.014

Valente, A., Maddalena, L., Robb, E., Moradi, F., & Stuart, J. (2017). A simple ImageJ macro tool for analyzing mitochondrial network morphology in mammalian cell culture. Acta Histochemica, 119(3), 315-326. doi: 10.1016/j.acthis.2017.03.001

van Spronsen, M., Mikhaylova, M., Lipka, J., Schlager, M., van den Heuvel, D., & Kuijpers, M. et al. (2013). TRAK/Milton Motor-Adaptor Proteins Steer Mitochondrial Trafficking to Axons and Dendrites. Neuron, 77(3), 485-502. doi: 10.1016/j.neuron.2012.11.027

Vandecandelaere, A., Pedrotti, B., Utton, M., Calvert, R., & Bayley, P. (1996). Differences in the regulation of microtubule dynamics by microtubule-associated proteins MAP1B and MAP2. Cell Motility And The Cytoskeleton, 35(2), 134-146. doi: 10.1002/(sici)1097-0169(1996)35:2<134::aid-cm6>3.0.co;2-a

Varidaki, A., Hong, Y., & Coffey, E. (2018). Repositioning Microtubule Stabilizing Drugs for Brain Disorders. Frontiers In Cellular Neuroscience, 12. doi: 10.3389/fncel.2018.00226

Vassy, J., Portet, S., Beil, M., Millot, G., Fauvel-Lafeve, F., & Karniguian, A. et al. (2001). The effect of weightlessness on cytoskeleton architecture and proliferation of human breast cancer cell line MCF-7. The FASEB Journal, 15(6), 1104-1106. doi: 10.1096/fj.00-0527fje

Verstraelen, P., Detrez, J., Verschuuren, M., Kuijlaars, J., Nuydens, R., Timmermans, J., & De Vos, W. (2017). Dysregulation of Microtubule Stability Impairs Morphofunctional Connectivity in Primary Neuronal Networks. Frontiers In Cellular Neuroscience, 11. doi: 10.3389/fncel.2017.00173

Vorselen, D., Roos, W., MacKintosh, F., Wuite, G., & Loon, J. (2013). The role of the cytoskeleton in sensing changes in gravity by nonspecialized cells. The FASEB Journal, 28(2), 536-547. doi: 10.1096/fj.13-236356

Withers, G., & Wallace, C. (2020). Transient lamellipodia predict sites of dendritic branch formation in hippocampal neurons. Cell And Tissue Research, 381(1), 35-42. doi: 10.1007/s00441-020-03194-w

Witze, A. (2020). Astronauts have conducted nearly 3,000 science experiments aboard the ISS. Nature. doi: 10.1038/d41586-020-03085-8

Wozniak, M., Melzer, M., Dorner, C., Haring, H., & Lammers, R. (2005). The novel protein KBP regulates mitochondria localization by interaction with a kinesin-like protein. BMC Cell Biology, 6(1). doi: 10.1186/1471-2121-6-35

Wuest, S., Gantenbein, B., Ille, F., & Egli, M. (2018). Electrophysiological experiments in microgravity: lessons learned and future challenges. Npj Microgravity, 4(1). doi: 10.1038/s41526-018-0042-3

Wuest, S., Richard, S., Kopp, S., Grimm, D., & Egli, M. (2015). Simulated Microgravity: Critical Review on the Use of Random Positioning Machines for Mammalian Cell Culture. Biomed Research International, 2015, 1-8. doi: 10.1155/2015/971474

Xicoy, H., Wieringa, B., & Martens, G. (2017). The SH-SY5Y cell line in Parkinson's disease research: a systematic review. Molecular Neurodegeneration, 12(1). doi: 10.1186/s13024-017-0149-0

Xu, K., Zhong, G., & Zhuang, X. (2013). Actin, Spectrin, and Associated Proteins Form a Periodic Cytoskeletal Structure in Axons. Science, 339(6118), 452-456. doi: 10.1126/science.1232251

Yang, F., Dai, Z., Tan, Y. & Li, Y. Effects of Altered Gravity on the Cytoskeleton of Neonatal Rat Cardiocytes. Microgravity Science and Technology 22, 45-52 (2008).

Yu, W., Cook, C., Sauter, C., Kuriyama, R., Kaplan, P., & Baas, P. (2000). Depletion of a Microtubule-Associated Motor Protein Induces the Loss of Dendritic Identity. The Journal Of Neuroscience, 20(15), 5782-5791. doi: 10.1523/jneurosci.20-15-05782.2000

Yuan, A., Rao, M., Veeranna, & Nixon, R. (2017). Neurofilaments and Neurofilament Proteins in Health and Disease. Cold Spring Harbor Perspectives In Biology, 9(4), a018309. doi: 10.1101/cshperspect.a018309

Yang, Q., Zhang, X., Pollard, T., & Forscher, P. (2012). Arp2/3 complex–dependent actin networks constrain myosin II function in driving retrograde actin flow. Journal Of Cell Biology, 197(7), 939-956. doi: 10.1083/jcb.201111052

Yu, W., Cook, C., Sauter, C., Kuriyama, R., Kaplan, P., & Baas, P. (2000). Depletion of a Microtubule-Associated Motor Protein Induces the Loss of Dendritic Identity. The Journal Of Neuroscience, 20(15), 5782-5791. doi: 10.1523/jneurosci.20-15-05782.2000

Yum, S., Zhang, J., Mo, K., Li, J., & Scherer, S. (2009). A novel recessiveNeflmutation causes a severe, early-onset axonal neuropathy. Annals Of Neurology, 66(6), 759-770. doi: 10.1002/ana.21728

Zhang, R., Jiang, M., Zhang, J., Qiu, Y., Li, D., & Li, S. et al. (2020). Regulation of the cerebrovascular smooth muscle cell phenotype by mitochondrial oxidative injury and endoplasmic reticulum stress in simulated microgravity rats via the PERK-eIF2α-ATF4-CHOP pathway. Biochimica Et Biophysica Acta (BBA) - Molecular Basis Of Disease, 1866(8), 165799. doi: 10.1016/j.bbadis.2020.165799

Zhang, Y., Gao, F., Popov, V., Wen, J., & Hamill, O. (2000). Mechanically gated channel activity in cytoskeleton-deficient plasma membrane blebs and vesicles from Xenopus oocytes. The Journal Of Physiology, 523(1), 117-130. doi: 10.1111/j.1469-7793.2000.t01-1-00117.x

Zheng, Y., Wildonger, J., Ye, B., Zhang, Y., Kita, A., & Younger, S. et al. (2008). Dynein is required for polarized dendritic transport and uniform microtubule orientation in axons. Nature Cell Biology, 10(10), 1172-1180. doi: 10.1038/ncb1777

Zhong, G., He, J., Zhou, R., Lorenzo, D., Babcock, H., Bennett, V., & Zhuang, X. (2014). Developmental mechanism of the periodic membrane skeleton in axons. Elife, 3. doi: 10.7554/elife.04581

Zhu, Q., Couillard-Després, S., & Julien, J. (1997). Delayed Maturation of Regenerating Myelinated Axons in Mice Lacking Neurofilaments. Experimental Neurology, 148(1), 299-316. doi: 10.1006/exnr.1997.6654

Zwetsloot, A., Tut, G., & Straube, A. (2018). Measuring microtubule dynamics. Essays In Biochemistry, 62(6), 725-735. doi: 10.1042/ebc20180035

Appendix A.

Supplementary Materials

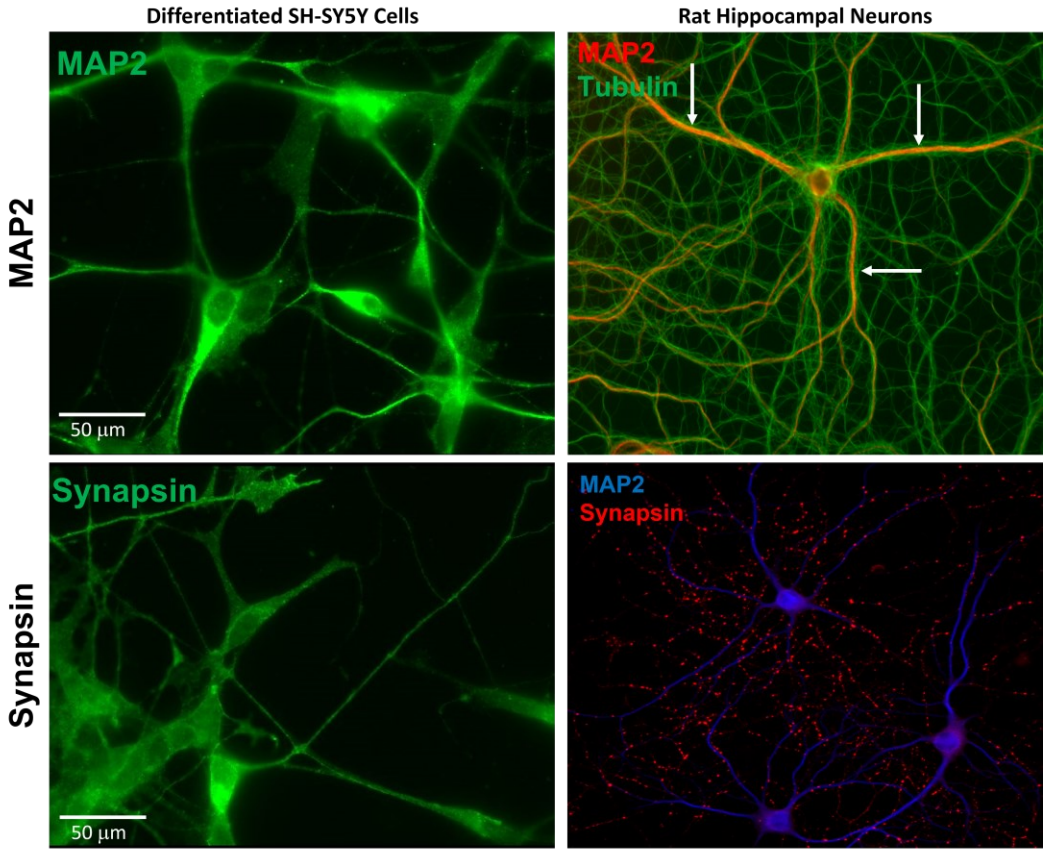

Figure A.1. Differentiated SH-SY5Y cells are not positive for mature synaptic markers

MAP2 and synapsin are not expressed in neuron-specific expression patterns when stained for in SH-SY5Y cells. MAP2 is highly expressed in dendrites and not axons when stained in mature neurons, but staining is not segregated in differentiated SH-SY5Y cells. Synapsin is highly expressed at synapses, where its function is fundamental to neurotransmitter release. Differentiated SH-SY5Y cells do not express synapsin in the distinct punctate patterns observable when stained for in neuronal cell lines.

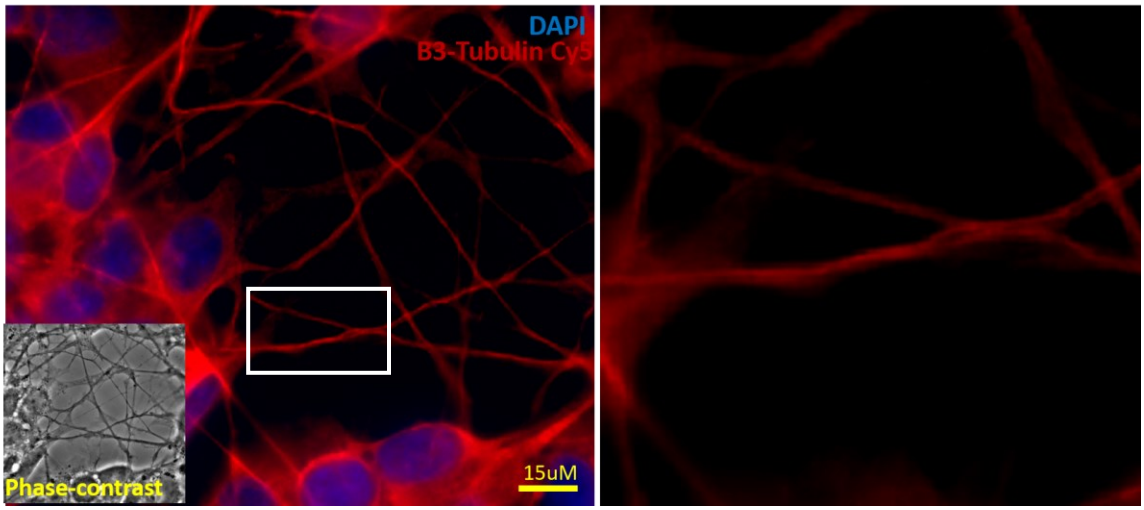

Figure A.2. SH-SY5Y cells differentiated with BDNF are positive for neuron-specific βIII-Tubulin

Differentiated SH-SY5Y cells positively stain for the neuron specific βIII-Tubulin variant. This result supports the conclusion that SH-SY5Y cells undergo biochemical differentiation following treatment with BDNF, expressing a distinct biochemical phenotype versus undifferentiated cells.

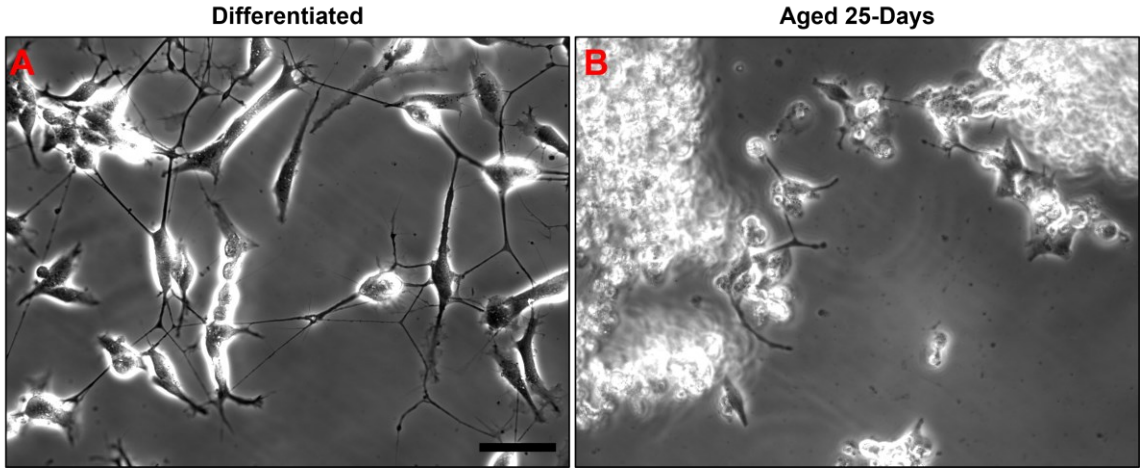

Figure A.3. SH-SY5Y long-term survivability and death in normal cell culture conditions

A) Representative phase-contrast image of fully differentiated SH-SY5Y cells. Cells aged 15-days total since induction (20-days total). Phase-bright cell bodies and long neurites are observable. B) Representative phase-contrast image of degenerated SH-SY5Y cells. Cells aged 20-days total since induction (25-days total). Majority of neurites have retracted, and no long neurites remain. Cellular debris abundant in field of view and few living cells remain. Scale bars: 50μM

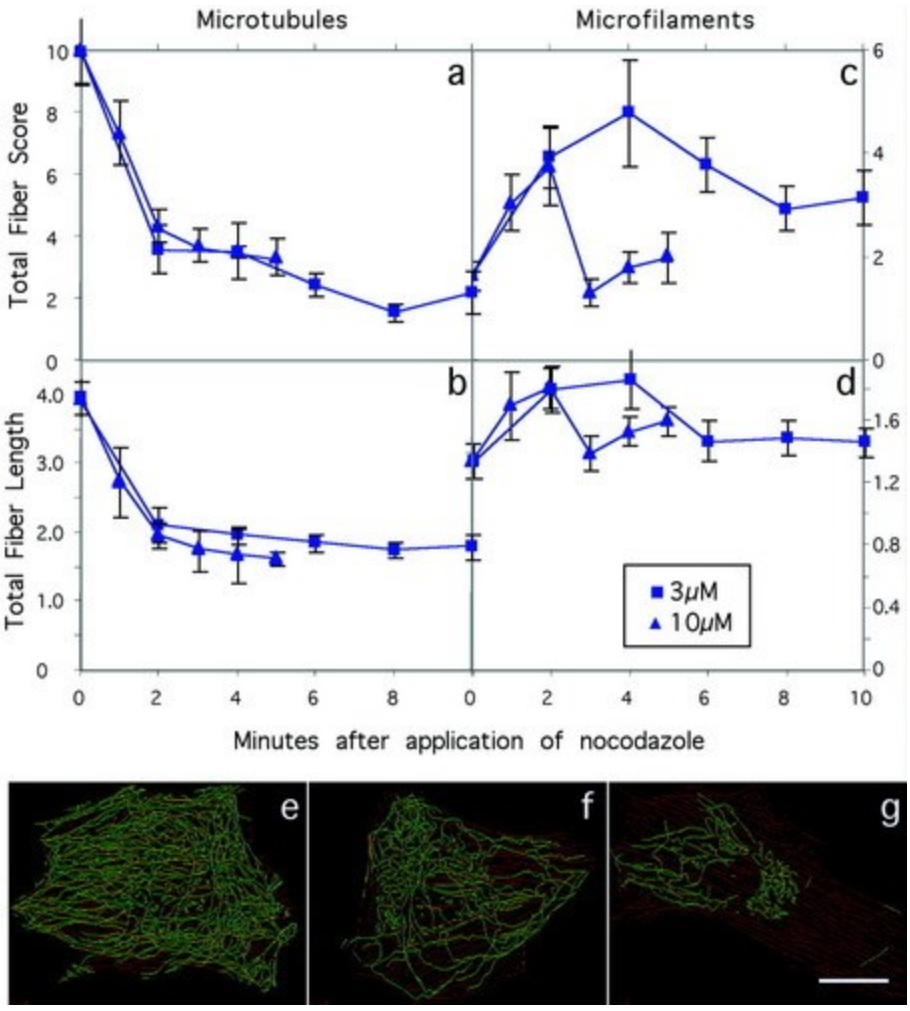

Figure A.4. Example of microtubule ultrastructure quantification via fiberscore algorithm in nocodazole-treated cells

The MatLab-based FiberScore algorithm reliably quantifies microtubule linearity following pharmaceutical treatment such as nocodazole. This protocol is an example of a potential quantitative approach for assessing disruption to microtubule structure following microgravity exposure.

Figure reproduced from Lichtenstein, N., Geiger, B., & Kam, Z. (2003). Quantitative analysis of cytoskeletal organization by digital fluorescent microscopy. Cytometry, 54A(1), 8-18. doi: 10.1002/cyto.a.10053. Reproduced under the terms of the Creative Commons Attribution 4.0 International License

Appendix B.

Supplementary Videos

Creator:

Matthew Danesh

Description:

This short video demonstrates a high-resolution recording of the trafficking of GFP-MTS in our transfected SH-SY5Y cell line. Visualization of short run length trafficking events is possible when GFP-MTS is observed at high magnification and resolution levels.

Filename:

GFP_63X_Video_Example.mov